

國立臺灣大學工學院應用力學研究所

博士論文

Department of Applied Mechanics


College of Engineering

National Taiwan University

Doctoral Dissertation

半古典晶格波滋曼方法

Semiclassical Lattice Boltzmann Method



洪立昕

Li-Hsin Hung

指導教授：楊照彥 博士

Advisor: Jaw-Yen Yang, Ph.D.

中華民國 99 年 10 月

October, 2010

## 誌 謝

終於走到這一步了，四年多前的熱情慢慢累積成一行行的程式、一篇篇的文章，也差不多消耗殆盡了。很高興也很欣慰能在不算太久的時間內走出台大大門。最感謝的是父母的支持，無論是精神上還是經濟上，都是給我最多幫助的。妹妹來自美國的鼓勵也幫助我不少，尤其妳比我更累的研究生活，更是鞭策我繼續向上的動力。謝謝珮君和冠孜，妳們的陪伴帶給我豐富而精采的精神生活，方能戰勝這漫長而艱辛的一役。

感謝指導教授 楊照彥博士四年多來的提攜，教授不論是嚴謹的研究態度還是充沛的精力跑遍各國都另人景仰和欽羨。

論文定稿之際，承蒙本校 許文翰教授、黃美嬌教授，清華大學 林昭安教授，中正大學 何正榮教授，成功大學 陳朝光教授、黃吉川教授以及楊玉姿教授的指導，讓我看到許多不同思考層面，更進一步精進論文內容，令我受益匪淺。

實驗室待了許久，相處過的學長學弟不可勝數，每個人都是我永遠的好友。特別感謝育炘帶我進入這全新的研究領域、澤揚在博後階段和我的討論，還有聖鑫及耀天在部分研究內容上的幫忙，讓我能夠發更多文章，順利畢業。最後，感謝許多我沒提及但仍愛我的人，少了你(妳)們，這一切也難以成真，謝謝。

## 摘要

本論文提出了半古典晶格波滋曼法，此方法是在波滋曼法的基礎下，使用量子統計(Bose-Einstein Statistics 和 Fermi-Dirac Statistics)取代古典統計(Maxwell-Boltzmann Statistics)後展開所得的方法。此方法可驗證在古典極限(Classical Limit)下可回復原本古典晶格波滋曼法，亦可由數值驗證得知古典極限下可得傳統晶格波滋曼法之結果。本文以此一新提出之模擬方法研究量子氣體運動問題，模擬之問題忽略粒子間交互作用，但因為使用量子統計之故，粒子在量子統計下的特性如泡立不相容原理(Pauli Exclusion Principle)、巨觀上傳輸係數之修正等等均有考慮在內。本文探討一維量子氣體之震波管問題、二維圓柱流問題、二維微管問題以及三維頂蓋流問題作為驗證半古典晶格波滋曼法之方式，模擬結果指出了量子統計和古典統計結果的主要差異。此外，本文亦提出了另一種雙分布函數熱晶格波滋曼法，可得出一般雙分布函數熱晶格波滋曼法所得結果，也可作為未來更進一步推廣半古典晶格波滋曼法之方向。

關鍵詞: 晶格波滋曼法、量子統計、波滋曼方程式

## Abstract

Unlike describing the physical phenomenon in coordinate or momentum spaces in quantum mechanics, semiclassical Boltzmann equation treats the system in phase space, and it is much easier to describe the dynamics of quantum gases. In this thesis, a class of semiclassical lattice Boltzmann methods is developed for solving quantum hydrodynamics and beyond. The present method is directly derived by projecting the Uehling-Uhlenbeck Boltzmann-BGK equations onto the tensor Hermite polynomials following Grad's moment expansion method. The intrinsic discrete nodes of the Gauss-Hermite quadrature provide the natural lattice velocities for the semiclassical lattice Boltzmann method. Formulations for the second-order and third order expansion of the semiclassical equilibrium distribution functions are derived and their corresponding hydrodynamics are studied. Gases of particles of arbitrary statistics can be considered. Simulations of one-dimensional compressible gas flow by using D1Q5 lattices, two dimensional microchannel flow, two dimensional flow over cylinder by using D2Q9 lattices and three dimensional lid driven cavity flow by using D3Q19 lattices are provided for validating this method. It is shown that the classical flow patterns such like vortex and vortices shedding in flow over cylinder simulations, temperature and pressure contours together with streamline patterns could be produced from the present method in classical limit. The results also indicate the distinct characteristics of the effects of quantum statistics when they are compared with fluid phenomena in classical statistics.

**Keywords:** Lattice Boltzmann Method, Semiclassical, Quantum.



# Contents

LIST OF TABLES . . . . .	v
LIST OF FIGURES . . . . .	1
<b>1 Introduction</b>	<b>1</b>
1.1 Overview . . . . .	1
1.2 Conventional LB method . . . . .	3
1.3 Basics of Semiclassical LB method . . . . .	5
1.4 Contents of the Dissertation . . . . .	8
<b>2 Semiclassical Kinetic Theory</b>	<b>9</b>
2.1 Overview . . . . .	9
2.2 Introduction to Quantum Gases . . . . .	10
2.3 Semiclassical Boltzmann Equation(UUB Equation) . . . . .	12
2.4 Semiclassical Hydrodynamic Equations . . . . .	14
<b>3 Semiclassical Lattice Boltzmann Method</b>	<b>21</b>
3.1 Overview . . . . .	21
3.2 The Derivations of Conventional LB method . . . . .	22
3.2.1 Time Discretization . . . . .	22
3.2.2 Space and Velocity Discretization . . . . .	23
3.3 The Derivations of Single Relaxation Time Semiclassical LB method . . . . .	28
3.3.1 Summary of Single Relaxation Time Semiclassical LB Method . . . . .	32
3.4 Generalized Semiclassical LB method . . . . .	35

<b>4</b>	<b>Initial Conditions and Boundary Conditions for Semiclassical LB method</b>	<b>43</b>
4.1	Overview . . . . .	43
4.2	Initial Conditions . . . . .	45
4.3	Boundary Conditions . . . . .	45
4.3.1	Periodic Boundary Condition . . . . .	45
4.3.2	Bounce Back Boundary Condition . . . . .	46
4.3.3	Non-Equilibrium Extrapolation Boundary Condition . . . . .	49
4.3.4	Immersed Boundary Condition . . . . .	52
4.3.5	Issues on Microchannel Boundaries . . . . .	53
<b>5</b>	<b>Numerical Results</b>	<b>63</b>
5.1	Overview . . . . .	63
5.2	One Dimensional Shock Tube . . . . .	64
5.3	Two Dimensional Microchannel Flow . . . . .	65
5.4	Two Dimensional Flow over Cylinder . . . . .	69
5.5	Two Dimensional Natural Convection and Rayleigh-Benard Convection Flow . . . . .	71
5.6	Three Dimensional Lid Driven Cavity Flow . . . . .	73
<b>6</b>	<b>Conclusions and Future Work</b>	<b>101</b>
6.1	Accomplishments . . . . .	101
6.2	Future Work . . . . .	103
<b>A</b>	<b>Nomenclature</b>	<b>107</b>
<b>B</b>	<b>Chapman-Enskog Analysis of semiclassical LB method</b>	<b>111</b>
B.1	Chapman-Enskog Analysis of Single Relaxation Time semiclassical LB method . . . . .	111

---

<b>C Derivations of Double Distribution Function LB method</b>	<b>117</b>
C.1 Two Relaxation Times Kinetic Model . . . . .	118
C.2 Expansion of the Equilibrium Distribution Functions . . . . .	121
C.3 Discretization of Velocity Space . . . . .	122
C.4 Time Discretization . . . . .	125
C.5 Chapman-Enskog Analysis of Double Distribution Functions LB method . . . . .	127
 <b>Bibliography</b>	 <b>133</b>





# List of Tables

3.1	D1Q5 quadratures and weights . . . . .	41
3.2	D2Q9 quadratures and weights . . . . .	41
3.3	D3Q19 quadratures and weights . . . . .	41
5.1	Comparisons of drag coefficient of different boundary conditions in LB method . . . . .	76
5.2	Comparisons of the average Nusselt number and the maximum velocity components across the cavity center. The data in parentheses are the locations of the maxima. . . . .	76





# List of Figures

2.1	Bose and Fermi functions in different fugacity $z$ . (a) Bose Function $g_{1.5}^{Bose}(z)$ , $g_{2.5}^{Bose}(z)$ , and $\frac{g_{2.5}^{Bose}(z)}{g_{1.5}^{Bose}(z)}$ , (b) Fermi Function $g_{1.5}^{Fermi}(z)$ , $g_{2.5}^{Fermi}(z)$ , and $\frac{g_{2.5}^{Fermi}(z)}{g_{1.5}^{Fermi}(z)}$ , (c) Comparing Bose $\frac{g_{2.5}^{Bose}(z)}{g_{1.5}^{Bose}(z)}$ and Fermi Function $\frac{g_{2.5}^{Fermi}(z)}{g_{1.5}^{Fermi}(z)}$ . . . . .	19
3.1	Comparisons of streamlines of uniform flow over a circular cylinder in a BE quantum gas in different expansion order with $z = 0.2$ and $Re_\infty = 40$ . (a) $N = 3$ , (b) $N = 2$ . . . . .	40
3.2	D1Q5 lattice structure . . . . .	41
3.3	D2Q9 lattice structure . . . . .	41
3.4	D3Q19 lattice structure . . . . .	41
4.1	Layout of the curved wall boundary in the regularly spaced lattices. . . . .	57
4.2	Periodic boundary conditions. . . . .	57
4.3	Layout of the curved wall boundary in the regularly spaced lattices. . . . .	58
4.4	Bounce back boundary conditions (a) $q < 1/2$ , (b) $q \geq 1/2$ . . .	59
4.5	The influences of different accommodation coefficients on velocity profile based on two different boundary conditions. (a) Bounce-back specular reflection boundary condition, (b) Discrete maxwellian boundary condition. . . . .	60
4.6	The influences of different boundary conditions on velocity profile based on the same accommodation $r = 0.8$ . (a) Kn=0.5, (b) Kn=2. . . . .	61

4.7	The velocity profile of different Knudsen number based on the same accommodation coefficient $r = 0.8$ for two different boundary conditions. (a) Bounce-back specular reflection boundary condition, (b) Discrete maxwellian boundary condition. . . . .	62
5.1	Convergence of solution with refined grids, the cells number is 100, 200, and 400. (a) Velocity, (b) Density, (a) Pressure, (d) Temperature. . . . .	78
5.2	Shock tube flow in a quantum gas. The effect due to different particle statistics; Bose-Einstein: BE, Fermi-Dirac: FD, Maxwell-Boltzmann: MB. (a) Density, (b) Velocity, (c) Pressure, (d) Temperature. . . . .	80
5.3	Shock tube flow in a quantum gas. The effect in high temperature limit; Bose-Einstein: BE, Fermi-Dirac: FD, Maxwell-Boltzmann: MB. (a) Density, (b) Velocity, (c) Pressure, (d) Temperature. . . . .	82
5.4	Velocity profiles in a channel flow of gases of arbitrary statistics (gas with $z = 0.2$ ). (a) $Kn=0.05$ , (b) $Kn=0.5$ , (c) $Kn=1$ . (d) Normalized mass flux in a channel flow as a function of $Kn$ number. . . . .	83
5.5	Drag and lift coefficients in classical limit. (a) $Re = 100$ , (b) $Re = 500$ . . . . .	84
5.6	Drag and lift coefficients in different boundary conditions (immersed boundary condition and bounce back boundary condition). (a) $Re = 100$ , (b) $Re = 200$ . . . . .	85



5.7	Streamlines of uniform flow over a circular cylinder in a quantum gas with $z = 0.2$ and $Re_\infty = 20$ . (a) BE gas, (b) MB gas, (c) FD gas. . . . .	86
5.8	Streamlines of uniform flow over a circular cylinder in a quantum gas with $z = 0.2$ and $Re_\infty = 40$ . (a) BE gas, (b) MB gas, (c) FD gas. . . . .	87
5.9	Streamlines of uniform flow over a circular cylinder in a quantum gas with $z = 0.2$ and $Re_\infty = 200$ . (a) BE gas, (b) MB gas, (c) FD gas. . . . .	88
5.10	Different contours and streamlines of uniform flow over a circular cylinder in a quantum gas in a classical limit with $Re_\infty = 200$ , steps=94200. (a) X-direction velocity( $u_x$ ), (b) y-direction velocity( $u_y$ ), (c) fugacity( $z$ ), (d) density( $\rho$ ), (e) temperature( $\theta$ ), (f) streamlines. . . . .	89
5.11	Streamlines for different Rayleigh numbers of natural convection. (a) $Ra = 10^3$ , (b) $Ra = 10^4$ , (c) $Ra = 10^5$ . . . . .	90
5.12	Isotherm lines for different Rayleigh numbers of natural convection. (a) $Ra = 10^3$ , (b) $Ra = 10^4$ , (c) $Ra = 10^5$ . . . . .	90
5.13	Streamlines of Rayleigh-Benard convection for different Rayleigh numbers. (a) $Ra = 4000$ , (b) $Ra = 10000$ , (c) $Ra = 50000$ . . .	91
5.14	Isotherms of Rayleigh-Benard convection for different Rayleigh numbers. (a) $Ra = 4000$ , (b) $Ra = 10000$ , (c) $Ra = 50000$ . . .	92
5.15	Grid refinement of three dimensional lid driven simulation, $Re = 400$ for two different centerlines. (a) (x,0,0), (b) (0,0,z). . . . .	93
5.16	Grid refinement of three dimensional lid driven simulation, $Re = 1000$ for two different centerlines. (a) (x,0,0), (b) (0,0,z). . . . .	93

5.17	Streamlines of MB statistics in three mid-planes, $Re = 100$ . (a) xy planes, (b) zy planes, (c) xz planes. . . . .	94
5.18	Streamlines of MB statistics in three mid-planes, $Re = 400$ . (a) xy planes, (b) yz planes, (c) xz planes. . . . .	94
5.19	Streamlines of MB statistics in three mid-planes, $Re = 1000$ . (a) xy planes, (b) yz planes, (c) xz planes. . . . .	94
5.20	Centerlines velocity of classical and semiclassical model. (a) Classical, (b) semiclassical . . . . .	95
5.21	Velocity vectors of BE statistics in three mid-planes, $Re = 100$ , $z = 0.2$ . (a) xy planes, (b) yz planes, (c) xz planes. . . . .	96
5.22	Pressure contours of BE statistics in three mid-planes, $Re = 100$ , $z = 0.2$ . (a) xy planes, (b) yz planes, (c) xz planes. . . . .	96
5.23	Streamlines patters of BE statistics in three mid-planes, $Re = 100$ , $z = 0.2$ . (a) xy planes, (b) yz planes, (c) xz planes. . . . .	96
5.24	Velocity vectors of FD statistics in three mid-planes, $Re = 100$ , $z = 0.2$ . (a) xy planes, (b) yz planes, (c) xz planes. . . . .	97
5.25	Pressure contours of FD statistics in three mid-planes, $Re = 100$ , $z = 0.2$ . (a) xy planes, (b) yz planes, (c) xz planes. . . . .	97
5.26	Streamlines patters of FD statistics in three mid-planes, $Re = 100$ , $z = 0.2$ . (a) xy planes, (b) yz planes, (c) xz planes. . . . .	97
5.27	Streamlines patters of FD statistics in three mid-planes, $Re = 400$ , $z = 0.2$ . (a) xy planes, (b) yz planes, (c) xz planes. . . . .	98
5.28	Streamlines patters of BE statistics in three mid-planes, $Re = 400$ , $z = 0.2$ . (a) xy planes, (b) yz planes, (c) xz planes. . . . .	98
5.29	Streamlines patters of FD statistics in three mid-planes, $Re = 1000$ , $z = 0.2$ . (a) xy planes, (b) yz planes, (c) xz planes. . . . .	98

5.30 Streamlines patters of BE statistics in three mid-planes,  $Re = 1000$ ,  $z = 0.2$ . (a) xy planes, (b) yz planes, (c) xz planes. . . . 99

5.31 Centerlines velocity of different quantum statistics,  $z = 0.1$  and  $z = 0.2$  . . . . . 100





# Introduction

---

## Contents

<b>1.1 Overview</b> . . . . .	<b>1</b>
<b>1.2 Conventional LB method</b> . . . . .	<b>3</b>
<b>1.3 Basics of Semiclassical LB method</b> . . . . .	<b>5</b>
<b>1.4 Contents of the Dissertation</b> . . . . .	<b>8</b>

---

## 1.1 Overview

After more than twenty years developments on lattice Boltzmann (LB) method since its introduction [1][2], the LB method is not just the extension of its ancestor lattice-gas automaton [3], and even not just a hydrodynamical equations solver. It has been another approach analyzing Boltzmann equation in compared with Chapman-Enskog expansion [4] and Grad moment method [5].

LB method is based on the kinetic equations for simulating fluid flow, see [6][7][8]. Over the past two decades, significant advances in the development of the LB method [2][9][10][11] based on classical Boltzmann equations with the relaxation time approximation of Bhatnagar, Gross and Krook (BGK) [12] have been achieved. The LB method has demonstrated its ability to simulate hydrodynamic systems, magnetohydrodynamic systems, multi-phase

and multi-component fluids, multi-component flow through porous media, and complex fluid systems, see [13]. The LB equations can also be directly derived in a *a priori* manner from the continuous Boltzmann equations [14][15][16]. Most of the classical LB methods are accurate up to the second order, i.e., Navier-Stokes hydrodynamics and have not been extended beyond the level of the Navier-Stokes hydrodynamics. A systematical method [17][16] was proposed for kinetic theory representation of hydrodynamics beyond the Navier-Stokes equations using Grad's moment expansion method [5][18]. The use of Grad's moment expansion method in other kinetic equations such as quantum kinetic equations and Enskog equations can be found in [19][20].

Despite their great success, however, most of the existing LB methods are limited to hydrodynamics of classical particles. Modern development in nanoscale transport requires carriers of particles of arbitrary statistics, e.g., phonon Boltzmann transport in nanocomposite and carrier transport in semiconductors. The extension and generalization of the successful classical LB method to quantum LB method for quantum particles is desirable. Analogous to the classical Boltzmann equations, a semiclassical Boltzmann equations for transport phenomenon in quantum gases has been developed by Uehling and Uhlenbeck [21][22]. Following the work of Uehling and Uhlenbeck based on the Chapman-Enskog procedure [4], the hydrodynamic equations of a trapped dilute Bose gas with damping have been derived [23]. In [19], the quantum Grad expansion using tensor Hermite polynomials has been applied to obtain the non-equilibrium density matrix which reduces to the classical Grad moment expansion if the gas obeys the Boltzmann statistics. The full Boltzmann equations is mathematically difficult to handle due to the collision integral in different types of collisions. To avoid the complexity of the collision term, the relaxation time model originally proposed by BGK model for the clas-

sical non-relativistic neutral and charged gases has been widely used. Also, BGK-type relaxation time models to capture the essential properties of carrier scattering mechanisms can be similarly devised for the UUB equations for various carriers and have been widely used in carrier transports [24]. Recently, kinetic numerical methods for ideal quantum gas dynamics based on Bose-Einstein(BE) and Fermi-Dirac(FD) statistics have been presented [25][26]. A gas-kinetic method for the semiclassical Boltzmann-BGK equations for non-equilibrium transport has been devised [27].

In this thesis, a new semiclassical LB method for the UUB-BGK equations based on Grad's moment expansion method by projecting the UUB-BGK equations onto Hermite polynomial basis has been derived. The relations between the relaxation time, viscosity and thermal conductivity are obtained by applying the Chapman-Enskog method [4] to the UUB-BGK equations for providing the basis for determining relaxation time used in the present semiclassical LB method. Hydrodynamics based on moments up to second and third order expansions are presented. Computational examples to illustrate the methods are given and the effects due to quantum statistics are delineated. In the rest of this dissertation, the conventional LB method and quantum LB method will be introduced, then comes the basics of semiclassical LB method which was first proposed in [28].

## 1.2 Conventional LB method

This section will describe the basic algorithm of the LB method. First, an overview of the historical development of LB method including recently developments and reviews will be given. Next, the method itself will be described. Finally, a derivation of the necessary equations and the lattice structures will

be discussed. The conventional LB method originated from its predecessor, the lattice gas cellular automata models [3] has become a competitive numerical tool for simulating fluid flows over a wide range of complex physical problems [2] [29] [30] [31] [32] [33]. The theoretical background of LB method is the kinetic theory and Boltzmann equation, which are connected with the macroscopic Navier-Stokes equation by the Chapman-Enskog expansion. The LB method can be regarded as a simplified kinetic scheme by using a finite set of discrete velocities and a simplified collision integral. Both the algorithm and the boundary conditions are easy to implement in LB method. As the LB method computes macroscopic behavior, such as the motion of a fluid, with equations describing microscopic scales, it operates on a mesoscopic level in between those two extremes. When compared to the traditional computational fluid dynamics techniques, the advantages of LB method are mostly on its clear physics and simple algorithm. While conventional solvers directly discretize the Navier-Stokes equations, the LB method is essentially a first order explicit discretization of the Boltzmann equation in a discrete phase-space. It can also be shown, that the LB method approximates the Navier-Stokes equations with good accuracy. A good review of LB method can be found, e.g., in [6][7][8]. In LB method, the simulation region is divided into a cartesian grid of cells, each of which only interacts with cells in its direct neighborhood. The LB method consists of two steps, the stream step, and the collide step. These are usually combined with no-slip boundary conditions for the domain boundaries or obstacles. The simplicity of the algorithm is especially evident when implementing it. Using a LB method, the particle movement is restricted to a limited number of directions. As shown in Fig. 3.3 and Fig. 3.4, a two-dimensional model with 9 velocities (commonly denoted as D2Q9), and three-dimensional model with 19 velocities (commonly denoted



as D3Q19) are provided.

### 1.3 Basics of Semiclassical LB method

Although Boltzmann Equation has been successfully applied to many field like dilute gas dynamics, multi-scale simulations, however, in recent years, micro and nano technology has been emerged quickly, and the transport phenomena in semiconductors at low temperatures is very important. There have been a successful theory in statistical mechanics which can predict the transport coefficients like shear viscosity and thermal conductivity of ideal quantum fluid such like electrons in the metal. The questions arise of whether quantum systems like that can be described similar to the one developed for the classical counterpart. When solving these kinds of problems, classical Boltzmann Equation is not enough and it require quantum mechanical treatments. In quantum mechanics identical particles are absolutely indistinguishable from one another and N-particle system can be described by a wave function with permutation symmetry. In nature, it is found that particles with antisymmetric wave functions are called fermions which obey FD statistics and particles with symmetric wave functions are called bosons which obey BE statistics. The statistical properties of fermion and boson systems are profoundly different at low temperature. However, in the classical limit, both quantum distributions reduce to the Maxwell-Boltzmann(MB) distribution. Boltzmann equation describes the dynamic behavior of ideal gas by a single-particle distribution function.

In general, there are three strategies to take for statistically treating a quantum system [34]. One is to use a kinetic equation governing the density matrix, another one is to use a kinetic equation with the Wigner distribution

function, the last one, which is also the method used in this thesis, is to assume a semiclassical kinetic equation such as the UUB [21][22] kinetic equation as a generalization of the classical one. In UUB equation, the collision term of the Boltzmann equation is rewritten with the quantum particle scattering form. The equilibrium distribution to semiclassical Boltzmann equation is the BE or FD distributions. The particles obey BE distribution are called bosons and FD distribution for fermions, no third category has yet been found.

Considering of the recently successful developing on LB method and well deriving semiclassical Boltzmann equation, it is natural to extend the conventional LB method to the semiclassical LB method for dealing with different quantum statistics. Although UUB equation introduced above has considered the quantum statistics and would reveal quantum effects in specific problems. However, dealing with UUB equation is still a challenge. In this dissertation, we proposed a new semiclassical LB method which extends well known LB method to solve semiclassical Boltzmann equation with BGK approximation. In [28], a new semiclassical LB-BGK method had been developed, and this method would describe quantum systems in different approaches. The following works about rarefied channel flow [35] and axisymmetric flow of quantum statistics [36] present different applications of this new method. The idea of extending the conventional LB method to semiclassical LB method is to adopt the Grad's moment method to find solutions to semiclassical Boltzmann equation by expanding  $f(\mathbf{x}, \boldsymbol{\zeta}, t)$  in terms of Hermite polynomials. And in simulations, the  $N$ -th finite order truncated distribution function  $f^N$  was considered. the details will be shown in chapter 3.

It is worth mentioning here the differences between the present method and *quantum LB method* which is proposed by Succi and Benzi [37][38]. In the quantum LB method, Dirac equation which is the most general equation de-

describing single particle motion in compliance with quantum theory and special relativity is solved by LB method. In [37], the procedure builds on a formal analogy between the Dirac equation and a special discrete kinetic equation known as LB method, it was then shown that the non-relativistic Schrödinger equation ensues from the Dirac equation under an adiabatic assumption that is formally similar to the one which takes the Boltzmann equation to the Navier-Stokes equations in kinetic theory. In [38], it was further shown that by a proper resort to operator splitting methods, the Dirac equation can be integrated as a sequence of three one dimensional LB equation evolving complex valued distribution function. In these works, LB method with complex distribution function is treated as a numerical tool for solving a complex equation. By using multiscale technique and the Chapman-Enskog expansion on complex variables, the complex partial differential equations could be recovered. Recent years, this procedure is applied for solving many different equations, for examples, the one-dimensional nonlinear Dirac equation[39], the nonlinear convection-diffusion equations in [40] and the complex Ginzburg-Landau equation in [41]. It should be also noticed that several quantum lattice gas cellular automata methods [37][42][43][44] have been recently presented which applying and extending the concept of classical lattice gas cellular automata models to treat the time evolution of wave functions for spinning particles and the Schrödinger equation or the Dirac equation directly. For a more detailed review, see [45]. However, present semiclassical LB method associated with the works presented in [25][26][27] are based on the semiclassical kinetic description. i.e., the particle motion (velocity or momentum) and position are treated in classical mechanics manner while the particles can be of quantum statistics. The procedure and physical meanings are much different.

## 1.4 Contents of the Dissertation

This Dissertation is organized as following.

Chapter 1 gives an overview of this dissertation, briefly describes the basic ideas of semiclassical LB method which combines the elements of semiclassical kinetic theory and LB method. History and recent developments of LB method are also given.

Chapter 2 describes the semiclassical kinetic theory. First, some important concepts of quantum kinetic theory are introduced, then comes the semiclassical Boltzmann equation which has been developed for several years since UUB equation [21][22]. Following the previous works, the corresponding semiclassical hydrodynamic equations are developed and compared with the classical hydrodynamic equations.

In chapter 3, the semiclassical LB method is derived based on expanding the BE and FD equilibrium distribution function onto the Hermite polynomials. The analysis of semiclassical LB method is also given. In chapter 4, the initial condition and the boundary conditions of the semiclassical LB method based on conventional LB method are introduced. Since LB method is a mature fluid simulating method, extending the boundary conditions from conventional LB method to semiclassical LB method is straightforward.

The numerical validation and examples are given in chapter 5, including one dimensional shock tube simulation, two dimensional flow over cylinder, natural convection flow, and three dimensional lid-driven cavity simulation. In chapter 6 the conclusions and future works are given. In Appendix 1, the Chapman-Enskog analysis of semiclassical LB method is given. Finally, a new thermal LB model is proposed for the future development of semiclassical LB method.

# Semiclassical Kinetic Theory

---

## Contents

2.1 Overview . . . . .	9
2.2 Introduction to Quantum Gases . . . . .	10
2.3 Semiclassical Boltzmann Equation(UUB Equation) . . . . .	12
2.4 Semiclassical Hydrodynamic Equations . . . . .	14

---

## 2.1 Overview

In quantum mechanics, the term **semiclassical** has different meanings and all refer to some approximations or situations that combine quantum and classical properties, for example, Wentzel-Kramers-Brillouin(WKB) approximation or UUB equation. In this chapter, from the basic concepts to quantum gases, the collision term of semiclassical Boltzmann equation is derived. Then, the approximation method, BGK method is introduced, and the equilibrium distribution function is proposed based on Boltzmann H theory. Finally, semiclassical hydrodynamic equations are derived from moment integration of the semiclassical Boltzmann equation with BGK approximation and the results are compared with their classical counterparts.

## 2.2 Introduction to Quantum Gases

Comparing with classical mechanics statistics and quantum mechanics statistics, **distinguishability** is a very important concept. In classical mechanics statistics, particles in a system are distinguishable even if they are identical. It is possible to label particles and track their phase space trajectories with certainty. Conversely, in quantum mechanics statistics the precise descriptions of particles motions are limited by Heisenberg uncertainty relation where the simultaneous measurements on momentum and position are not allowed. Under these fuzzy descriptions, the particles become untrackable and the property of **indistinguishability** is inherent. The distinguishable property makes the configuration different and the corresponding microstate distinct as particle interchanges. The number of microstates are usually very large and microstates will continually change as time goes on. The time-average behavior of the system will be identical to the average behavior of all sort microstates corresponding to the macrostates at time  $t$ . The average behaviors on all the collection of microstates in any systems are called ensembles of the systems. In statistical theory, there are three different statistics which are microcanonical ensemble, canonical ensemble and grand canonical ensemble. In canonical ensemble the macrostates are characterized by  $(N, V, T)$ , and the partition function is written as  $Q_N(V, T) = \sum_E e^{-\beta E}$ , wherein  $\beta = 1/k_b T$ . In the ideal quantum gas system, the energy eigenvalues  $E$  are composed of single particle states in occupation set  $\{n_\varepsilon\}$ ,  $\varepsilon$  is the single-particle energy, and  $E$  can be expressed in terms of  $\varepsilon$  as  $E = \sum_\varepsilon n_\varepsilon \varepsilon$ . The values of the numbers  $n_\varepsilon$  must satisfy the condition

$$\sum_\varepsilon n_\varepsilon = N \quad (2.1)$$

According to the discussions of distinguishable property given above, we

can write down the statistical weight factor for FD, BE and MB statistics as:

$$W_{FD}\{n_\varepsilon\} = \begin{cases} 1 & \text{if all } \varepsilon = 0 \text{ or } 1 \\ 0 & \text{otherwise} \end{cases}, \quad (2.2)$$

$$W_{BE}\{n_\varepsilon\} = 1, \quad (2.3)$$

$$W_{MB} = \prod_{\varepsilon} \frac{1}{n_\varepsilon!}. \quad (2.4)$$

We can further write the partition function of a N particle system

$$Q_N(V, T) = \sum'_{\{n_\varepsilon\}} W\{n_\varepsilon\} e^{-\beta \sum_{\varepsilon} n_\varepsilon \varepsilon} \quad (2.5)$$

$\sum'$  means the summation over all distribution sets that satisfies (2.1). To work out the partition function within  $\sum'$  is relatively complicated since the summation is under some constraints. Now substituting (2.3) and (2.2) into (2.5), one has

$$Q_N(V, T) = \sum'_{\{n_\varepsilon\}} e^{-\beta \sum_{\varepsilon} n_\varepsilon \varepsilon}.$$

The differences between BE and FD statistics arises from the values that the number  $n_\varepsilon$  can take. However, the restriction (2.1) makes the canonical ensemble cumbersome here. The grand partition function seems to provide an efficient way

$$\begin{aligned} \vartheta(z, V, T) &\equiv \sum_{N=0}^{\infty} z^N Q_N(V, T) = \sum_{N=0}^{\infty} \left[ \sum'_{\{n_\varepsilon\}} \prod_{\varepsilon} (ze^{-\beta\varepsilon})^{n_\varepsilon} \right] \\ &= \sum_{\{n_0, n_1, \dots\}} (ze^{-\beta\varepsilon_0})^{n_0} (ze^{-\beta\varepsilon_1})^{n_1} (\dots) \\ &= \begin{cases} \prod_{\varepsilon} (1 - ze^{-\beta\varepsilon})^{-1} & \text{BE case, } ze^{-\beta\varepsilon} < 1 \\ \prod_{\varepsilon} (1 + ze^{-\beta\varepsilon}) & \text{FD case} \end{cases} \end{aligned}$$

The average occupation number in state  $\varepsilon$

$$\begin{aligned} \langle n_\varepsilon \rangle &= \frac{1}{\vartheta} \left[ -\frac{1}{\beta} \left( \frac{\partial \vartheta}{\partial \varepsilon} \right)_{z,T,all} \right] \\ &= \frac{1}{z^{-1} e^{\beta \varepsilon} + \eta} \end{aligned}$$

where  $\eta = -1$  for bosons,  $\eta = -1$  for fermions,  $\eta = 0$  for MB gas. It is convenient to define the thermodynamic potential  $q$  to find the average number and energy

$$q(z, V, T) \equiv \ln \vartheta = \frac{PV}{kT} = \eta \sum_{\varepsilon} \ln(1 + \eta z e^{\beta \varepsilon}) \quad (2.6)$$

$$\bar{N} = z \left( \frac{\partial q}{\partial z} \right)_{V,T} = \sum_{\varepsilon} \frac{1}{z^{-1} e^{\beta \varepsilon} + \eta} \quad (2.7)$$

$$\bar{E} = - \left( \frac{\partial q}{\partial \beta} \right)_{z,V} = \sum_{\varepsilon} \frac{\varepsilon}{z^{-1} e^{\beta \varepsilon} + \eta} \quad (2.8)$$

## 2.3 Semiclassical Boltzmann Equation(UUB Equation)

Boltzmann equation is successful in describing dilute classical monatomic gases. People showed the derivation of the Boltzmann equation from the Newtonian of motion for the many particle system under suitable assumptions. Hereinafter, the semiclassical Boltzmann equation (also called UUB equation) is used for describing the flow of fermions and bosons. The generalized Boltzmann equation is

$$\partial_t f + \frac{\mathbf{p}}{m} \cdot \nabla_{\mathbf{x}} f + \mathbf{F} \cdot \nabla_{\xi} f = \mathbf{R}(f), \quad (2.9)$$

where  $\mathbf{F} = m\mathbf{a}$  is the external force. The quantum particles are assumed to obey the streaming mythology like the left hand side of the Boltzmann



equation. It should be emphasized here that the major and only difference between semiclassical Boltzmann equation and classical Boltzmann equation is the collision term  $\mathbf{R}(f)$ . In the classical one, collision term is derived based on classical mechanics [46] while it is derived by quantum scattering theory in the semiclassical one [23]. The collision term for semiclassical Boltzmann equation is described below [21].

$$\begin{aligned} \mathbf{R}(f) = \int d\mathbf{p}_1 \int d\Omega K(\mathbf{p}, \mathbf{p}_1, \Omega) \{ & [1 + \eta f(\mathbf{p}, t)][1 + \eta f(\mathbf{p}_1)]f(\mathbf{p}^*, t)f(\mathbf{p}_1^*, t) \\ & - [1 + \eta f(\mathbf{p}^*, t)][1 + \eta f(\mathbf{p}_1^*)]f(\mathbf{p}, t)f(\mathbf{p}_1, t) \}, \end{aligned} \quad (2.10)$$

where the function  $K$  is the collision kernel,  $\Omega$  is the solid angle.  $\eta = +1$  denotes the case of BE statistics and  $\eta = -1$  denotes the case of FD statistics. We observe that the Pauli exclusion principle is included in the case of fermion and a population factor for boson is included. It is noted that the Boltzmann equation of the classical statistics is included in (2.10) as a special case when  $\eta = 0$ . The population in final state is neglected. This shows the classical collision term can be recovered when considering dilute, non-degenerate classical gases.

Although semiclassical Boltzmann equation has been derived from considering quantum particles collisions, the complexity of the collision term is still a obstacle for computation. One straightforward way to solve this problem is to approximate the complex collision term  $\mathbf{R}(f)$  with BGK approximation  $\frac{f-f^{eq,Q}}{\tau}$  which was first proposed in [12]. BGK approximation makes the direct solution of the BGK-Boltzmann equation tractable. After introducing the BGK approximation, (2.9) could be rewritten as

$$\frac{\partial}{\partial t} f + \boldsymbol{\xi} \cdot \nabla_x f + \mathbf{a} \cdot \nabla_{\boldsymbol{\xi}} f = -\frac{f - f^{eq}}{\tau}. \quad (2.11)$$

In this BGK-Boltzmann equation,  $f^{eq}$  could be quantum equilibrium distribution function  $f^{eq,Q}$  or classical equilibrium distribution function  $f^{eq,C}$ .  $f^{eq}$  means the probability of particles (electrons, phonons, photons, etc...) occupying a specific quantum state in equilibrium, such that, the physical meaning of  $f^{eq}$  is the same as  $\langle n \rangle$  which has been derived in last section. The generalized equilibrium distribution function is

$$f^{eq,Q}(\varepsilon) = \langle n_\varepsilon \rangle = \frac{1}{z^{-1}e^{\beta\varepsilon} + \eta} \quad (2.12)$$

where  $z \equiv e^{-\beta\mu}$  is the fugacity and  $\varepsilon = m(\boldsymbol{\xi} - \mathbf{u})^2/2$  is the energy of particle.

The parameter  $\eta$  determines which statistics  $f^{eq,Q}$  belong to.

## 2.4 Semiclassical Hydrodynamic Equations

The semiclassical hydrodynamic equations are obtained by taking moments  $\psi = [1, m\boldsymbol{\xi}, m\xi^2/2]$  on the semiclassical Boltzmann equation of (2.9) with the collision term (2.10), then integrating the resulting equations over all  $\boldsymbol{\xi}$ .

$$\partial_t \int \psi f d\boldsymbol{\Xi} + \nabla_x \int \psi \boldsymbol{\xi} f d\boldsymbol{\Xi} - \mathbf{a} \int \psi \nabla_{\boldsymbol{\xi}} f d\boldsymbol{\Xi} = \int \mathbf{R}(f) \psi d\boldsymbol{\Xi} \quad (2.13)$$

The integrals of the collision terms in all three cases should preserve the conservation property. That means the conservation of mass, momentum and energy need to be satisfied all the time, which is called the *compatibility condition*,

$$\int \mathbf{R}(f) \psi d\boldsymbol{\Xi} = 0, \quad \psi = \begin{bmatrix} 1 \\ m\boldsymbol{\xi} \\ \frac{1}{2}m(\xi_x^2 + \xi_y^2 + \xi_z^2) \end{bmatrix}, \quad (2.14)$$

where  $d\boldsymbol{\Xi} = m^3 d\boldsymbol{\xi}/h^3$  is the infinitesimal volume in momentum space. We note that the collision in BGK model should also preserve the *compatibility*

condition,

$$\frac{1}{\tau} \int (f - f^{eq}) \psi d\Xi dt = 0, \quad \psi = \begin{bmatrix} 1 \\ \xi_i \\ \frac{1}{2}m(\xi_i^2 + \xi_j^2 + \xi_k^2) \end{bmatrix}. \quad (2.15)$$

The definitions of the number density, number density flux, and energy density are given, respectively, by

$$\begin{aligned} n(\mathbf{x}, t) &= \int f d\Xi, \\ \mathbf{j}(\mathbf{x}, t) &= m \int \boldsymbol{\xi} f d\Xi, \\ E(\mathbf{x}, t) &= m \int \frac{\xi^2}{2} f d\Xi. \end{aligned}$$

Other definitions of higher order moments such as internal energy density  $\varepsilon(\mathbf{x}, t)$ , stress tensor  $P_{ij}(\mathbf{x}, t)$ , heat flux vector  $q_i(\mathbf{x}, t)$  are also given,

$$\begin{aligned} \varepsilon(\mathbf{x}, t) &= \frac{m}{2} \int |\boldsymbol{\xi} - \mathbf{u}|^2 f(\boldsymbol{\xi}, \mathbf{x}, t) d\Xi \\ P_{ij}(\mathbf{x}, t) &= m \int (\xi_i - u_i)(\xi_j - u_j) f(\boldsymbol{\xi}, \mathbf{x}, t) d\Xi \\ q_i(\mathbf{x}, t) &= \frac{m}{2} \int |\boldsymbol{\xi} - \mathbf{u}|^2 (\xi_i - u_i) f(\boldsymbol{\xi}, \mathbf{x}, t) d\Xi. \end{aligned}$$

We can have the familiar form of hydrodynamic equations,

$$\frac{\partial n}{\partial t} + \frac{\partial n u_i}{\partial x_i} = 0 \quad (2.16)$$

$$\rho \frac{d u_i}{d t} + \frac{\partial P_{ij}}{\partial x_j} = \rho a_i \quad (2.17)$$

$$\rho \frac{d \varepsilon}{d t} + P_{ij} \frac{\partial u_i}{\partial x_j} = \frac{\partial q_i}{\partial x_j}, \quad (2.18)$$

where,  $\frac{d}{dt} = \frac{\partial}{\partial t} + u_i \frac{\partial}{\partial x_i}$ . We have briefly described the equilibrium distribution including MB, FD, and BE distributions. The next step is to derive the corresponding hydrodynamic equations under these statistics. Although the

hydrodynamic equations are the same in both classical and semiclassical version, the transport coefficients are different due to the differences between  $f^{eq.Q}$  and  $f^{eq.C}$ . After some straightforward algebraic manipulations, the equation of state of pressure  $p$ , the number density  $n$  and total energies  $E$  in classical and quantum statistics as:

$$\begin{aligned} p_c &= nk_B T \\ n_c &= \frac{z}{\Lambda^3} \\ E_c &= \frac{3}{2}nk_B T + \frac{D}{2}mnu^2, \end{aligned}$$

and

$$\begin{aligned} p_q &= nk_B T \frac{g_{5/2}(z)}{g_{3/2}(z)} \\ n_q &= \frac{g_{3/2}(z)}{\Lambda^3} \\ E_q &= \frac{3}{2}nk_B T \frac{g_{5/2}(z)}{g_{3/2}(z)} + \frac{D}{2}mnu^2. \end{aligned}$$

$g_\nu$  is the generalized FD/BE function which is defined as

$$g_\nu(z) \equiv \frac{1}{\Gamma(\nu)} \int_0^\infty \frac{x^{\nu-1}}{z^{-1}e^x + \eta} dx, \quad (2.19)$$

wherein  $\Gamma(\nu)$  is the Gamma function. Notice that in classical limit,  $g_\nu(z)$  will approach  $z$  no matter what the number  $\nu$  is. We can check that the pressure  $p_q$ , number density  $n_q$  and total energies  $E_q$  will approach the classical counterpart in classical limit. We can also check the specific heat  $\gamma = C_p/C_v$ , in ideal classical gas,  $\gamma_c = 5/3$  for monatomic gas, but  $\gamma_q = \frac{5}{3} \frac{g_{5/2}(z)g_{1/2}(z)}{g_{3/2}^2(z)}$  in ideal quantum gas, which depends on the fugacity  $z$  and not constant. Obviously,  $\gamma_q$  approaches  $\gamma_c$  in classical limit. Moreover, more hydrodynamical

coefficients like viscosity and thermal conductivity are given by

$$\begin{aligned}\mu_q &= \tau n k_B T \frac{g_{5/2}(z)}{g_{3/2}(z)} = \tau P \\ \kappa_q &= \tau \frac{5k_B}{2m} \left[ \frac{7g_{7/2}(z)}{2g_{3/2}(z)} - \frac{5g_{5/2}(z)}{2g_{3/2}^2(z)} \right] n k_B T,\end{aligned}\quad (2.20)$$

and the classical coefficients are also listed for comparing:

$$\begin{aligned}\mu_c &= \tau n k_B T = \tau P \\ \kappa_c &= \tau \frac{5k_B}{2m} n k_B T = \tau \frac{5k_B}{2m} P.\end{aligned}\quad (2.21)$$

All the semiclassical coefficients will approach their classical counterparts and Prandtl number equals 1 in classical coefficients. However, in semiclassical model, the Prandtl number depends on the fugacity  $z$  and is no more a constant number. Similar results could be found in linearized semiclassical Boltzmann equations [23]. Until now, the semiclassical Boltzmann Equation and the semiclassical hydrodynamical equations have been introduced and compared with their classical counterparts. In those descriptions there appears an important parameter  $z$  which is not shown in classical Boltzmann equation or MB statistics. The physical meaning of the fugacity  $z$  is described below: Recall number density in semiclassical representation  $n_q = \frac{g_{3/2}(z)}{\Lambda^3}$ , if we consider  $0 < z < 1$ , then  $g_{3/2}(z) \simeq z$ , we have  $z = n_q (h^2/2\pi m k_B T)^{3/2} = n_q \Lambda^3$ . From this equation,  $z$  can be interpreted as the ratio of  $\Lambda^3$  to average volume occupied by particles. In other words, it is the ratio of occupied length to particles thermal wavelength. When  $z$  is small, it means the order of spatial dimension is larger than the thermal wavelength and we can neglect the degeneracy effect of particles (highly non-degenerate gas). For large  $z$ , the degeneracy effect is important (highly degenerate gas) because the order of thermal wavelength is comparable to the spatial dimension. Moreover, the thermal wavelength is proportional to  $T^{-1/2}$ , that means when the number

density is in normal condition this effect will be obvious especially in the low temperature. In summary, when  $z \rightarrow 0$  the quantum distribution will coincide with the classical one, and the physical explanation is that the length dimension of particle is larger than the particle de Broglie wavelength. The wave property will not be important. When  $z$  is considerably large, two length scales become comparable and one cannot omit the quantum effect anymore. So, we can think the fugacity  $z$  is the index of the degree of degeneracy. The fugacity  $z$  has some restrictions in two different quantum distributions. In the case of Boson,  $z$  should not exceed 1 because of the non-negative density, and in the Fermion case there are no such restrictions on  $z$ .

Finally, the actual correction values of the generalized Fermi function is shown in Fig. 2.1. One finds the BE and FD curves overlap MB curve in  $z \rightarrow 0$  limit, that means the classical statistics could only work in the classical limit ( $z \rightarrow 0$ ) of quantum statistics. Moreover,  $z$  is restricted in  $0 \leq z \leq 1$  for Bose gas, the function  $g_{3/2}(z)$  increases monotonically with  $z$  and is bounded, its largest value being  $g_{3/2}(1) = 2.612$ .

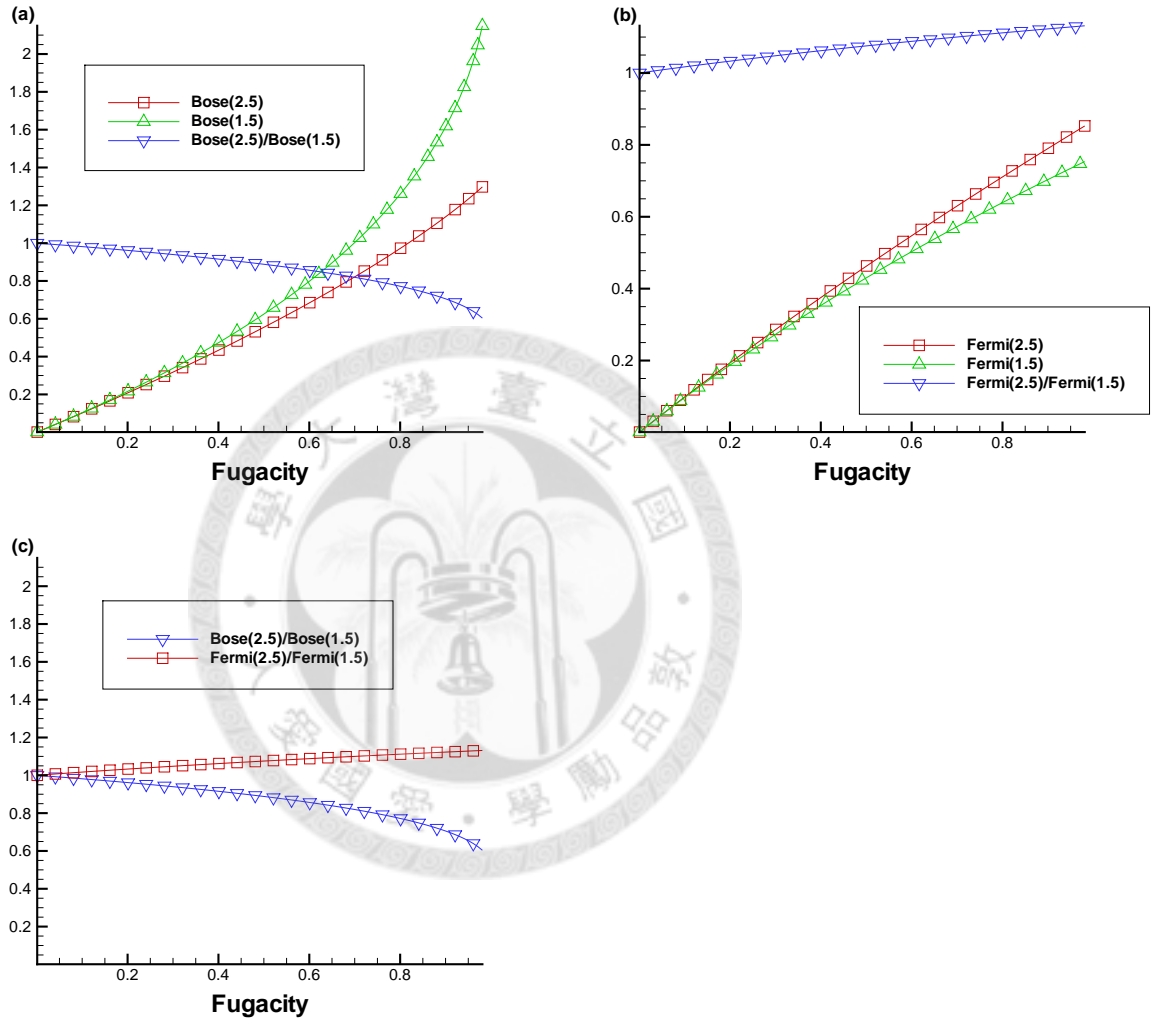


Figure 2.1: Bose and Fermi functions in different fugacity  $z$ . (a) Bose Function  $g_{1.5}^{Bose}(z)$ ,  $g_{2.5}^{Bose}(z)$ , and  $\frac{g_{2.5}^{Bose}(z)}{g_{1.5}^{Bose}(z)}$ , (b) Fermi Function  $g_{1.5}^{Fermi}(z)$ ,  $g_{2.5}^{Fermi}(z)$ , and  $\frac{g_{2.5}^{Fermi}(z)}{g_{1.5}^{Fermi}(z)}$ , (c) Comparing Bose  $\frac{g_{2.5}^{Bose}(z)}{g_{1.5}^{Bose}(z)}$ , and Fermi Function  $\frac{g_{2.5}^{Fermi}(z)}{g_{1.5}^{Fermi}(z)}$





# Semiclassical Lattice Boltzmann Method

---

## Contents

<b>3.1 Overview</b>	<b>21</b>
<b>3.2 The Derivations of Conventional LB method</b>	<b>22</b>
3.2.1 Time Discretization	22
3.2.2 Space and Velocity Discretization	23
<b>3.3 The Derivations of Single Relaxation Time Semiclassical LB method</b>	<b>28</b>
3.3.1 Summary of Single Relaxation Time Semiclassical LB Method	32
<b>3.4 Generalized Semiclassical LB method</b>	<b>35</b>

---

## 3.1 Overview

In this chapter, the semiclassical LB method will be derived from semiclassical Boltzmann equation with BGK approximation (2.11). In general, there are two steps for deriving LB method from the continuous Boltzmann equation. First, the time discretization is achieved by integrating the Boltzmann

equation along characteristic line. Second, the discretization of space is done by low Mach expansion or Hermite polynomials expansion. The derivations of semiclassical LB method is following the Hermite expansion procedures and the results are extended to multiple relaxation time version. The derived equations could be validated by reducing the SLB equation to classical one in classical limit.

## 3.2 The Derivations of Conventional LB method

Just like other numerical methods, discretization of time and space before simulating continuous models or equations on a discrete digital computer is necessary, the detailed procedures are listed below.

### 3.2.1 Time Discretization

Consider the semiclassical Boltzmann equation with BGK approximation (2.11), and neglect the forcing term here:

$$\partial_t f + \boldsymbol{\xi} \cdot \nabla f = \mathbf{R}_{BGK}(f) = -\frac{1}{\tau}[f - f^{eq}] \quad (3.1)$$

Rewrite the Boltzmann BGK Equation (3.1) in the form:

$$D_t f + \frac{1}{\tau} f = \frac{1}{\tau} f^{eq} \quad (3.2)$$

where  $D_t \equiv \partial_t + \boldsymbol{\xi} \cdot \nabla$ . Then, integrating (3.2) over a time step  $\delta_t$  along characteristics:

$$f(\mathbf{x} + \boldsymbol{\xi}\delta_t, \boldsymbol{\xi}, t + \delta_t) = e^{-\delta_t/\tau} f(\mathbf{x}, \boldsymbol{\xi}, t) + \frac{1}{\tau} e^{-\delta_t/\tau} \int_0^{\delta_t} e^{t'/\tau} f^{eq}(\mathbf{x} + \boldsymbol{\xi}\delta_t', \boldsymbol{\xi}, t + \delta_t') dt' \quad (3.3)$$

By using Taylor expansion, and neglecting the high order terms  $O(\delta_t^2)$ , also with  $\tau^* = \tau/\delta_t$ , the standard LB equation is derived as:

$$f(\mathbf{x} + \boldsymbol{\xi}\delta_t, \boldsymbol{\xi}, t + \delta_t) - f(\mathbf{x}, \boldsymbol{\xi}, t) = \mathbf{R}_{BGK}(f) = -\frac{1}{\tau^*}[f(\mathbf{x}, \boldsymbol{\xi}, t) - f^{eq}(\mathbf{x}, \boldsymbol{\xi}, t)], \quad (3.4)$$

This equation indicates the basic procedures of LB method: streaming and collision. Since we have got the time discretization LB equation, the following processes will focus on discretizing the equilibrium distribution function  $f^{eq}(\mathbf{x}, \boldsymbol{\xi}, t)$  on velocity space .

### 3.2.2 Space and Velocity Discretization

In LB method, computational domain is discretized on a regular lattice with fixed grid spacing which makes this method simple. Although original LB method is empirically derived from lattice gas automata, however, modern LB method is derived from continuous Boltzmann equation and has a concrete physical interpretation compared with those come from empirical derivations. The two different approaches to discretizing the computational domain are **low mach number expansion** and **hermite polynomials expansion**. In the following derivations, particles are in high temperature, low density and under classical statistics are assumed. That means, the distribution follows the classical MB statistics. And the MB equilibrium distribution function is:

$$f^{eq,C} = \frac{n}{(2\pi\theta)^{D/2}} \exp\left[-\frac{\mathbf{c}^2}{2\theta}\right] \quad (3.5)$$

wherein  $n$  is the number density,  $D$  is the space dimension,  $\theta = RT$  the temperature and the peculiar velocity  $\mathbf{c} = \boldsymbol{\xi} - \mathbf{u}$ .  $\boldsymbol{\xi}$  is the molecular velocity and  $\mathbf{u}$  the mean velocity. C means classical equilibrium distribution function here.

### 3.2.2.1 Low Mach Number Expansion

Expanding (3.5) by Taylor expansion, we can get the discrete equilibrium distribution function as:

$$f^{eq,C} \approx \frac{n}{(2\pi\theta)^{D/2}} \exp\left(-\frac{\xi^2}{2\theta}\right) \left[1 + \frac{\xi \cdot \mathbf{u}}{\theta} + \frac{(\xi \cdot \mathbf{u})^2}{2\theta^2} - \frac{u^2}{2\theta}\right] \quad (3.6)$$

After choosing some suitable weighting and quadrature points to recover the original moment integration, it will become the frequently used LB model. We use D2Q9 model for example for presenting these procedures. First, we need to discretize the momentum space  $\xi$  properly. The integration is replaced by the summations as:

$$\int \psi(\xi) f^{eq,C}(\mathbf{x}, \xi, t) d\xi = \sum_a W_a \psi(\xi_a) f^{eq,C}(\mathbf{x}, \xi_a, t), \quad (3.7)$$

where  $\psi(\xi)$  is the polynomial of  $\xi$ . Then, the above integral is evaluated by a Gaussian-type quadrature:

$$I = \int \exp\left(-\frac{\xi^2}{2\theta}\right) \psi(\xi) d\xi = \sum_a W_a \exp\left(-\frac{\xi_a^2}{2\theta}\right) \psi(\xi_a), \quad (3.8)$$

A cartesian coordinate system is used to recover the D2Q9 model. Therefore, we set  $\psi(\xi) = \xi_x^m \xi_y^n$ , where  $\xi_x$  and  $\xi_y$  are the  $x$  and  $y$  components of  $\xi$ . Such that, the integrand  $I$  will be

$$I = (\sqrt{\theta})^{(m+n+2)} I_m I_n, \quad (3.9)$$

where  $I_m = \int_{-\infty}^{+\infty} e^{-\varsigma} \varsigma^m d\varsigma$  and  $\varsigma = \xi_x/\sqrt{2\theta}$  or  $\varsigma = \xi_y/\sqrt{2\theta}$ . For D2Q9 model, the third-order Hermite formula for evaluating  $I_m$  is chosen, i.e.  $I_m = \sum_{j=1}^3 \omega_j \varsigma_j^m$ .

The three abscissas of the quadrature are:

$$\begin{aligned} \varsigma_1 &= -\sqrt{3/2} \\ \varsigma_2 &= 0 \\ \varsigma_3 &= \sqrt{3/2}, \end{aligned} \quad (3.10)$$

and the corresponding weight coefficients are:

$$\begin{aligned}\omega_1 &= \sqrt{\pi}/6 \\ \omega_2 &= 2\sqrt{\pi}/3 \\ \omega_3 &= \sqrt{\pi}/6.\end{aligned}\tag{3.11}$$

After this integrating, the equilibrium distribution function of the D2Q9 model is:

$$f_a^{(0),C} = \omega_a n \left[ 1 + \frac{3\xi_a \cdot \mathbf{u}}{c^2} + \frac{9(\xi_a \cdot \mathbf{u})^2}{2c^4} - \frac{3\mathbf{u}^2}{2c^2} \right],\tag{3.12}$$

where  $c = \sqrt{3\theta} \equiv \frac{\delta x}{\delta t}$ .  $\delta x$  is the space between two adjacent lattices. Similarly, other models like D2Q7 and D3Q27 can be derived in a similar manner.

### 3.2.2.2 Hermite Polynomials Expansion

Hermite polynomials expanding of the distribution function for LB method was firstly presented in [17], then well developed in [47] and [16]. This method is inspired by [5], [18] and [48]. The brief descriptions are described below. Following the approaches in [17][16][47], we adopt the Grad's moment approach and seek solutions to (3.4) by expanding  $f(\mathbf{x}, \boldsymbol{\xi}, t)$  in terms of Hermite polynomials,

$$f(\mathbf{x}, \boldsymbol{\xi}, t) = \omega(\boldsymbol{\xi}) \sum_{n=0}^{\infty} \frac{1}{n!} \mathbf{a}^{(n)}(x, t) \mathcal{H}^{(n)}(\boldsymbol{\xi})\tag{3.13}$$

And the expansion coefficients  $\mathbf{a}^{(n)}$  are given by

$$\mathbf{a}^{(n)}(\mathbf{x}, t) = \int f(\mathbf{x}, \boldsymbol{\xi}, t) \mathcal{H}^{(n)}(\boldsymbol{\xi}) d\boldsymbol{\xi}\tag{3.14}$$

where  $\omega(\boldsymbol{\xi}) = \frac{1}{(2\pi)^{3/2}} e^{-\boldsymbol{\xi}^2/2}$  is the weighting function,  $\mathbf{a}^{(n)}$  and  $\mathcal{H}^{(n)}(\boldsymbol{\xi})$  are rank- $n$  tensors and the product on the right-hand side denotes full contraction. Here and throughout the dissertation, the shorthand notations of Grad [5] for fully symmetric tensors have been adopted.

Some of the first few tensor Hermite polynomials are given here,

$$\begin{aligned}\mathcal{H}^{(0)}(\boldsymbol{\xi}) &= 1 \\ \mathcal{H}_i^{(1)}(\boldsymbol{\xi}) &= \xi_i \\ \mathcal{H}_{ij}^{(2)}(\boldsymbol{\xi}) &= \xi_i \xi_j - \delta_{ij} \\ \mathcal{H}_{ijk}^{(3)}(\boldsymbol{\xi}) &= \xi_i \xi_j \xi_k - \xi_i \delta_{jk} - \xi_j \delta_{ik} - \xi_k \delta_{ij}\end{aligned}$$

The first few expansion coefficients can be easily identified with the familiar hydrodynamic variables:

$$\begin{aligned}\mathbf{a}^{(0)} &= \int f d\boldsymbol{\xi} = n \\ \mathbf{a}^{(1)} &= \int f \boldsymbol{\xi} d\boldsymbol{\xi} = n\mathbf{u} \\ \mathbf{a}^{(2)} &= \int f(\boldsymbol{\xi}^2 - \delta) d\boldsymbol{\xi} = \mathbf{P} + n(\mathbf{u}^2 - \delta) \\ \mathbf{a}^{(3)} &= \int f(\boldsymbol{\xi}^3 - \boldsymbol{\xi}\delta) d\boldsymbol{\xi} = \mathbf{Q} + \mathbf{u}(\mathbf{a}^{(2)} - 2n\mathbf{u}^2)\end{aligned}\quad (3.15)$$

Where the momentum flux tensor is defined as  $\mathbf{P} = P_{ij} \equiv \int f c_i c_j d\mathbf{c}$ , the heat flux tensor is defined as  $\mathbf{Q} = g_{ijk} \equiv \int f c_i c_j c_k d\mathbf{c}$ , and We also have  $\varepsilon = \frac{1}{2}[\mathbf{a}_{ii}^{(2)} - n(\mathbf{u}\mathbf{u} - 3)]$ . The orthogonality of Hermite polynomials implies that the leading moments of a distribution function up to the  $N$ th order are preserved by truncations of the higher-order terms in its Hermite expansion. Thus, a distribution function of the Boltzmann-BGK equation can be approximated by its projection onto a Hilbert space spanned by the first  $N$  Hermite polynomials without affecting the first  $N$  moments. Here, up to  $N$ th order,  $f^N(\mathbf{x}, \boldsymbol{\xi}, t)$  has exactly the same velocity moments as the original  $f(\mathbf{x}, \boldsymbol{\xi}, t)$  does. This guaranties that a LB method gas dynamic system can be constructed by a finite set of macroscopic variables. As a partial sum of Hermite series with finite terms, the truncated distribution function  $f^N$  can be completely and uniquely determined by its values at a set of discrete abscissae in the velocity

space. This is possible because with  $f$  truncated to order  $N$ , the integrand on the right-hand side of (3.14) can be expressed as:

$$f^N(\mathbf{x}, \boldsymbol{\xi}, t) \mathcal{H}^{(n)}(\boldsymbol{\xi}) = \omega(\boldsymbol{\xi}) q(\mathbf{x}, \boldsymbol{\xi}, t) \quad (3.16)$$

where  $q(\mathbf{x}, \boldsymbol{\xi}, t)$  is a polynomial in  $\boldsymbol{\xi}$  of a degree no greater than  $2N$ . Using the Gauss-Hermite quadrature,  $\mathbf{a}^{(n)}$  can be precisely calculated as a weighted sum of functional values of  $q(\mathbf{x}, \boldsymbol{\xi}, t)$ :

$$\begin{aligned} \mathbf{a}^{(n)}(\mathbf{x}, t) &= \int_{-\infty}^{\infty} \omega(\boldsymbol{\xi}) q(\mathbf{x}, \boldsymbol{\xi}, t) d\boldsymbol{\xi} = \sum_1^l w_a q(\mathbf{x}, \boldsymbol{\xi}_a, t) \\ &= \sum_1^l \frac{w_a}{\omega(\boldsymbol{\xi}_a)} f^N(\mathbf{x}, \boldsymbol{\xi}_a, t) \mathcal{H}^{(n)}(\boldsymbol{\xi}_a), \end{aligned} \quad (3.17)$$

where  $w_a$  and  $\boldsymbol{\xi}_a, a = 1, \dots, l$ , are, respectively, the weights and abscissae of a Gauss-Hermite quadrature of degree  $\geq 2N$ . Thus,  $f^N$  is completely determined by the set of discrete functional values,  $f^N(\mathbf{x}, \boldsymbol{\xi}_a, t); a = 1, \dots, l$ , and therefore its first  $N$  velocity moments, and vice versa. The set of discrete distribution functions  $f^N(\mathbf{x}, \boldsymbol{\xi}_a, t)$  now serve as a new set of fundamental variables (in physical space) for defining the fluid system in place of the conventional hydrodynamic variables.

Next, we expand the equilibrium distribution  $f^{eq,C}$  in the Hermite polynomial basis to the same order as  $f^N$ , i.e.,  $f^{eq,C}(\mathbf{x}, \boldsymbol{\xi}, t) \approx f^{(0),C,N}(\mathbf{x}, \boldsymbol{\xi}, t)$ , and we have

$$f^{(0),C,N}(\mathbf{x}, \boldsymbol{\xi}, t) = \omega(\boldsymbol{\xi}) \sum_{n=0}^N \frac{1}{n!} \mathbf{a}_0^{(n)}(\mathbf{x}, t) \cdot \mathcal{H}^{(n)}(\boldsymbol{\xi}) \quad (3.18)$$

$$\mathbf{a}_0^{(n)}(\mathbf{x}, t) = \int f^{eq,C}(\mathbf{x}, \boldsymbol{\xi}, t) \mathcal{H}^{(n)}(\boldsymbol{\xi}) d\boldsymbol{\xi} \quad (3.19)$$

These coefficients  $\mathbf{a}_0^{(n)}$  can be evaluated exactly and we have

$$\begin{aligned}\mathbf{a}_0^{(0)} &= n, \quad \mathbf{a}_0^{(1)} = n\mathbf{u}, \\ \mathbf{a}_0^{(2)} &= n[\mathbf{u}\mathbf{u} + (\theta - 1)\delta], \\ \mathbf{a}_0^{(3)} &= n[\mathbf{u}\mathbf{u}\mathbf{u} + (\theta - 1)\delta\mathbf{u}]\end{aligned}\quad (3.20)$$

where  $n, \mathbf{u}$  and  $\theta$  are in non-dimensional form hereinafter.

Denote  $f_a^{(0),C} \equiv w_a f^{eq,C}(\boldsymbol{\xi}_a)/\omega(\boldsymbol{\xi}_a)$  and for  $N = 3$ , we get the explicit Hermite expansion of the MB distribution at the discrete velocity  $\boldsymbol{\xi}_a$  as:

$$\begin{aligned}f_a^{(0),C,3} &= w_a n \left\{ 1 + \boldsymbol{\xi}_a \cdot \mathbf{u} + \frac{1}{2} [(\mathbf{u} \cdot \boldsymbol{\xi}_a)^2 - u^2 + (\theta - 1)(\boldsymbol{\xi}_a^2 - D)] \right. \\ &\quad \left. + \frac{\boldsymbol{\xi}_a \cdot \mathbf{u}}{6} [(\mathbf{u} \cdot \boldsymbol{\xi}_a)^2 - 3u^2 + 3(\theta - 1)(\boldsymbol{\xi}_a^2 - D - 2)] \right\}.\end{aligned}\quad (3.21)$$

where  $D = \delta_{ii}$ . We could check if  $\theta = 1$  which means isothermal here. Then (3.21) up to second order will be as the same as (3.6).

### 3.3 The Derivations of Single Relaxation Time Semiclassical LB method

The left hand side of UUB-BGK equation is as the same as the conventional Boltzmann-BGK equation (3.1). The only difference of this two equation is the equilibrium distribution function on the right hand side, that means, the classical equilibrium distribution function  $f^{eq,C}$  (3.5) is replaced by the quantum equilibrium distribution function  $f^{eq,Q}$  (3.22) in UUB-BGK equation. The quantum equilibrium distribution function which includes BE equilibrium distribution function and FD equilibrium distribution function has been derived as (2.12) and rewritten here as:

$$f^{eq,Q} = \left\{ z^{-1} \exp\left[\frac{(\boldsymbol{\xi} - \mathbf{u})^2}{2\theta}\right] - \eta \right\}^{-1}, \quad (3.22)$$



### 3.3. The Derivations of Single Relaxation Time Semiclassical LB method 29

First, The macroscopic variables is defined as

$$\Phi(\mathbf{x}, t) = \int \frac{m^3 d\boldsymbol{\xi}}{h^3} \phi f. \quad (3.23)$$

For examples, the number density

$$n(\mathbf{r}, t) = \int_{-\infty}^{\infty} \frac{m^3 d\boldsymbol{\xi}}{h^3} f^{eq,Q} = \frac{1}{\Lambda^3} g_{3/2}(z) \quad (3.24)$$

the pressure is

$$p(\mathbf{x}, t) \equiv P_{ii}/3 = 2\varepsilon/3 = \frac{k_B T}{\Lambda^3} g_{5/2}(z) \quad (3.25)$$

wherein,  $\Lambda = [h^2/2\pi m^2 \theta]^{1/2}$  is the de Broglie thermal wavelength,  $g_\nu$  the generalized FD/BE function which has been defined in Ch2 (2.19) together with the calculation approximations is listed as

$$g_\nu(z) \equiv \frac{1}{\Gamma(\nu)} \int_0^\infty \frac{x^{\nu-1}}{z^{-1}e^x + \eta} dx = \sum_{l=1}^{\infty} (-\eta)^{l-1} \frac{z^l}{l^\nu}. \quad (3.26)$$

Notice that the series is valid only when  $z < 1$ . In deriving semiclassical LB method, the particle velocity dimension  $d$  and space dimension  $D$  do not need to be the same, such that we could have the more generalized results. Following the same procedures applied to classical gases in [16] and already briefly described above, defining  $\boldsymbol{\zeta} = \frac{m^d \boldsymbol{\xi}}{h^d}$ , and  $d\boldsymbol{\zeta} = m^d d\boldsymbol{\xi}/h^d$ , such that the coefficients  $a_0^{(n)}$  which is defined as (3.14) of the semiclassical expansion can be calculated as

$$\begin{aligned} a_0^{(0)} &= \frac{g_{d/2}}{\Lambda^d} = n \\ a_0^{(1)} &= n\mathbf{u} \\ a_0^{(2)} &= n[\mathbf{u}\mathbf{u} + \frac{d}{D}\theta \frac{g_{d/2+1}}{g_{d/2}} \hat{\boldsymbol{\delta}} - \boldsymbol{\delta}] \\ a_0^{(3)} &= n[\mathbf{u}\mathbf{u}\mathbf{u} + (\frac{d}{D}\theta \frac{g_{d/2+1}}{g_{d/2}} \hat{\boldsymbol{\delta}} - \boldsymbol{\delta})\mathbf{u}]. \end{aligned} \quad (3.27)$$

Notice that the coefficients  $a_0^{(N)}$  here is not yet non-dimensional, and  $\boldsymbol{\delta}$  has the same dimension as  $\mathbf{u}\mathbf{u}$ ,  $\hat{\boldsymbol{\delta}}$  represents delta without dimension. To nondi-

dimensionalize those coefficients we choose some reference variables as:

$$\Lambda_{ref} = \frac{h}{m(2\pi\theta_{ref})^{\frac{1}{2}}} \quad (3.28)$$

$$u_{ref} = \sqrt{\theta_{ref}} \quad (3.29)$$

$$n_{ref} = \frac{1}{\Lambda_{ref}^d} \quad (3.30)$$

$$\hat{\theta} = \frac{\theta}{\theta_{ref}}, \quad (3.31)$$

and notice the non-dimensional coefficients are:

$$\begin{aligned} \hat{a}_0^{(0)} &= \frac{a_0^{(0)}}{n_{ref}} \\ \hat{a}_0^{(1)} &= \frac{a_0^{(1)}}{n_{ref}u_{ref}} \\ \hat{a}_0^{(2)} &= \frac{a_0^{(2)}}{n_{ref}u_{ref}^2} \\ \hat{a}_0^{(3)} &= \frac{a_0^{(3)}}{n_{ref}u_{ref}^3}. \end{aligned} \quad (3.32)$$

Combine (3.27) and (3.32), the non-dimensional coefficients are derived as below:

$a_0^{(0)}$ :

$$\begin{aligned} a_0^{(0)} &= \frac{g_{d/2}}{\Lambda^d} = n \\ \hat{a}_0^{(0)} \cdot n_{ref} &= \frac{g_{d/2}}{\Lambda^d} = \hat{n} \cdot n_{ref} \\ \hat{a}_0^{(0)} &= \frac{\Lambda_{ref}^d g_{d/2}}{\Lambda^d} = \hat{n} \\ \hat{a}_0^{(0)} &= \hat{\theta}^{d/2} g_{d/2} \end{aligned} \quad (3.33)$$

$a_0^{(1)}$ :

$$\begin{aligned} a_0^{(1)} &= nu \\ \hat{a}_0^{(1)} \cdot n_{ref}u_{ref} &= \hat{n} \cdot n_{ref}\hat{\mathbf{u}} \cdot u_{ref} \\ \hat{a}_0^{(1)} &= \hat{n}\hat{\mathbf{u}} \end{aligned} \quad (3.34)$$

$a_0^{(2)}$ :

$$\begin{aligned}
 a_0^{(2)} &= n\left[\frac{d}{D}\theta\frac{g_{d/2+1}}{g_{d/2}}\hat{\delta} - \delta\right] + n\mathbf{u}\mathbf{u} \\
 \hat{a}_0^{(2)} \cdot n_{ref}u_{ref}^2 &= \hat{n} \cdot n_{ref}\left[\frac{d}{D}\hat{\theta} \cdot u_{ref}^2\frac{g_{d/2+1}}{g_{d/2}}\hat{\delta} - \hat{\delta} \cdot u_{ref}^2\right] + \hat{n}\hat{\mathbf{u}}\hat{\mathbf{u}} \cdot n_{ref}u_{ref}^2 \\
 \hat{a}_0^{(2)} &= \hat{n}\left[\frac{d}{D}\hat{\theta}\frac{g_{d/2+1}}{g_{d/2}} - 1\right]\hat{\delta} + \hat{n}\hat{\mathbf{u}}\hat{\mathbf{u}}
 \end{aligned} \tag{3.35}$$

$a_0^{(3)}$ :

$$\hat{a}_0^{(3)} = \hat{n}[\hat{\mathbf{u}}\hat{\mathbf{u}}\hat{\mathbf{u}} + \left(\frac{d}{D}\hat{\theta}\frac{g_{d/2+1}}{g_{d/2}} - 1\right)\hat{\delta}\hat{\mathbf{u}}] \tag{3.36}$$

Finally, we take off  $\hat{\cdot}$  on every variables and all the non-dimensional coefficients are listed as:

$$\begin{aligned}
 a_0^{(0)} &= \theta^{d/2}g_{d/2} = n \\
 a_0^{(1)} &= n\mathbf{u} \\
 a_0^{(2)} &= n\left[\frac{d}{D}\theta\frac{g_{d/2+1}}{g_{d/2}} - 1\right]\delta + n\mathbf{u}\mathbf{u} \\
 a_0^{(3)} &= n[\mathbf{u}\mathbf{u}\mathbf{u} + \left(\frac{d}{D}\theta\frac{g_{d/2+1}}{g_{d/2}} - 1\right)\delta\mathbf{u}]
 \end{aligned} \tag{3.37}$$

Put (3.37) into (3.13) and notice the variable  $\xi$  has been replaced by  $\zeta$  now, we can get the expansion of the quantum equilibrium distribution function.

$$\begin{aligned}
 f_a^{(0),Q,3} &= \omega_a n \left\{ 1 + \zeta_a \cdot \mathbf{u} + \frac{1}{2} [(\zeta_a \cdot \mathbf{u})^2 - u^2 + \frac{d}{D}\theta\frac{g_{\frac{d}{2}+1}}{g_{\frac{d}{2}-1}}(\zeta_a^2 - D)] \right. \\
 &\quad \left. + \frac{\zeta_a \cdot \mathbf{u}}{6} [(\zeta_a \cdot \mathbf{u})^2 - 3u^2 + 3\left(\frac{d}{D}\theta\frac{g_{\frac{d}{2}+1}}{g_{\frac{d}{2}-1}\right)}(\zeta_a^2 - D - 2)] \right\}.
 \end{aligned} \tag{3.38}$$

To validate this result, we note that in classical limit  $z \ll 1$ , the generalized FD function  $g_\nu(z)$  will approximately equal  $z$  no matter what the order  $\nu$  is. That means,  $\frac{g_{d/2+1}(z)}{g_{d/2}(z)} = 1$  in (3.38), such that, the semiclassical equilibrium

distribution function (3.38) in classical limit will become

$$(3.38)^{In\_Classical\_Limit} = \omega_a n \{1 + \boldsymbol{\zeta}_a \cdot \mathbf{u} + \frac{1}{2} [(\boldsymbol{\zeta}_a \cdot \mathbf{u})^2 - u^2 + \frac{d}{D} \theta (\boldsymbol{\zeta}_a^2 - D)] + \frac{\boldsymbol{\zeta}_a \cdot \mathbf{u}}{6} [(\boldsymbol{\zeta}_a \cdot \mathbf{u})^2 - 3u^2 + 3(\frac{d}{D} \theta) (\boldsymbol{\zeta}_a^2 - D - 2)]\}. \quad (3.39)$$

Comparing this result with (3.21), when  $d$  equals  $D$ , (3.21) and (3.39) are the same in the classical limit.

### 3.3.1 Summary of Single Relaxation Time Semiclassical LB Method

Once we have obtained  $f^N$  and  $f^{eq,Q,N}$  at the discrete velocity abscissae  $\boldsymbol{\zeta}_a$ , we are ready to set up the whole system for solving (3.1) in the physical configuration space. We use (3.4) for solving (3.1) in the following simulations. For clearly (3.4) is listed below.

$$f_a(\mathbf{x} + \boldsymbol{\zeta}_a, t + 1) - f_a(\mathbf{x}, t) = -\frac{1}{\tau} [f_a - f_a^{(0),Q}]. \quad (3.40)$$

where  $f_a^{(0),Q}$  is given by (3.38) and  $\tau$  could be calculated from (2.20). Applying Gauss-Hermite quadrature to the moment integration, we have the macroscopic quantities, the number density, number density flux, and energy density. And the macroscopic variables become:

$$\begin{aligned} n(\mathbf{x}, t) &= \sum_{a=1}^l f_a(\mathbf{x}, t), \\ n\mathbf{u} &= \sum_{a=1}^l f_a \boldsymbol{\zeta}_a, \\ n(D\theta \frac{g_{5/2}(z)}{g_{3/2}(z)} + u^2) &= \sum_{a=1}^l f_a \boldsymbol{\zeta}_a^2. \end{aligned} \quad (3.41)$$

In summary, (3.40) and (3.41) form a closed set of differential equations governing the set of variables  $f_a(\mathbf{x}, t)$  in the physical configuration space. All the

macroscopic variables and their fluxes can be calculated directly from their corresponding moment summations.

We should note that there appears the fugacity  $z$  in this semiclassical LB method that not shown in classical LB method, such that, we need some additional procedures to calculate the fugacity  $z$ . The detail calculating procedures are shown below. First, the density can be calculated as

$$\sum_a f_a = n \tag{3.42}$$

and the velocity is calculated as

$$\sum_a f_a \zeta_a = n \mathbf{u}_a \tag{3.43}$$

Then, recall the two formulas:

$$n = \theta^{d/2} g_{d/2} \tag{3.44}$$

$$\sum_a f_a \zeta_a^2 = nd\theta \frac{g_{d/2+1}}{g_{d/2}} + nu^2 = 2E, \tag{3.45}$$

where  $E$  is the total energy. Combining (3.44) and (3.45), we can get

$$2E - d\left(\frac{n}{g_{d/2}}\right)^{\frac{2+d}{d}} g_{d/2+1} - nu^2 = 0 \tag{3.46}$$

By solving(3.46) with Newton method, we can get the fugacity  $z$ . then we can get temperature  $\theta$  from (3.44). Since the derivation is based on expanding distribution function  $f$  onto Hermite polynomials as [16], the lattices and corresponding weights listed in [16] also could be used. The D2Q9 lattice model for two dimensional flow and D3Q19 lattice model for three dimensional flow are listed in Fig. 3.3, Table 3.2 and Fig. 3.4, Table 3.3. The subscript  $fs$  denotes a fully symmetric set of points.

The present semiclassical LB method is derived from expanding distribution function onto Hermite polynomials. The accuracy of semiclassical LB method should be carefully discussed. According to [16], the second order  $N = 2$  kinetic theory of hydrodynamics is necessary for representing  $n, u, \theta$  and the momentum flux tensor  $P$ . On the other hand, to describe the dynamics of the internal energy of a fluid system, the third-order  $N = 3$  Hermite terms must be retained. The most important principle we should notice is that the higher order  $N$  we expand the equilibrium distribution function  $f$ , the higher quadrature degree  $n$  of lattice structure we should use. The relation between them is  $n \geq 2N$ . Such that, an accurate Navier-Stokes level of description for an isothermal momentum equation requires a quadrature of a degree of precision greater than 6. And we should include the Hermite expansion up to  $N \geq 4$ , and the quadrature degree up to  $n \geq 8$  to ensure accuracy up to the Burnett order for isothermal fluids. See the details in [16]. Since the semiclassical LB method is also derived from expanding the equilibrium distribution function onto Hermite polynomials, the principle of  $n \geq 2N$  may be followed. But, we can not forget in deriving both classical LB method and semiclassical LB method, there are still higher order terms have been drop off, and the total influences of different order method are worth studying. A two dimensional cylinder flow is considered here for studying this issue of accuracy. we consider a uniform two-dimensional viscous flow over a circular cylinder in a BE quantum gas to illustrate the present semiclassical LB method in different order on D2Q9 lattices.  $N = 2$  and  $N = 3$  expansion equations are both set for this case. The computation domain is  $(-1, 1) \times (-1, 1)$  and set by  $201 \times 201$  lattices, and the cylinder is set at the center of the computation domain with the radius  $D = 0.1$ . Uniform Cartesian grid system is used. The free stream velocity is  $u_\infty = 0.1$ , free stream temperature  $\theta_\infty = 0.5$

and the Reynolds number  $Re_\infty = u_\infty D/\nu$ . Notice according to the relation  $n \geq 2N$ , the D2Q9 lattices with quadrature degree 5 suppose to be only used on  $N = 2$  but not  $N = 3$ . The results are depicted in Fig. 3.1, the vortices in the wake region in both cases are clearly shown. The differences of the streamline pattern is not easy to delineate. However, in [16], the accuracy of different quadrature degree is validated by shear decay simulations.

### 3.4 Generalized Semiclassical LB method

Numerical stability and dispersion are important issues in numerical simulations. The semiclassical LB method derived above is based on the BGK model which involves the single relaxation time approximation. The single relaxation time semiclassical LB method-BGK equation should have the same deficits as the classical counterpart such like numerical instability and the fixed Prandtl number which is unity. To overcome the LB method-BGK deficiencies. The generalized LB method [49] which is also called multiple relaxation time LB method has been proposed and examined recently by [50]. The generalized LB method is of better numerical stability and has attract much attention in recent years. Its basic idea is that in the single relaxation time LB method, the bulk and shear viscosities are both determined by the same relaxation time  $\tau$ . In another way, the generalized LB method use several relaxation times to relax different modes such that the bulk and shear viscosities could be adjusted independently. Consequently, the stability and dispersion could be tuned into a better situation. In this section, the single relaxation time semiclassical LB method derived above is extended to the generalized semiclassical LB method. The derivations of generalized semiclassical LB method is based on the steps in [51] and [52]. At first, consider the equation (3.4), We expand distribution

function on Hermite polynomials, namely, the following finite expansion for  $f$ :

$$f(\mathbf{x}, \boldsymbol{\xi}, t) = \sum_{n=0}^N \frac{1}{n!} \mathbf{a}^{(n)}(x, t) \mathcal{H}^{(n)}(\boldsymbol{\xi}). \quad (3.47)$$

The Hermite coefficients of  $f$  and  $f^{eq}$  are noted by  $a^{(n)}$  and  $a_0^{(n)}$  respectively. Due to the conservation laws,  $\mathbf{a}^{(0)} = \mathbf{a}_0^{(0)}$ ,  $\mathbf{a}^{(1)} = \mathbf{a}_0^{(1)}$  and  $Tr(\mathbf{a}^{(2)}) = Tr(\mathbf{a}_0^{(2)})$ , where  $Tr$  denotes the trace of the second order tensors. The BGK collision model can be written as:

$$\mathbf{R}_{BGK}(f) = -\frac{1}{\tau} \sum_{n=2}^N \frac{1}{n!} [\mathbf{a}^{(n)} - \mathbf{a}_0^{(n)}] \mathcal{H}^{(n)}. \quad (3.48)$$

Assumes that relaxation time is different from different order expansions.

$$\mathbf{R}_{BGK}(f) = -\sum_{n=2}^N \frac{1}{\tau_n n!} [\mathbf{a}^{(n)} - \mathbf{a}_0^{(n)}] \mathcal{H}^{(n)}, \quad (3.49)$$

and integrating (3.1) over  $\mathbf{c}d\mathbf{c}$

$$\int \left( \frac{\partial f}{\partial t} + \boldsymbol{\xi} \cdot \delta f \right) \mathbf{c}d\mathbf{c} = -\sum_{n=2}^N \frac{1}{\tau_n n!} [\mathbf{a}^{(n)} - \mathbf{a}_0^{(n)}] \mathcal{H}^{(n)} \int \mathcal{H}^{(n)} \mathbf{c}d\mathbf{c}. \quad (3.50)$$

Noticing that  $\mathbf{c}\mathbf{c} = \mathcal{H}^{(2)}(\boldsymbol{\xi}) - \mathbf{u}\mathcal{H}^{(1)}(\boldsymbol{\xi}) + \mathbf{u}\mathbf{u} + \boldsymbol{\delta}$ , the right hand side is simply

$$-\frac{1}{\tau_2} [\mathbf{a}^{(2)} - \mathbf{a}_0^{(2)}]. \quad (3.51)$$

That means,

$$\mathbf{a}^{(2)} - \mathbf{a}_0^{(2)} = -\tau_2 \int \left( \frac{\partial f}{\partial t} + \boldsymbol{\xi} \cdot \delta f \right) \mathbf{c}d\mathbf{c}. \quad (3.52)$$

Since we already have  $\mathbf{a}_0^{(2)}$  in previous procedures, what we should do now is to calculate  $\mathbf{a}^{(2)}$ . The first step to get  $\mathbf{a}^{(2)}$  is from continuity equation and momentum equation which could be easily got by integrating the governing equation (3.1). In the following derivations, Einstein summation convention



is used for convenience.

$$\partial_t n + \partial_i(nu_i) = 0 \quad (3.53)$$

$$\partial_t(nu_i) + \partial_j(nu_i u_j) = -\partial_i(n\theta). \quad (3.54)$$

Then, summing (3.53) and (3.54),

$$\partial_t u_i + u_j \partial_j u_i = \frac{-1}{n} \partial_i(n\theta). \quad (3.55)$$

Calculating  $\partial_t(\int f^{eq,Q} \xi_i \xi_j)$  and  $\partial_k \int f^{eq,Q} \xi_i \xi_j \xi_k$ :

$$\begin{aligned} \partial_t(\int f^{eq,Q} \xi_i \xi_j) &= \partial_t(nu_i u_j + n\theta \frac{g_{d/2}}{g_{d/2+1}} \delta_{ij}) \\ &= \partial_t(nu_i)u_j + nu_i \partial_t u_j + \theta \frac{g_{d/2}}{g_{d/2+1}} \delta_{ij} \partial_t n + n \delta_{ij} \partial_t \theta \frac{g_{d/2}}{g_{d/2+1}} \\ &= -\partial_k(nu_i u_j)u_j - \partial_i(n\theta \frac{g_{d/2}}{g_{d/2+1}})u_j - nu_i u_j \partial_k u_j - u_i \partial_j(n\theta \frac{g_{d/2}}{g_{d/2+1}}) \\ &\quad - \partial_k(nu_k) \theta \frac{g_{d/2}}{g_{d/2+1}} \delta_{ij} - nu_k \partial_k(\theta \frac{g_{d/2}}{g_{d/2+1}} \delta_{ij}) - \frac{2}{3} n \partial_k u_k \theta \frac{g_{d/2}}{g_{d/2+1}} \\ &= -\partial_k(nu_i u_j u_k) - \partial_j(n\theta \frac{g_{d/2}}{g_{d/2+1}})u_i - \partial_i(n\theta \frac{g_{d/2}}{g_{d/2+1}})u_j - \partial_k(n\theta \frac{g_{d/2}}{g_{d/2+1}} u_k) \delta_{ij} \\ &\quad - \frac{2}{3} n \theta \frac{g_{d/2}}{g_{d/2+1}} \partial_k u_k \end{aligned} \quad (3.56)$$

$$\partial_k \int f^{eq,Q} \xi_i \xi_j \xi_k = \partial_j(n\theta \frac{g_{d/2}}{g_{d/2+1}} u_i) + \partial_i(n\theta \frac{g_{d/2}}{g_{d/2+1}} u_j) + \partial_k(n\theta \frac{g_{d/2}}{g_{d/2+1}} u_k) \delta_{ij} + \partial_k(nu_i u_j u_k) \quad (3.57)$$

Summing (3.56) and (3.57):

$$n\theta \frac{g_{d/2}}{g_{d/2+1}} (\partial_i u_j + \partial_j u_i) - \frac{2}{3} n \theta \frac{g_{d/2}}{g_{d/2+1}} \partial_k u_k = n\theta \frac{g_{d/2}}{g_{d/2+1}} \Lambda_{ij}. \quad (3.58)$$

Recall  $a_0^{(2)} = n\theta \frac{g_{d/2}}{g_{d/2+1}} \delta_{ij}$  such that, the overall momentum stress tensor is derived as:

$$P_{ij} \equiv \int f c_i c_j dc = n\theta \frac{g_{d/2}}{g_{d/2+1}} \delta_{ij} - \tau_2 n \theta \frac{g_{d/2}}{g_{d/2+1}} \Lambda_{ij} \quad (3.59)$$

After getting the stress tensor, we need to calculate the conduction coefficient along with an additional relaxation time. In the similar steps, we calculate  $\int [\frac{\partial f^{eq,Q}}{\partial t} + \boldsymbol{\xi} \cdot \nabla f^{eq,Q}] \mathbf{c} \cdot \mathbf{c}^2 d\mathbf{c}$ . First, the zeroth order energy conservation equation is derived from integrating (3.1)  $\times c^2$  over  $\boldsymbol{\xi}$

$$3\partial_t(n\theta \frac{g_{d/2}}{g_{d/2+1}}) + \partial_i \int f \xi_i c^2 d\boldsymbol{\xi} + 2n\theta \frac{g_{d/2}}{g_{d/2+1}} \partial_i u_i + O(\partial^2) = 0 \quad (3.60)$$

and notice that

$$\int f \xi_i c^2 d\boldsymbol{\xi} = \int f^{eq,Q} \xi_i c^2 d\boldsymbol{\xi} = 3n\theta \frac{g_{d/2}}{g_{d/2+1}} u_i + O(\partial^2) \quad (3.61)$$

combine (3.60) with (3.53) and (3.61)

$$\partial_t \theta \frac{g_{d/2}}{g_{d/2+1}} + u_i \partial_i \theta \frac{g_{d/2}}{g_{d/2+1}} = -\frac{2}{3} \partial_i u_i \theta \frac{g_{d/2}}{g_{d/2+1}} + O(\partial^2) \quad (3.62)$$

$$\begin{aligned} \int \partial_t f^{eq,Q} \xi_i (\xi - u)^2 d\boldsymbol{\xi} &= \partial_t \int f^{eq,Q} \xi_i (\xi - u)^2 + 2 \int f^{eq,Q} \xi_i (\xi_k - u_k) \partial_t u_k \\ &= \partial_t (3n\theta \frac{g_{d/2}}{g_{d/2+1}} u_i) + 2n\theta \frac{g_{d/2}}{g_{d/2+1}} \partial_t u_i \\ &= 3\theta \frac{g_{d/2}}{g_{d/2+1}} [-\partial_j (n u_i u_j) - \partial_i (n\theta \frac{g_{d/2}}{g_{d/2+1}})] + 3n u_i (-u_j \partial_j \theta \frac{g_{d/2}}{g_{d/2+1}} - \frac{2}{3} \partial_j u_j \theta \frac{g_{d/2}}{g_{d/2+1}}) \\ &\quad + 2n\theta \frac{g_{d/2}}{g_{d/2+1}} [-u_j \partial_j u_i - \frac{1}{n} \partial_i (n\theta \frac{g_{d/2}}{g_{d/2+1}})] \\ &= \partial_j (-3\theta \frac{g_{d/2}}{g_{d/2+1}} n u_i u_j) - 2n\theta \frac{g_{d/2}}{g_{d/2+1}} \partial_j (u_i u_j) - 5\theta \frac{g_{d/2}}{g_{d/2+1}} \partial_i (n\theta \frac{g_{d/2}}{g_{d/2+1}}) \end{aligned} \quad (3.63)$$

$$\begin{aligned} \int \partial_j f^{eq,Q} \xi_i \xi_j c^2 d\boldsymbol{\xi} &= \partial_j \int f^{eq,Q} \xi_i \xi_j c^2 + 2 \int f^{eq,Q} \xi_i \xi_j (\xi_k - u_k) \partial_j u_k \\ &= \partial_i \int f^{eq,Q} c_i c_j c^2 d\boldsymbol{\xi} - \partial_j (3n\theta \frac{g_{d/2}}{g_{d/2+1}} u_i u_j) + 2n\theta \frac{g_{d/2}}{g_{d/2+1}} (u_i \partial_j u_j + u_j \partial_j u_i) \\ &= \partial_i (5n\theta \frac{g_{d/2}}{g_{d/2+1}})^2 + \partial_j (3n\theta \frac{g_{d/2}}{g_{d/2+1}} u_i u_j) + 2n\theta \frac{g_{d/2}}{g_{d/2+1}} \partial_j (u_i u_j) \end{aligned} \quad (3.64)$$

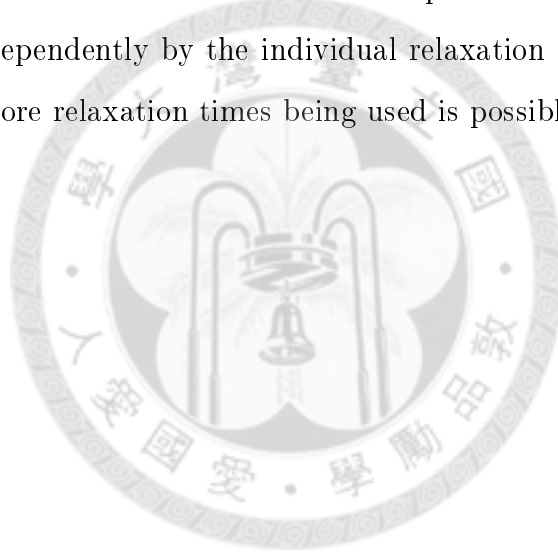
Finally, Combine (3.63) and (3.64) to get heat flux.

$$(3.63) + (3.64) = 5n\theta \frac{g_{d/2}}{g_{d/2+1}} \partial_i \theta \frac{g_{d/2}}{g_{d/2+1}} \quad (3.65)$$

$$q_i = -2\lambda \frac{\partial \theta \frac{g_{d/2}}{g_{d/2+1}}}{\partial x_i} = -(D+2)\tau_3 \rho \theta \frac{g_{d/2}}{g_{d/2+1}} \frac{\partial \theta \frac{g_{d/2}}{g_{d/2+1}}}{\partial x_i} \quad (3.66)$$

$$\kappa = \frac{\lambda}{\rho c_p} = \frac{\frac{D+2}{2}\tau_3 \rho \theta \frac{g_{d/2}}{g_{d/2+1}}}{\rho c_p} = \tau_3 \theta \frac{g_{d/2}}{g_{d/2+1}} \quad (3.67)$$

In this section, we show that the single relaxation time semiclassical LB method can be extended to include multiple relaxation times using Hermite decomposition. The viscous and thermal transport coefficients are shown to be governed independently by the individual relaxation times. Higher order moments and more relaxation times being used is possible.



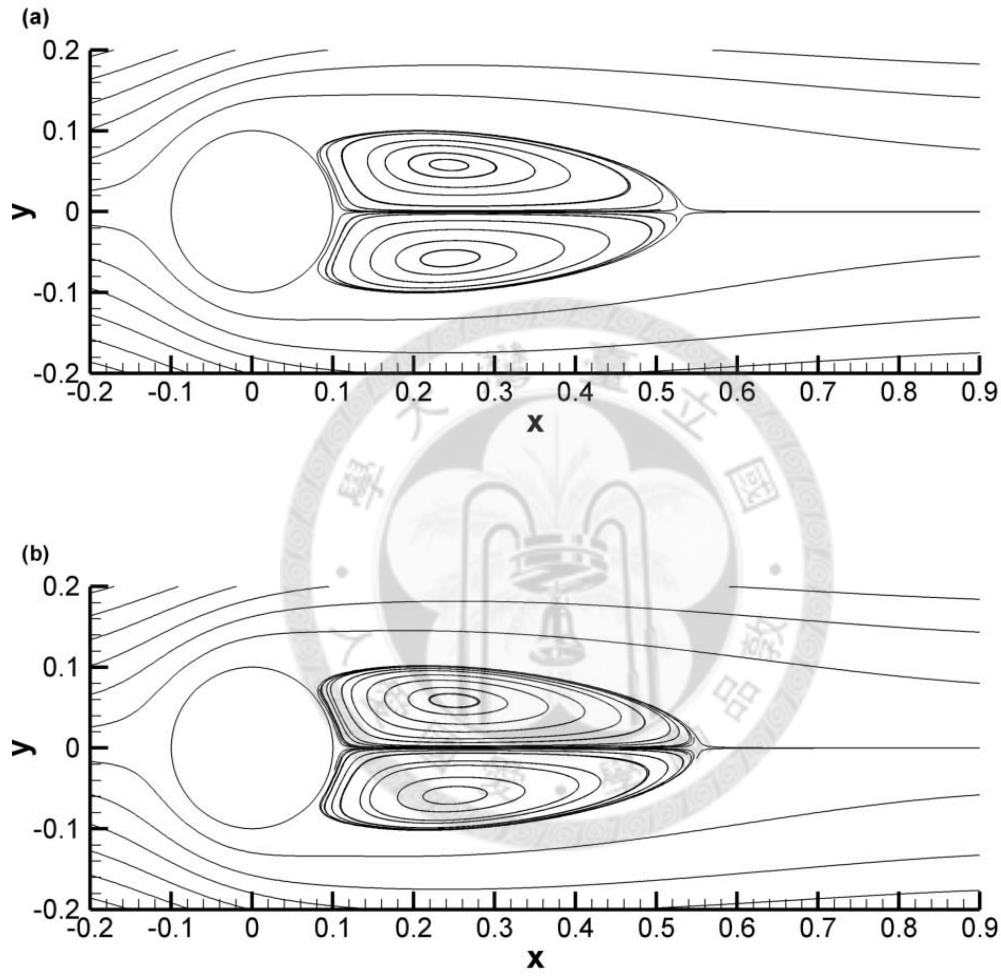


Figure 3.1: Comparisons of streamlines of uniform flow over a circular cylinder in a BE quantum gas in different expansion order with  $z = 0.2$  and  $Re_\infty = 40$ . (a)  $N = 3$ , (b)  $N = 2$ .

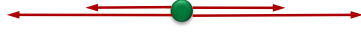


Figure 3.2: D1Q5 lattice structure

Table 3.1: D1Q5 quadratures and weights

$\zeta_a$	$w_a$
0	8/15
$\pm\sqrt{5 - \sqrt{10}}$	$(7 + 2\sqrt{10})/60$
$\pm\sqrt{5 + \sqrt{10}}$	$(7 - 2\sqrt{10})/60$

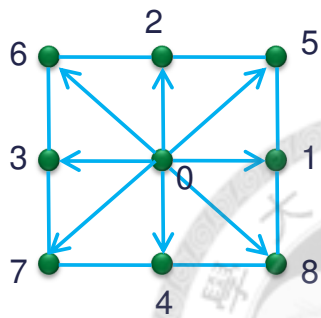


Figure 3.3: D2Q9 lattice structure

Table 3.2: D2Q9 quadratures and weights

$\zeta_a$	$w_a$
(0, 0)	4/9
$(\sqrt{3}, 0)_{fs}$	1/9
$(\pm\sqrt{3}, \pm\sqrt{3})$	1/36

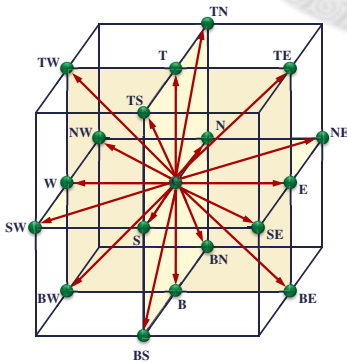


Figure 3.4: D3Q19 lattice structure

Table 3.3: D3Q19 quadratures and weights

$\zeta_a$	$w_a$
(0, 0, 0)	1/3
$(\sqrt{3}, 0, 0)_{fs}$	1/18
$(\pm\sqrt{3}, \pm\sqrt{3}, \pm\sqrt{3})_{fs}$	1/36



# Initial Conditions and Boundary Conditions for Semiclassical LB method

---

## Contents

<b>4.1 Overview</b> . . . . .	<b>43</b>
<b>4.2 Initial Conditions</b> . . . . .	<b>45</b>
<b>4.3 Boundary Conditions</b> . . . . .	<b>45</b>
4.3.1 Periodic Boundary Condition . . . . .	45
4.3.2 Bounce Back Boundary Condition . . . . .	46
4.3.3 Non-Equilibrium Extrapolation Boundary Condition . . . . .	49
4.3.4 Immersed Boundary Condition . . . . .	52
4.3.5 Issues on Microchannel Boundaries . . . . .	53

---

## 4.1 Overview

This section focuses on the implementation of initial conditions and boundary conditions for the semiclassical LB method. The choices of initial conditions

and boundary conditions influence the stability, accuracy and efficiency of the numerical scheme [53][54]. In semiclassical LB method, the primitive variables are the distribution functions  $f_a$  just as in the usual LB method, but not the hydrodynamic variables  $n$ ,  $u$ , and  $\theta$ (or  $T$ ). Most of the boundary conditions used in the classical LB method, including periodic boundary conditions, extrapolation boundary condition, bounce back boundary condition, non-equilibrium boundary condition should also work in semiclassical LB method since they are all dealing with distribution functions. In view of the complex boundaries, the real curves of the boundary are not always on lattice points, the layout of the curved wall boundary in the regularly spaced lattices is shown on Fig. 4.1, the circles represent the fluid nodes, the rectangles represent solid nodes, the real boundary does not always lay on the solid nodes but on the intersections between solid nodes and fluid nodes. The real boundary intersection point is labeled by triangle. Obviously, simple bounce back boundary condition can not be applied to this situation and some interpolation skills should be used, more discussions will be given below. For a lattice node near a boundary, density distributions entering the fluid domain after the propagation step are not available, the boundary conditions must then be implemented by specifying the unknown distribution function  $f_a$  entering the simulation domain across boundaries, such that the macroscopic velocity and pressure requirements are satisfied. These stipulations pose some difficulties in the LB method implementation. In this section, some important boundary conditions will be introduced, especially those suitable for semiclassical LB method. In the end of this section, a special issue about the boundary conditions for microchannel flow will be discussed.



## 4.2 Initial Conditions

In general, the steady state problem is not sensitive to the initial conditions. Such that, in many cases we can just set initial conditions of the distribution functions as its equilibrium state. That is,  $f_i^{initial} = f_i^{eq,Q}(n_0, u_0, \theta_0, z_0)$ , wherein  $n_0$ ,  $u_0$ ,  $\theta_0$  and  $z_0$  are the initial macroscopical variables. Since in this thesis the problems we consider are not sensitive to initial conditions, the initial distribution functions are simply set by the equilibrium distribution functions as described above. In conventional LB method, there are other methods applying initial conditions. For example, in [53] the non-equilibrium initial condition is considered. In [55] and [56] pressure is solved from Poisson equation and used to initialize the distribution functions. It should be noticed that some nonlinear flow problems like turbulence and multi-phase flow are sensitive to initial conditions [57].

## 4.3 Boundary Conditions

### 4.3.1 Periodic Boundary Condition

When a system exhibits symmetric or periodic features in space, symmetric, or periodic boundary conditions can be utilized to reduce the domain size for a better computational efficiency. Due to the particulate nature, these boundary conditions can be easily implemented in LB method. Fig. 4.2 illustrates a horizontal symmetry boundary along the inlet and outlet of the computational domain. The basic idea is that an unknown incoming distribution across a symmetry boundary is exactly the reflection image of this required distribution about the symmetry boundary. For periodic boundaries, all particles leave the domain across a periodic boundary re-enter the domain from

the opposite side. Therefore, the actual system being simulated is then an infinitely long horizontal domain with identical repeated units. To impose a pressure gradient along the periodic direction, for example, along a channel, the periodic boundary condition can be modified to incorporate the pressure drop between the domain inlet and outlet [58]. Periodic boundary condition is widely used since it is easily and directly implemented on the distribution functions. For example, referring to Fig. 4.2, the boundary conditions are set as:  $f_{6,3,7}(nx, j) = f_{6,3,7}(1, j)$  and  $f_{1,5,8}(1, j) = f_{1,5,8}(nx, j)$ , such that the periodic boundary conditions are applied on inlet and outlet of the two dimensional computational domain.

### 4.3.2 Bounce Back Boundary Condition

The **no-slip** boundary condition at a solid-liquid interface is important for our understanding of liquid mechanics. In conventional computational fluid dynamics, the vast majority of problems are concerned with solving the Navier-Stokes equations for incompressible flow

$$\begin{aligned} \nabla \cdot \mathbf{u} &= 0 \\ (\partial_t + \mathbf{u} \cdot \nabla) \mathbf{u} &= -\frac{\nabla p}{\rho} + \nu \nabla^2 \mathbf{u}. \end{aligned}$$

Most of these studies assume the validity of the no-slip boundary condition which means that all components of the fluid velocity on a solid surface are equal to the respective velocity components of the surface. In mesoscopical computational tools like LB method, smoothed-particle hydrodynamics et al., there should be a method corresponding to the no-slip boundary condition in macroscopical world, and it is called "Bounce Back Boundary Condition" in LB method. The success of LB method is mainly due to the most widely used bounce back boundary condition which evolved from the boundary conditions

of lattice gas and is well documented in the literature [59][60][61][62][63]. The standard bounce back boundary condition is simple to implement and shown here: a particle will reverse its momentum when it hits on a solid surface. Suppose a lattice site  $x_b$  is designated as a solid site on a boundary, and a lattice site  $x_f$  is designated as a fluid site next to the boundary. The bounce back boundary conditions can be simply expressed as

$$f_a(x_f) = f_{\bar{a}}(x_b)$$

where  $\bar{a}$  means the oppose direction of  $a$ , but this standard bounce back boundary condition has only first order accuracy. Recent research reveals that keeping the real boundary on the link between two adjacent lattices will get second order accuracy. Although this modified bounce back boundary condition is second-order accurate when the solid boundary resides on the midpoint of the link, this is not the case for an arbitrary surface or, say, complex boundary, for which the accuracy of the bounce-back method degrades into a first-order-accurate velocity field. The research of bounce back boundary condition for complex boundary has long history on the development of LB method, and we will discuss it here by dividing these methods into two groups: Node-based methods and Link-based methods. Node-based methods treat the lattices most closing to the real physical boundaries as solid lattices, the standard bounce back boundary condition belongs to this kind of group. In contrast of this method, the link-based methods always put the real physical boundaries on the middle of the link of two adjacent lattices, the modified bounce back boundary condition belongs to this kind of group. The node-based method keeps the real physical boundary on the lattices and increases the accuracy of the fluid solid coupling through the direct alteration of fluid nodes adjacent to the solid surface. Early methods based on the work

of [64] and [65] alter the collision operator with forcing terms dependent on the volume fraction of solid in the given lattice cell. This method requires the accurate calculation of the solid fraction for each of these cells, which is complicated for arbitrarily shaped particles in three dimensions. Without an accurate calculation of the partially filled fluid cell volume fraction, spikes in particle force and torque are reported [66]. In [67], the no-slip condition is enforced directly on fluid nodes adjacent to the solid in a method called the external boundary force LB method. For link-based methods, the standard bounce back method is altered by interpolation or extrapolation to make the real physical boundary lie at the midpoint of the link. Filippova et al. use interpolation methods on standard bounce back method [68], then Mei et al. improved this kind of method [69]. In [70] Bouzidi et al. proposed a new method combining bounce-back and space interpolation for dealing with the complex boundary. In [71] Lallemand and Luo improved the methods from Bouzidi et al.. In the following context, the modified bounce-back method is based on the works of [71] and extended to semiclassical LB method. According to Fig. 4.4, the circle points F, E and A are fluid lattices, the square point B is solid lattice. The dashed line represents the real wall, the particle from fluid lattice A toward to wall lattice B will hit the real wall and bounce back to the solid circle point D. Before continuing the following discussions, define a quantity  $q$  as a fraction of the total link distance  $q = \frac{AC}{AB}$ . For the case when the solid boundary is closer than the link midpoint,  $0 < q < 1/2$  in Fig. 4.4(a). The distribution function with velocity moving to the wall (the arrow in Fig. 4.4(a)) at the fluid grid point A would end up at the point D located at a distance  $(1 - 2q)\delta_x$  away from the fluid grid point A. Because D is not a grid point, the distribution function  $f_3$  at the grid point A needs to be reconstructed. Noticing that according to the standard bounce back rule,

the  $f_1$  from grid point D would become  $f_3$  at grid point D after one time step, such that, what we should do is to construct the values of  $f_1$  at the point D by a interpolation involving three distribution function  $f_1$ :  $f_1(A)$ ,  $f_1(E)$  and  $f_1(F)$ . The similar procedures are applied to the case of  $q \geq 1/2$  depicted in Fig. 4.4(b). The interpolation formulas are ( where the  $\hat{f}_a$  and  $f_a$  denote the post-collision distribution functions before and after advection):

For  $q < \frac{1}{2}$ ,

$$f_{\bar{a}}(\xi_A, t) = q(1 + 2q)\hat{f}_a(\xi_A, t) + (1 - 4q^2)\hat{f}_a(\xi_E, t) - q(1 - 2q)\hat{f}_a(\xi_F, t).$$

For  $q \geq \frac{1}{2}$ ,

$$f_{\bar{a}}(\xi_A, t) = \frac{1}{q(1 + 2q)}\hat{f}_a(\xi_A, t) + \frac{2q - 1}{q}\hat{f}_a(\xi_E, t) - \frac{2q - 1}{2q + 1}\hat{f}_a(\xi_F, t).$$

Although these kind of methods are accurate, there also exists an error in the boundary location that is dependent on the viscosity [72] [73]. This error exists for standard bounce back methods, even with the boundary located at the midpoint of two adjacent lattices, and for the linear and quadratic interpolation methods mentioned above. We should also notice that there is a disadvantage to all interpolation methods due to the lack of mass conservation. Although the magnitude of mass leakage for the multi reflection and equilibrium interpolated methods is small, it may be important in cases such as the simulation of deformable capsules, in which mass leakage results in an overall change in particle volume.

### 4.3.3 Non-Equilibrium Extrapolation Boundary Condition

The usually used bounce-back scheme is easy for implementation as described above. However, the standard bounce-back scheme is only of first order in nu-

merical accuracy at boundaries [59][73]. There are many alternative boundary conditions proposed for solving the accuracy degrading problem in complex geometry, for example, half-way bounce-back scheme [63], the non-equilibrium bounce-back scheme [74] and the extrapolation scheme [75] and so on. However, there still exist some disadvantages and will introduce some additional errors [76]. Guo et al. introduced non-equilibrium extrapolation boundary condition in [76] to solve those problems, they used this method to deal with the curved boundaries, and in the following years it had been widely used on many numerical simulations [77][78][79][80] due to its easy implementation and stabilization. Before introducing the present boundary condition, we recall the extrapolation boundary condition introduced in [75], this method is easily applied and it keeps zero derivative in the present boundary. It is derived from simple finite difference method and could be illustrated as:

$$f_a(1, j) = f_a(2, j)$$

$$f_a(nx, j) = f_a(nx - 1, j)$$

In which  $i = 1$  and  $i = nx$  are inlet and outlet boundaries. We can also use second order finite difference method to derive the extrapolation boundary condition and it will be shown as:

$$f_a(1, j) = 2f_a(2, j) - f_a(3, j)$$

$$f_a(nx, j) = 2f_a(nx - 1, j) - f_a(nx - 2, j)$$

This method is suitable for many different boundaries like Dirichlet and Neumann boundary conditions because it is derived from the finite difference method. However, some researches shows this kind of extrapolation boundary conditions will degrade the numerical stability [74][76]. The non-equilibrium extrapolation boundary condition first introduced in [76] is separating the unknown distribution functions on the wall into equilibrium and non-equilibrium

parts, where the equilibrium part is determined by the macroscopic variables, and the non-equilibrium part is determined by that of the distribution function at the nearest neighbor nodes in the fluid region. For example, D2Q9 model is used for describing this principle, and we consider Fig. 4.3, after streaming, the distribution functions  $f_1, f_5$  and  $f_8$  on left open boundary are unknown, we can represent it by equilibrium and non-equilibrium parts as:

$$f_a(x_b, t) = f_a^{eq}(x_b, t) + f_a^{neq}(x_b, t), a = 1, 5, 8,$$

where  $f^{neq}$  represents the non-equilibrium part. Since we do not know the non-equilibrium part  $f^{neq}$  on the wall, we use the nearest fluid nodes approximating it.

$$f_a^{neq}(x_b, t) = f_a^{eq}(x_f, t) - f_a^{eq}(x_b, t), a = 1, 5, 8,$$

such that, the non-equilibrium extrapolation boundary condition can be described as:

$$f_a(x_b, t) = f_a^{eq}(x_b, t) + (f_a(x_f, t) - f_a^{eq}(x_f, t)), a = 1, 5, 8.$$

For another example, referring to Fig. 4.2, adiabatic wall and isothermal wall boundary conditions are important in thermal flow simulation. According to this approach, the distribution function  $f_a(x_b)$  can be assigned new values by setting  $u_b = 0$ , and, for adiabatic wall  $\theta_b = \theta_f$ , for isothermal wall  $\theta_b = \theta_H$ , or  $\theta_b = \theta_L$ . Here,  $\theta_H$  means the high temperature at the isothermal wall and the  $\theta_L$  means the low temperature one. Finally, the distribution functions on the boundary points are calculated as:

$$f_a(x_b) = f_a^{eq,Q}(x_b, u_b, \theta_b) + [f_a(x_f, u_f, \theta_f) - f_a^{eq,Q}(x_f, u_f, \theta_f)], a = 1, 5, 8.$$

where  $\rho_b, \theta_b, u_b$  denote the hydrodynamic variables at the boundary points and  $\rho_f, \theta_f, u_f$  denote the corresponding ones at the nearest neighborhood. Non-

equilibrium boundary condition has been proven for its stability and accuracy in numerous cases.

#### 4.3.4 Immersed Boundary Condition

Immersed boundary method (IBM) was invented by [81] to simulate cardiac mechanics and associated blood flow. The feature of this method is implementing entire simulations on a cartesian grid without conforming to the geometry of the rigid body. In another words, IBM is replacing the effect boundaries acting on the surrounding fluid by the force added in the governing equations. Based on the work of Peskin, numerous modifications and refinements have been proposed and a number of variants of this approach now exist. [2-10]. Among the remarkable works, Goldstein et al. [82] proposed a model named virtual boundary method which permits simulations with complex geometries. Lai and Peskin [83] proposed a second-order accurate immersed boundary method with adoption of a well-chosen Dirac delta function. Linnick and Fasel [84] proposed a high-order modified immersed interface method for the two-dimensional, unsteady, incompressible Navier-Stokes equations in the stream function-vorticity formulation, which employs an explicit fourth-order Runge-Kutta scheme for time integration and the fourth-order compact finite-difference schemes for approximation of spatial derivatives. Lima E Silva et al. [85] proposed a version named physical virtual model, which is based on the conservation laws, and simulated an internal channel flow and the flow around a circular cylinder. Due to the common feature of using Cartesian mesh in the LB method (LB method) and IBM, some researchers tried to combine these two methods into an efficient one. The first such attempt was made by Feng and Michaelides [86][87]. In their work, the restoration force due to deformation is computed by the penalty method [86] or the direct-forcing



scheme [87]. The penalty method introduces a user-defined spring parameter which may have a significant effect on the computational efficiency and accuracy. The direct-forcing immersed boundary [88] in order to overcome the drawbacks of the virtual boundary force method, and its improved versions [89] are very suitable for finite difference applications to simulate flows in complex domains. However, the direct-forcing scheme requires solving the N-S equations by the finite-difference method, which may spoil the merits of LB method. In recent years, IBM is introduced in LB method, Since the Cartesian mesh is used in both LB method and IBM, the combinations of IBM and LB method should make the computations easy, efficient and suitable for complex boundaries. A boundary treatment using the immersed boundary velocity correction method proposed in [86][90][91] which enforcing the physical boundary condition is also adopted here. Since the immersed boundary method is dealing with real curved geometries in simulation, it must be better than the standard bounce back method. The detailed comparisons between immersed boundary method and bounce back method are given in Fig. 5.6. In this case, we used flow over cylinder to test the accuracy of two different boundary conditions. We could find that immersed boundary method is much better than the bounce back method while dealing with complex geometries. And also referring to Table. 5.1, the results of standard bounce back boundary condition oscillate in different Reynolds number and can not reveal the real physical phenomena well.

#### 4.3.5 Issues on Microchannel Boundaries

Microchannel flow has drawn a lot of attentions in recent years, there are several interesting phenomenons in microchannel flow like slip velocity, temperature jump and Knudsen minimum [92], simulating microchannel flow and

these phenomena is a challenging problem. Conventionally, direct simulation monte carlo method has been used wildly on this topic and got good results. Recently, LB method is also applied to this topic and got accurate results. In the developing of LB method on microchannel flow, there are two important issues, one is the relations between Knudsen number  $Kn$  and the relaxation time  $\tau$ , the other is the boundary conditions. The detailed descriptions covering the first issue will be discussed in Chapter 5. Here introducing and comparing the state of art boundary conditions for microchannel simulations, and the adequate boundary condition is chosen, modified and adopted on semiclassical microchannel flow simulations in Chapter 5. In microchannel simulations, diffusive boundary conditions are the most important and worth to introduce in detail. Ansumali et al. disclosed the first idea of diffusive boundary conditions [93]. In their work, derivation of the LB method from the continuous kinetic theory [14][17] is extended to obtain boundary conditions. For the model of a diffusively reflecting moving solid wall, the boundary condition for the discrete set of velocities is derived. This diffusive boundary condition is formulated in the continuous kinetic theory and listed in equation (10) of [93] then expanded and discretized on the hermite polynomials. In 2005, Tang et al. followed the idea and introduced the discrete maxwellian method which use the discrete kinetic theory boundary conditions to get the slip velocity at the solid boundaries [94]. According to the bottom wall, shown in Fig. 4.3, the discrete maxwellian method is described as:

$$\begin{aligned}
 f_2 &= f'_4 \\
 f_5 &= rK f_5^{eq}(\rho_w, \mathbf{u}_w) + (1-r)f'_8 \\
 f_6 &= rK f_6^{eq}(\rho_w, \mathbf{u}_w) + (1-r)f'_7
 \end{aligned} \tag{4.1}$$

where  $\rho_w$  and  $\mathbf{u}_w$  are the density and velocity of wall, and  $K$  is a factor defined as:  $K = \frac{f'_4 + f'_7 + f'_8}{f_2^{eq}(\rho_w, \mathbf{u}_w) + f_5^{eq}(\rho_w, \mathbf{u}_w) + f_6^{eq}(\rho_w, \mathbf{u}_w)}$ . There is another diffusive boundary conditions which reflects the sum of incoming distribution function to the wall according to the weight of each distribution function come to the fluids. the detail descriptions also referring to the bottom wall of 4.3 is described as:

$$\begin{aligned} f_2 &= Q \times f'_2 / (f'_2 + f'_5 + f'_6) \\ f_5 &= Q \times f'_5 / (f'_2 + f'_5 + f'_6) \\ f_6 &= Q \times f'_6 / (f'_2 + f'_5 + f'_6) \end{aligned} \quad (4.2)$$

where  $Q = f'_4 + f'_7 + f'_8$  is the sum of incoming distribution function to the wall,  $f'_2 / (f'_2 + f'_5 + f'_6)$  is the weight of  $f_2$  comes to the fluid. The diffusive boundary conditions are applied to microchannel flow simulations and got great success. In 2002, Succi et al. combined bounce back and specular reflection methods to capture the gas slip velocity in the microflows [95], which is called bounce-back specular reflection method here. Referring to the bottom wall of Fig. 4.3. The bounce-back specular reflection method is introduced as:

$$\begin{aligned} f_2 &= f'_4 \\ f_5 &= r f'_7 + (1 - r) f'_8 \\ f_6 &= r f'_8 + (1 - r) f'_7 \end{aligned} \quad (4.3)$$

$$\begin{aligned} f_2 &= f'_4 + r f'_7 + r f'_8 \\ f_5 &= (1 - r) f'_8 \\ f_6 &= (1 - r) f'_7 \end{aligned} \quad (4.4)$$

Microchannel flow simulation is used for comparing the influences of different boundary conditions, In these different boundary conditions, all of them have a tunable variable  $r$ . It can be tuned to match the experimental data. Here we

use classical microchannel flow simulation to validate and compare different boundary conditions and the influences of accommodation coefficients. First, we compare the influences of different accommodation coefficients on velocity profile based on two different boundary conditions are shown in Fig. 4.5. From the results of this figure, the accommodation coefficient  $r$  represents the magnitude of the specular, and  $1-r$  means the magnitude of the bounce-back. That means, the higher  $r$  makes slip velocity more obvious. Next, we consider the influences of different boundary conditions on velocity profile based on the same accommodation  $r = 0.8$ . We chose two  $Kn$  number,  $Kn = 0.5$  and (b) for  $Kn = 2$ , and the results are in Fig. 4.6. We found that slip boundary condition and discrete Maxwellian boundary condition both reveals the same velocity profile in low  $Kn$  number, but the velocity profiles will split in high  $Kn$  number. As shown in Fig. 4.6(b), different boundary conditions indeed affect the slip velocity on the wall, the slip boundary condition has the maximum slip velocity on the wall. Finally, we consider the velocity profile of different Knudsen number based on the same accommodation  $r = 0.8$  for two different boundary conditions, as shown in Fig. 4.7(a) for bounce-back specular reflection boundary condition and Fig. 4.7(b) for discrete Maxwellian boundary condition respectively, we found that different  $Kn$  number really affects the slip velocity. In high Knudsen number, the velocity slip is obvious.

We should notice that there are still many other boundary conditions for the slip velocity boundaries not discussed here, for example, [96] introduced a modified LB model with a stochastic relaxation mechanism mimicking virtual wall collisions between free streaming particles and solid walls. Virtual wall collisions model combined with bounce back method or diffusive boundary conditions [93] were compared to show that this model can help the latter two methods work in high  $Kn$  number flow.

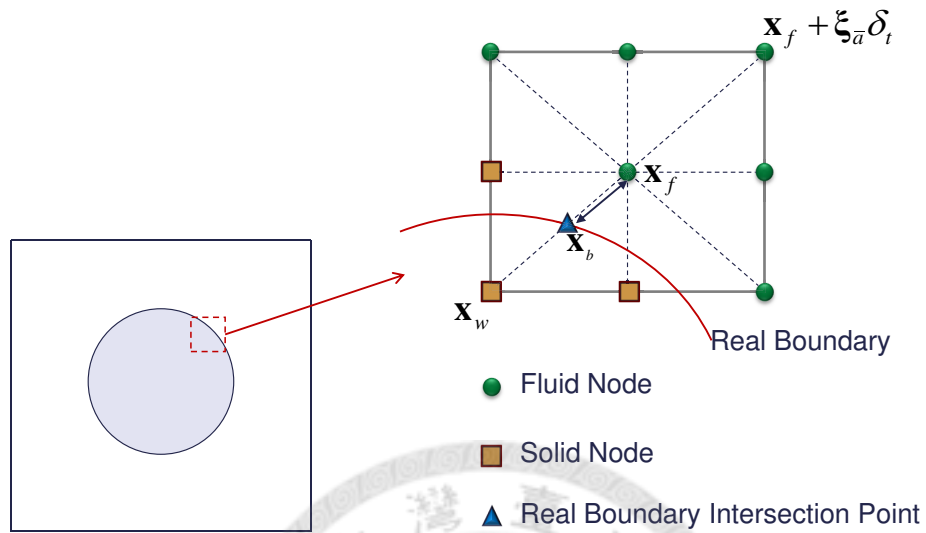


Figure 4.1: Layout of the curved wall boundary in the regularly spaced lattices.

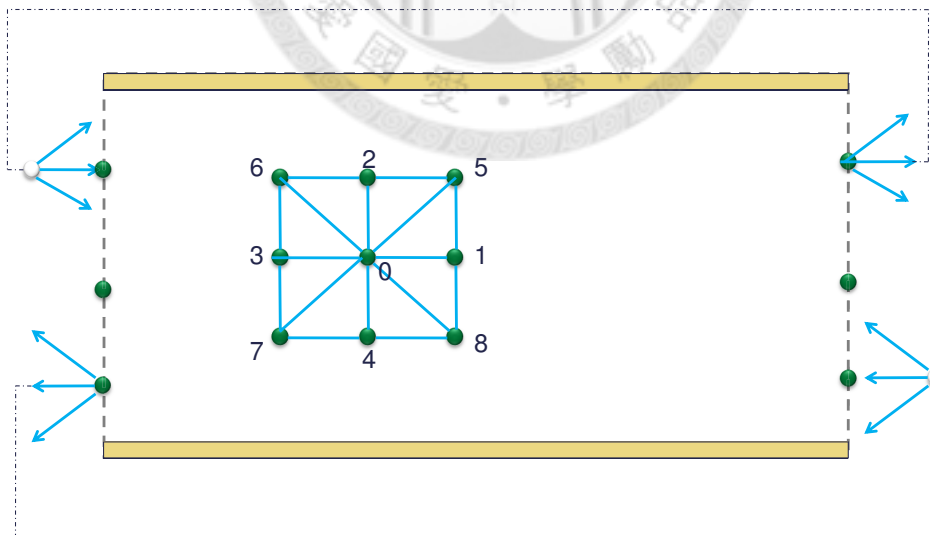


Figure 4.2: Periodic boundary conditions.

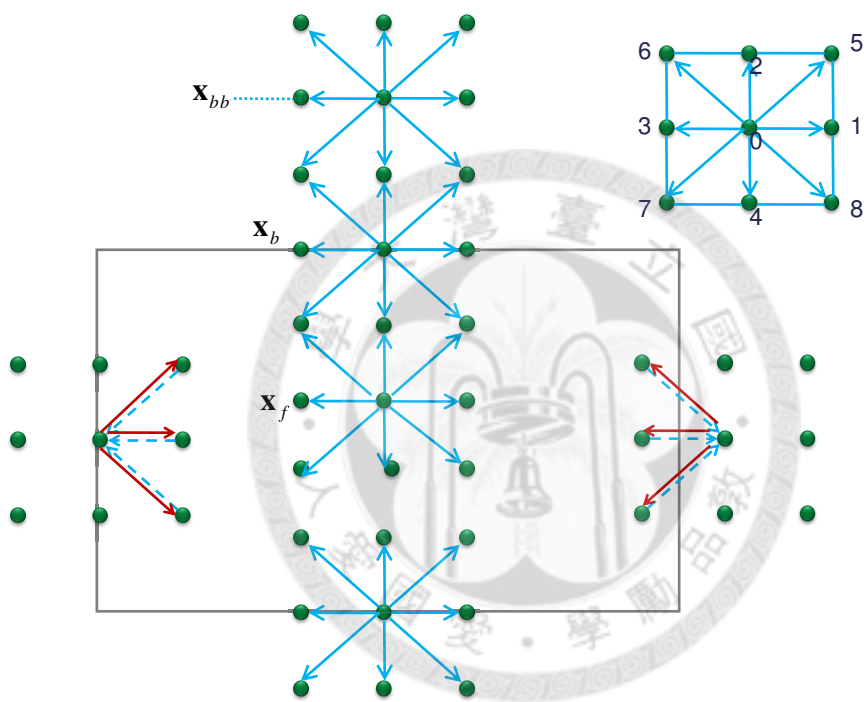
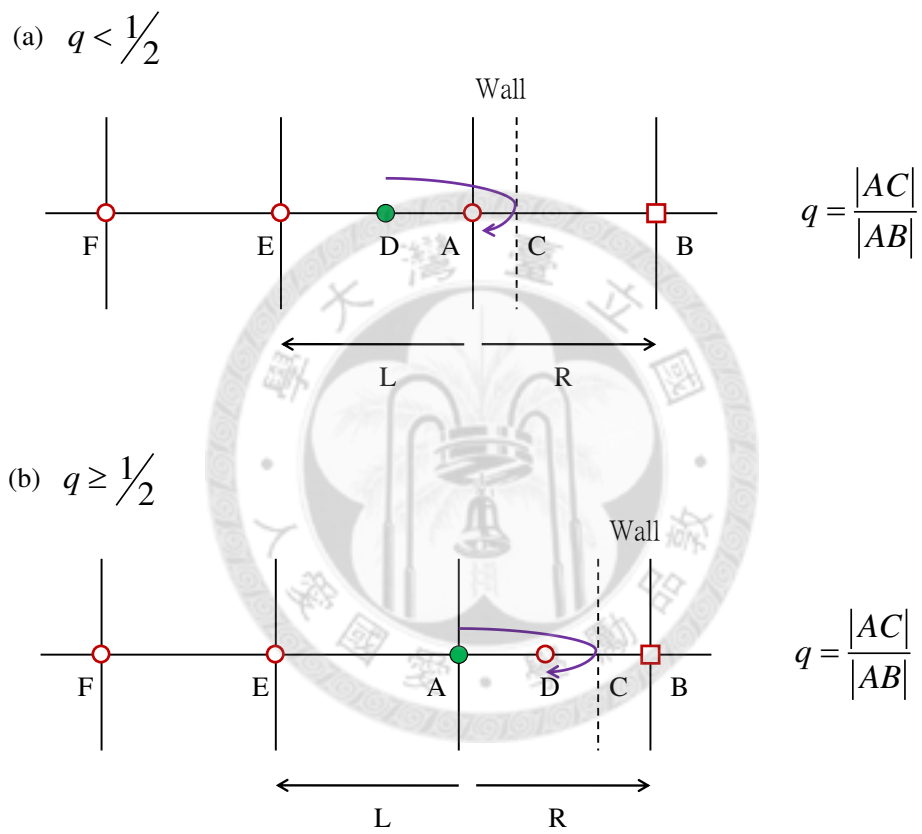


Figure 4.3: Layout of different boundary conditions in semiclassical LB method.

Figure 4.4: Bounce back boundary conditions (a)  $q < 1/2$ , (b)  $q \geq 1/2$ .

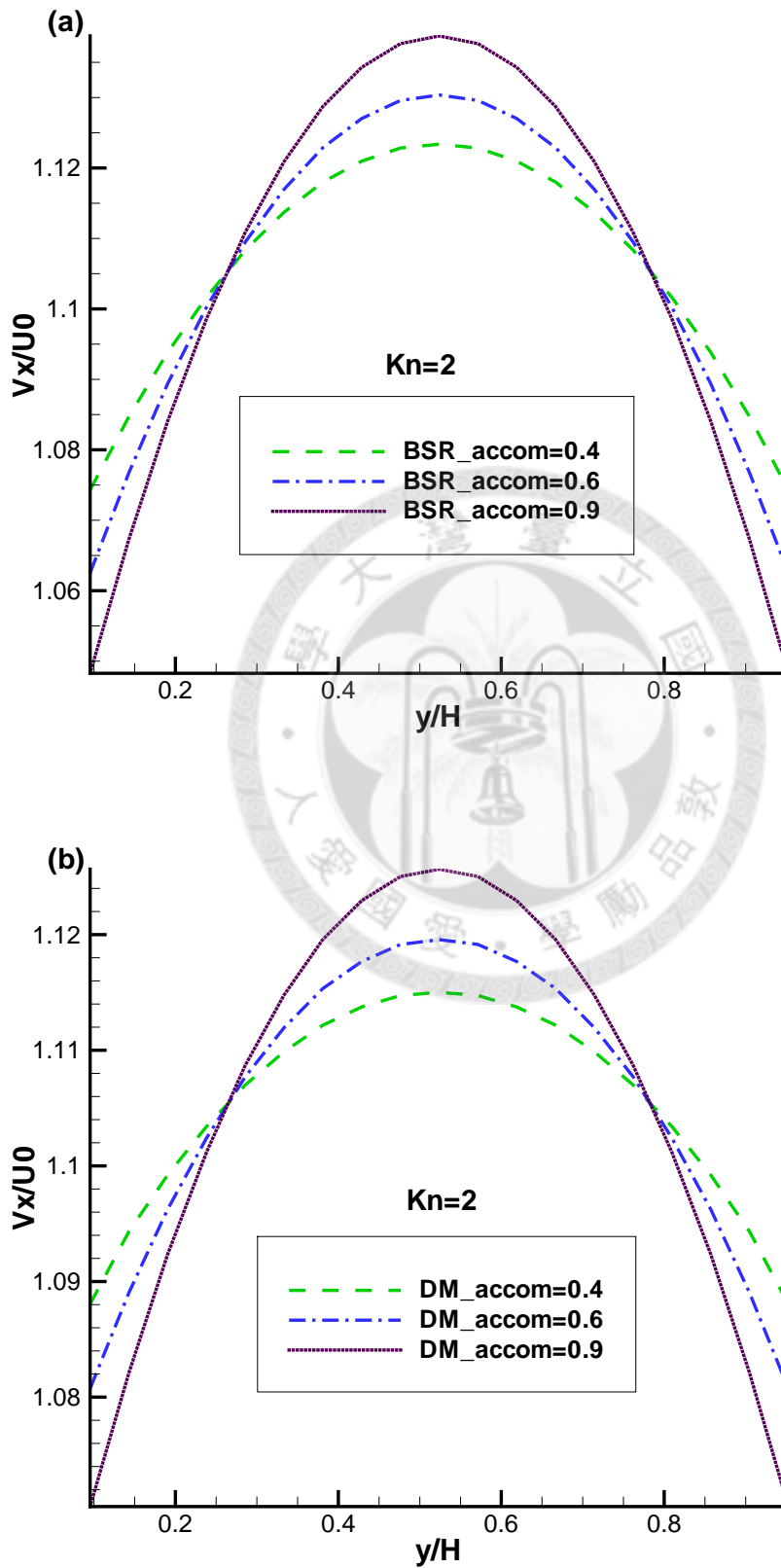


Figure 4.5: The influences of different accommodation coefficients on velocity profile based on two different boundary conditions. (a) Bounce-back specular reflection boundary condition, (b) Discrete Maxwellian boundary condition.



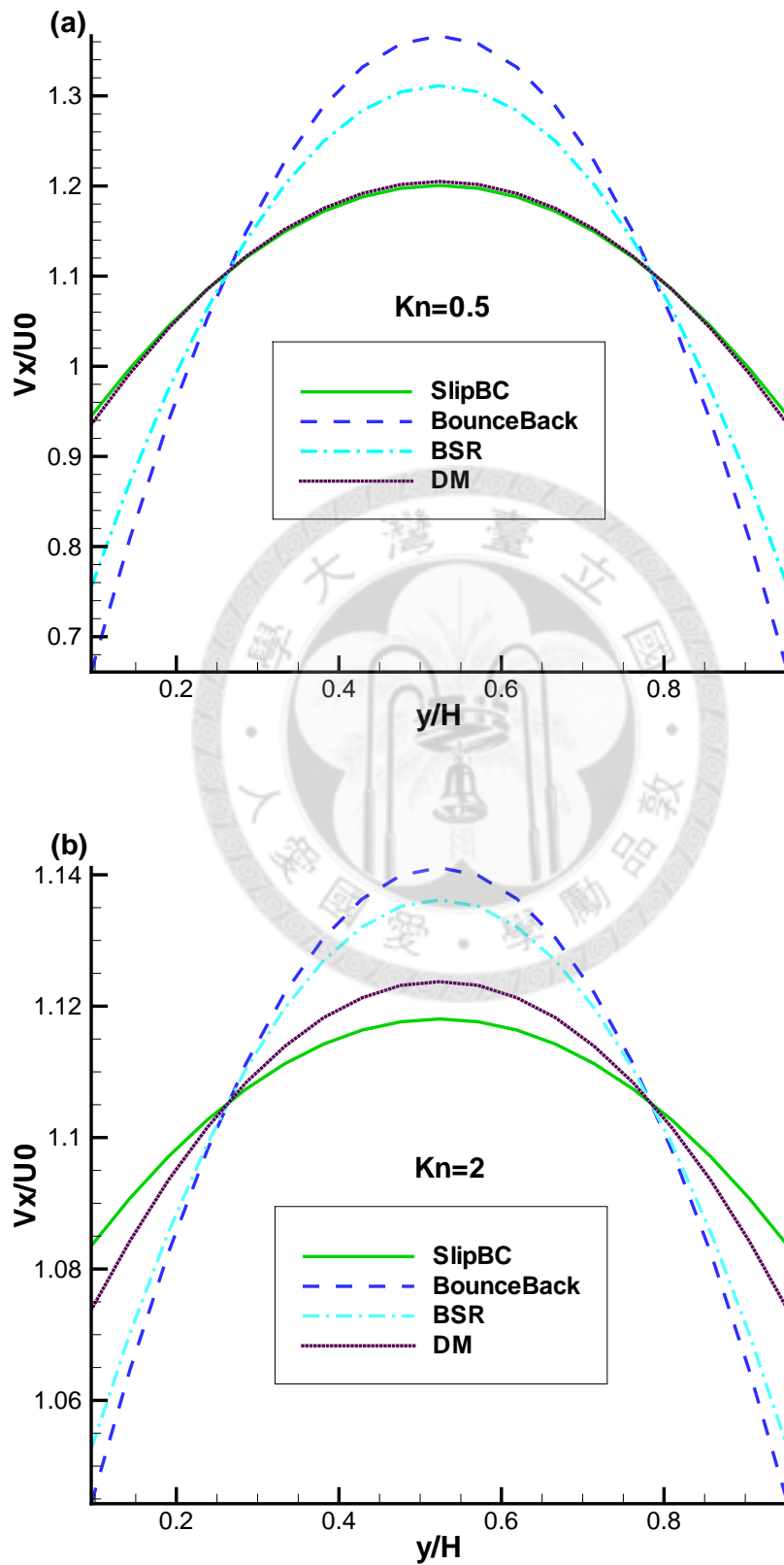


Figure 4.6: The influences of different boundary conditions on velocity profile based on the same accommodation  $r = 0.8$ . (a)  $Kn=0.5$ , (b)  $Kn=2$ .

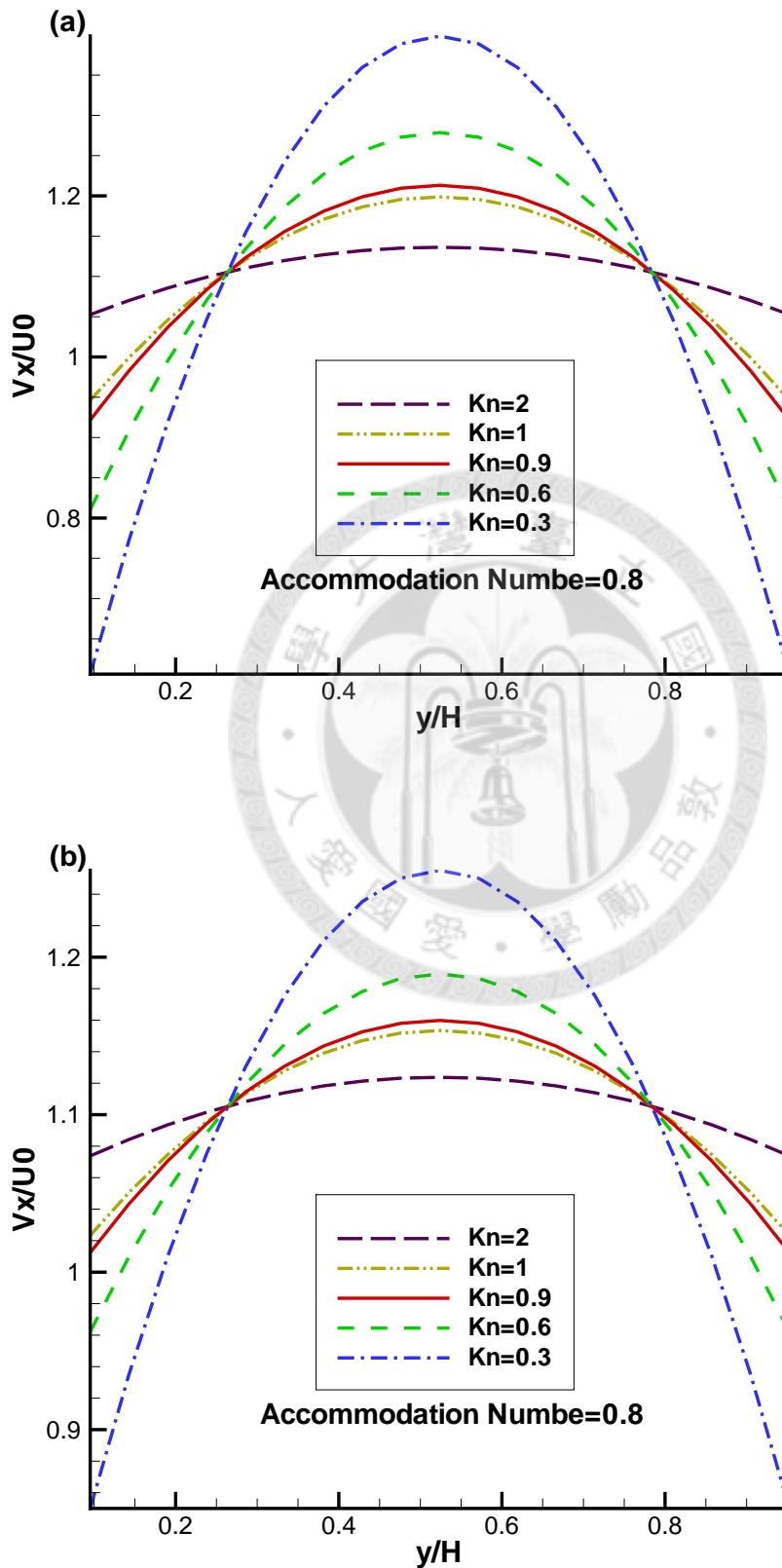


Figure 4.7: The velocity profile of different Knudsen number based on the same accommodation coefficient  $r = 0.8$  for two different boundary conditions. (a) Bounce-back specular reflection boundary condition, (b) Discrete

# Numerical Results

---

## Contents

---

5.1	Overview . . . . .	63
5.2	One Dimensional Shock Tube . . . . .	64
5.3	Two Dimensional Microchannel Flow . . . . .	65
5.4	Two Dimensional Flow over Cylinder . . . . .	69
5.5	Two Dimensional Natural Convection and Rayleigh- Beñard Convection Flow . . . . .	71
5.6	Three Dimensional Lid Driven Cavity Flow . . . . .	73

---

## 5.1 Overview

In this chapter, Some numerical examples for testing theory and illustrating the present semiclassical LB method are reported. For validation and comparison purposes, the present single relaxation time semiclassical LB method is applied to one-dimensional quantum gas flows in a shock tube, two-dimensional quantum gas flow over cylinder, two-dimensional quantum gas microchannel flow and three-dimensional quantum gas flow lid-driven cavity. Moreover, a new thermal LB method presented in Appendix 2 is validated by two dimensional natural convection flow and two-dimensional Rayleigh-Beñard thermal

convection.

## 5.2 One Dimensional Shock Tube

The constant relaxation time  $\tau = 0.001$  is used in testing the applicability of the present methods. The D1Q5 discrete velocities scheme as Table 3.1 is employed. The expansion equations up to the  $N = 3$  order, i.e., (3.38), is used for this one-dimensional problem. The computational domain is  $0 \leq x \leq 1$  and is divided into uniform cells of size  $1/L$ , where  $L$  is the number of cells. The diaphragm is initially located at  $x = 0.5$ . The initial conditions at the left and right sides of the diaphragm in the shock tube are  $(n_l, u_l, \varepsilon_l) = (1.0, 0.0, 1.0)$  and  $(n_r, u_r, \varepsilon_r) = (0.7, 0.0, 1.5)$ , the fugacity is set as  $z = 0.2$  everywhere. The relaxation time is set to constant  $\tau = 0.001$ . Here, we adopt the conventional finite volume schemes on those equations, in which (3.4) is solved by first order upwind scheme. In this case, (3.40) is treated as a system consisting of five one-dimensional linear wave equations. After applying first order upwind scheme, the discrete equations become

$$\begin{aligned} \frac{f_{a,i}^{n+1} - f_{a,i}^n}{\delta t} + \zeta_a^+ \frac{f_{a,i}^n - f_{a,i-1}^n}{\delta x} + \zeta_a^- \frac{f_{a,i+1}^n - f_{a,i}^n}{\delta x} \\ = - \frac{(f_{a,i}^n - f_{a,i}^{eq})}{\tau} \end{aligned} \quad (5.1)$$

where  $\zeta_a^+ = \max(\zeta_a, 0)$  and  $\zeta_a^- = \min(\zeta_a, 0)$  and the superscript  $n$  denotes the time level. We first performed a grid refinement test using  $L = 100, 200$ , and 400 cells to ensure the convergence of solution which are shown in Fig. 5.1. The convergence of solution is evident. Next, we compare the different behaviors due to the three statistics, namely, BE, FD, and MB statistics. The initial conditions at the left and right sides of the diaphragm in the shock tube are  $(n_l, u_l, \theta_l) = (1.0, 0.0, 2.0)$  and  $(n_r, u_r, \theta_r) = (0.7, 0.0, 1.8)$  and the same con-

stant relaxation time is used. The results using  $L = 200$  cells for the three statistics are shown in Fig. 5.2. The main features of a typical shock tube flow, namely, the shock wave, contact discontinuity and the expansion fan, are well represented. We can clearly delineate the difference of three statistics. It is shown that under different statistics although the initial temperature, density, and relaxation time are the same, the pressure, internal energy, and the temperature are different. It is noted that the results of MB statistics always lie between those of BE and FD statistics. Finally, we increase the temperature and keep other parameters the same as  $(n_l, u_l, \theta_l) = (1.0, 0.0, 10.0)$  and  $(n_r, u_r, \theta_r) = (0.7, 0.0, 12.0)$ . The results in Fig. 5.3 show that the dilute quantum gas in high temperature represent the quantum gas in classical limit, the difference of three different statistics can not be delineated. The results are in consistent with the characters in classical limit: high temperature and low density.

### 5.3 Two Dimensional Microchannel Flow

The transition from molecular to viscous flow was one of the main subjects of the early experiments of Knudsen [92] in which the Knudsen minimum phenomenon was first discovered where experimentally observed that the volumetric flow rate per unit pressure drop across a long capillary does not vanish as the mean pressure reduces to very small values. Since then, the capturing the Knudsen minimum phenomena in rarefied gas channel flows have been a challenging and long investigating problem [97][98][99][100][101]. This phenomenon not only occurs in classical dilute gas but also in liquid helium at low temperature which indicates a flow minimum in phonon system [51]. The fundamental physics of the phenomena of Knudsen minimum is associated with

rarefied gas flows in the slip- and transition-flow regimes and the boundary effects of the kinetic boundary layer and so-called Knudsen layer is dominant. This type of flow is also found in micro- and nano-scale fluidic applications typically involved in MEMS. The Navier-Stokes equations with no-slip boundary conditions often fail to explain important experimental observations, e.g., that the measured flow rate is higher than expected while the drag and friction factor are lower than expected [102]. The main reason is that the Navier-Stokes equations can only describe flows that are close to local thermodynamic equilibrium. When the mean free path of the gas molecules approaches the length scale of the device, the flow lacks scale separation and is unable to achieve local equilibrium [103]. Gas flows in miniaturized devices are often in the slip regime ( $0.001 < Kn < 0.1$ ) or the transition regime ( $0.1 < Kn < 10$ ). In these regimes, the gas can no longer be described as continuous quasi-equilibrium fluid nor as a free molecular flow [104]. Also, the flows encountered in micro system typically involve low Mach numbers. The LB method offers an attractive technique for micro- and nano-scale fluidic applications where the microscopic and macroscopic behavior are coupled. The method retains a computational efficiency comparable to Navier-Stokes solvers but is a more physically accurate method for gas flows, over a broad range of Knudsen numbers due to its original link to kinetic theory. The LB equations can be directly derived in a *priori* manner from the continuous Boltzmann equations [102][103]. In this section, our objective is to study the planar channel flow of gas particles of arbitrary statistics in the slip and transition regimes and in particular, we investigate the Knudsen minimum phenomena using semi-classical LB method. While considering the microchannel flow simulations, one of the two most important issues is the boundary conditions which have been discussed in Ch. 4, and another one is the relation between Knudsen

number  $Kn$  and relaxation time  $\tau$ . In the literatures, there are many methods of calculating  $\tau$  from  $Kn$ . However, generally we can write down the relation as  $\tau = \frac{1}{2} + \frac{c}{c^*} y_{Dim} \times Kn$ ,  $y_{Dim}$  is the lattice number in the y direction,  $c$  is the sound speed in the present lattices, which will be  $\sqrt{3}$  in our D2Q9 model, and  $c^*$  is different in many literatures, for example,  $c^* = \sqrt{8\theta/\pi}$  in [105] which is the average speed of molecular. Others chose  $c^* = \sqrt{3\theta}$  or  $c^* = \sqrt{\theta\pi/2}$ . Even more, Zhang et al. disclosed an idea of wall function that can provide a correction to the mean free path [51]. Such that, the mean free path is variable from wall to fluid, as a result,  $c^*$  becomes the function of Knudsen number  $Kn$ . We consider a uniform two-dimensional pressure-driven channel flow in a quantum gas. The channel length is  $L$  and height  $H$  and  $L/H = 25$ . With the given fugacity  $z_{inlet} = 0.2$ ,  $z_{outlet} = 0.09835$  for the Fermi gas,  $z_{inlet} = 0.2$ ,  $z_{outlet} = 0.10191$  for the Bose gas, and  $z_{inlet} = 0.2, z_{outlet} = 0.1$  for the classical limit, the temperature is  $\theta_{inlet} = 0.5$ ,  $\theta_{outlet} = 0.5$ , then the pressure ratio will be  $(P_{inlet}/P_{outlet}) = (n\theta \frac{g_{\frac{5}{2}}(z)}{g_{\frac{3}{2}}(z)})_{inlet} / (n\theta \frac{g_{\frac{5}{2}}(z)}{g_{\frac{3}{2}}(z)})_{outlet} = g_{\frac{5}{2}}(z_{inlet}) / g_{\frac{5}{2}}(z_{outlet}) = 2$  for the three cases. Since the D2Q9 square lattice is applied,  $L$  can be written as  $L = (N_x - 1)\delta_x$ , and  $H = (N_y - 1)\delta_y$  where  $N_x$  and  $N_y$  are the number of lattice nodes in the  $x$ - and  $y$ -direction, respectively. The accommodation coefficient  $\sigma = 0.6$  is used in the simulation. Other values can also be calculated. To begin with the computation, the desired  $Kn = \lambda/H$  is first input, where  $H$  is the height of the channel. We also set the lattice spacing  $\delta_x = \delta_y = 1$ . In the simulations of these cases,  $c^* = \sqrt{8\theta/\pi}$  is chosen, such that the relaxation time  $\tau$  can be expressed as

$$\tau = Kn(N_y - 1) \times \sqrt{\frac{3\pi}{8}} + 0.5. \quad (5.2)$$

Having  $Kn$  defined, appropriate  $N_y$  and  $\tau$  could be chosen, which could then be used in the determination of mesh size and the collision propagation updat-

ing procedure, respectively. We used the  $N = 2$  expansion equations set for all the cases computed. The computation domain is  $(0 \leq x \leq 500, 0 \leq y \leq 20)$  and  $501 \times 21$  uniform lattices were used. Several Knudsen numbers covering near continuum, slip and transition flow regimes are calculated. The steady velocity profiles for the three statistics, BE, MB, and FD gases for the case of  $z = 0.2$  are shown in Fig. 5.4 (a), (b) and (c), respectively, for three different Knudsen numbers to represent the Knudsen, slip and Poiseuille regions. For the small Knudsen number,  $Kn = 0.05$ , the characteristic parabolic velocity profile is evident and for  $Kn = 0.2$ , the velocity slip at the walls can be clearly observed. Again, the profile for MB gas lies always in between that of the BE and FD gas and for small Knudsen number, the three profiles get closer to each other. The mass flow rates for all three statistics, BE, MB, and FD gases for the case of  $z = 0.2$  for Knudsen number covering Knudsen, slip and Poiseuille regions are shown in Fig. 5.4 (d). Seven values of Knudsen number from 0.06 to 6.0 were calculated. The Knudsen minimum can be clearly identified for all three statistics and the profile for MB gas lies always in between that of the BE and FD gas. The Knudsen minimum is found to be near  $Kn = 0.6$ . Basically, the Knudsen minimum of a pipe or channel flow can be viewed and explained as a phenomena that appears when the flow passing through the competition between the classical Poiseuille continuum flow and the Knudsen flow and the value of Knudsen number at this minimum should lie in the slip and transition regime. It is also found that the Knudsen number value at Knudsen minimum is very sensitive to the specular condition (specified by  $\sigma$ ) of the wall surface. Our value obtained here is in agreement with that reported in the literatures (See [106][107][108]). For example, in [106], first observation of the Knudsen minimum in normal liquid  ${}^3He$  was reported and the position of Knudsen minimum was found to lie at Knudsen number of



$\simeq 0.5$  as compared to the value of 0.75. Also, Knudsen minima for phonons at Knudsen numbers of  $0.87 \pm 0.13$  and 0.65, respectively, have been reported, see [107][108]. Theoretically, as comparing with particles of classical statistics, the effects of quantum statistics at finite temperatures (non-degenerate case) are approximately equivalent to introducing an interaction between particles [109]. This interaction is attractive for bosons and repulsive for fermions and operates over distances of order of the thermal wavelength  $\Lambda$ . Our present simulation examples seem to be able to illustrate and explore the manifestation of the effect of quantum statistics.

## 5.4 Two Dimensional Flow over Cylinder

Next we consider a uniform two-dimensional viscous flow over a circular cylinder in a quantum gas to illustrate the present semiclassical LB method in practical flow simulation. We used the  $N = 2$  expansion equations set for this case. The computation domain is  $(-1, 1) \times (-1, 1)$  and set by  $201 \times 201$  lattices, and the cylinder is set at the center of the computation domain with the radius  $D = 0.1$ . Uniform Cartesian grid system is used. The free stream velocity is  $u_\infty = 0.1$ , free stream temperature  $T_\infty = 0.5$  and the Reynolds number  $Re_\infty = u_\infty D / \nu$ . First, we simulate the dilute quantum gas in classical limit and compare the results with the classical LB method to validate semiclassical LB method in this case. The drag and lift coefficients are defined as  $C_d = \frac{2F_D}{\rho u_\infty^2 A}$  and  $C_l = \frac{2F_L}{\rho u_\infty^2 A}$  respectively,  $F_D$  and  $F_L$  are the drag and lift forces,  $A$  is the planform area.  $C_d$  and  $C_l$  of different Reynolds number  $Re = 100$  and  $Re = 500$  are depicted in Fig. 5.5, we found the oscillation amplitude is consistent with the results from conventional LB method. After that, We consider two cases with  $Re_\infty = 20$  and  $Re_\infty = 40$  in three differ-

ent statistics. The kinematic viscosity  $\nu$  of the fluid could be obtained from the given Reynolds number and the relaxation time  $\tau$  is calculated according to (2.20), rather than the classical one (2.21), and both of them come from the Chapman-Enskog analysis [110] which considers the numerical viscosity in LB scheme. The equilibrium density distribution function with the given free stream velocity and density is used to implement the boundary conditions at the far fields. A boundary treatment using the immersed boundary velocity correction method proposed in [86][91] and described in Sec. 4.3.4 which enforcing the physical boundary condition is adopted at the cylinder surface. The D2Q9 velocity lattice used is as Table 3.2. The streamline patterns for all three statistics, BE, MB, and FD gases for the case of  $Re_\infty = 20$  are shown in Fig. 5.7. For this low Reynolds number, the flow patterns are symmetric and the wake vortices are larger for the FD gas and smaller for the BE gas as compared with the classical MB gas. Similarly, the results for the case  $Re_\infty = 40$  are shown in Fig. 5.8. The flow patterns are symmetric and the vortices in the wake region become larger as compared with  $Re_\infty = 20$  case. Again, the size of the vortex for the MB gas is always larger than that of BE gas and smaller than that of FD gas. This reflects the fact that the MB distribution always lies in between the BE and FD distributions. Moreover, Fig. 5.9 shows the streamline patterns for higher  $Re$  number,  $Re_\infty = 200$  with  $z = 0.2$  when time steps equals 65000. The vortex shedding is obvious, and we could see that the streamline patterns in the same time steps are different due to different quantum statistics. Finally, Fig. 5.10 shows different contours and streamlines of uniform flow over a circular cylinder in a quantum gas in classical limit with  $Re_\infty = 200$  when time steps equals 94200. The velocity contours of both x-direction  $u_x$  and y-direction  $u_y$  are shown, and we can find out that density  $\rho$ , fugacity  $z$  and temperature  $\theta$  have similar

patterns because of the formula  $n = \theta^{\frac{95/2}{93/2}}$ . Theoretically, as comparing with particles of classical statistics, the effects of quantum statistics at finite temperatures (non-degenerate case) are approximately equivalent to introducing an interaction between particles [109]. This interaction is attractive for bosons and repulsive for fermions and operates over distances of order of the thermal wavelength  $\Lambda$ . Our present simulation examples seem to be able to illustrate and explore the manifestation of the effect of quantum statistics.

## 5.5 Two Dimensional Natural Convection and Rayleigh-Bènard Convection Flow

In Appendix 2, a new coupled thermal LB method is given, and it should be extended to double distribution function semiclassical LB method. In this section, we report some numerical examples to test the coupled thermal LB method derived in Appendix 2. For validation and comparison purposes, we apply the numerical method to natural convection flows in a square cavity. Before the numerical simulations, we should notice that the local temperature  $\theta = RT$  is coupled in both the equilibrium velocity distribution function  $f^{(0),3}$  and equilibrium total energy distribution function  $h^{(0),2}$ , since the numerical case is low speed flow, we can average the local temperature computed from velocity distribution function and the total energy distribution function, respectively. A boundary treatment using the non-equilibrium exploration boundary conditions proposed in [79] and described in 4.3.3 is applied. The D2Q9 velocity lattice listed in Table 3.2 is used. On the left and right sides of the cavity, the isothermal boundary conditions with  $\theta_{left} = \theta_H$ ,  $\theta_{right} = \theta_L$  are applied. On the top and bottom sides of the cavity, the adiabatic boundary conditions are applied. No-slip conditions  $\mathbf{u} = 0$  are set on the four

sides. The convection flow induced by the temperature difference is characterized by the Prandtl number  $Pr = \frac{c\nu\mu}{\kappa} = \gamma \frac{\tau_f^{-0.5}}{\tau_h^{-0.5}}$  and Rayleigh number  $Ra = \frac{g\beta\Delta TH^3 Pr}{\nu^2}$ , where  $\Delta T = T_H - T_L$  is the temperature difference, or we can represent  $Ra$  number as  $Ra = \frac{g\hat{\beta}\Delta TH^3 Pr}{T_0\nu^2} = \frac{g\hat{\beta}\Delta\theta H^3 Pr}{\theta_0\nu^2}$ , where  $T_0$  is the reference temperature, and  $\hat{\beta} = T_0\beta$ . The computational domain is  $129 \times 129$  for  $Ra = 10^3$  and  $Ra = 10^4$ , and  $257 \times 257$  for  $Ra = 10^5$ . We set  $\theta_H = 1.04$  and  $\theta_L = 1.0$ . The initial temperature is set at  $(\theta_H + \theta_L)/2$  and initial density is  $\rho = 1.0$ . Notice that there are three unknowns  $\tau_f$ ,  $\tau_h$  and  $\beta$  relating to two parameters  $Pr$  and  $Ra$ . We set  $\frac{1}{\tau_f} = 1.5$  in all cases, then the  $\tau_h$  and  $\beta$  can be determined once the Prandtl number and Rayleigh number are specified. Here we set  $Pr = 0.71$ . The streamline patterns for several Rayleigh numbers are shown in Fig. 5.11. With the increase of the Rayleigh number, the fluid motion becomes stronger because of the larger buoyancy. The heat is transferred mainly by conduction at small Rayleigh number and by convection at large Rayleigh number. For low Rayleigh number a vortex appears at the center. As Rayleigh number increases, the vortex tends to become elliptic and breaks up into two vortices at  $Ra = 10^5$ . Similarly, the results for isothermal lines are shown in Fig. 5.12. The isothermal lines are nearly vertical at small Rayleigh number, and become horizontal at large Rayleigh number. To quantify the results, we define the average Nusselt number as  $Nu_{ave} = 1 + \langle u_x T \rangle \frac{H}{\chi(T_H - T_L)} = 1 + \langle u_x \theta \rangle \frac{H}{\chi(\theta_H - \theta_L)}$ , where  $\langle \rangle$  means the system average, and  $\chi = \frac{\kappa}{\rho c_p}$  is the thermal diffusivity. We also calculate the maximum velocities along the horizontal and vertical lines through the cavity center. The results are listed in Table I together with previous data. Our present simulation examples are able to illustrate and explore the manifestation of the effect of thermal Navier-Stokes flows. All of these results are in good agreement with those reported in [79]. Next, we also consider the

Rayleigh-Bénard convection flow which is a classical benchmark on coupled thermal LB models. The calculation of Rayleigh-Bénard convection is similar to the natural convection case. The fluid is enclosed between two parallel stationary walls with hot (bottom) and cold (top) temperatures and subjected to the gravitation force. Density variations induced by the temperature difference will drive the flow and the viscous force will counteract to balance it. The calculation domain is set as  $200 \times 100$  lattices, the top and bottom sides are set at the isothermal boundary conditions which are  $\theta_L$  and  $\theta_H$  corresponding to low temperature and high temperature accordingly. The x-direction is set with periodic boundary conditions. The simulations are corresponding to three different  $Ra$  number which are  $Ra = 4000$ ,  $Ra = 1000$  and  $Ra = 50000$ . We set  $\theta_H = 1.04$  and  $\theta_L = 1.0$ . The initial temperature is set at  $(\theta_H + \theta_L)/2$  and initial density is  $\rho = 1.0$ . We set  $\frac{1}{\tau_f} = 1.5$  and  $Pr = 0.71$  in all cases, then the  $\tau_h$  and  $\beta$  can be determined once the Prandtl number and Rayleigh number are specified just as described above. Top and bottom walls are applied by isothermal boundary condition, and left and right walls are applied by periodic boundary conditions. The streamlines and isotherms patterns for several Rayleigh numbers are shown in Fig. 5.13 and Fig. 5.14. With the increase of the Rayleigh number, the fluid motion becomes stronger because of the larger buoyancy. The heat is transferred mainly by conduction at small Rayleigh number and by convection at large Rayleigh number.

## 5.6 Three Dimensional Lid Driven Cavity Flow

Since all the components for simulating in real world are in three dimensional spaces. It is important to extend present semiclassical LB methods to three dimensional simulation. In this section we consider a benchmark three

dimensional lid driven cavity filled with dilute quantum gas. We used the  $N = 2$  expansion equations set for this case. The computational domain is  $(-0.5, 0.5) \times (-0.5, 0.5) \times (-0.5, 0.5)$  and set by  $51 \times 51 \times 51$  lattices. Uniform Cartesian grid system is used. The top wall velocity is  $u_{lid} = 0.02$ , free stream temperature  $T_\infty = 0.5$  and the Reynolds number is defined as  $Re_\infty = u_\infty D/\nu$ . Before doing the semiclassical LB method experiments, we consider three cases with  $Re_\infty = 100$ ,  $Re_\infty = 400$  and  $Re_\infty = 1000$  to validate the D3Q19 conventional LB method in three dimensional calculation. The kinematic viscosity  $\nu$  of the fluid could be obtained from the given Reynolds number and the relaxation time  $\tau$  is calculated according to  $\tau_c = \frac{\nu}{T} + \frac{\delta t}{2}$ , which comes from the Chapman-Enskog analysis [110] which considers the numerical viscosity in LB scheme. The equilibrium density distribution function with the given top wall velocity and density is used to implement the boundary conditions at top wall. A bounce back boundary treatment which enforcing the physical boundary condition is also adopted on all the walls except the top wall. The D3Q19 velocity lattice used is as Table 3.3. The convergence condition is set as  $\max_{x,y,z} \frac{|u(\mathbf{x},t) - u(\mathbf{x},t-\Delta t)|}{u_{lid}} \leq 10^{-5}$ . The convergence validation is shown in Fig. 5.15 and Fig. 5.15. The streamlines profiles of different Reynolds number of  $Re_\infty = 100$ ,  $Re_\infty = 400$  and  $Re_\infty = 1000$  for classical gases are shown in Fig. 5.19, Fig. 5.18 and Fig. 5.19. The results are in good agreement with previous works [111], [112] and [113]. The second comparison of this three dimensional lid driven cavity flows is the velocity profiles along the centerlines  $(x, 0, 0)$  and  $(0, 0, z)$  of both classical case and semiclassical case in classical limit shown in Fig. 5.20, we found Fig. 5.20(a) is in good agreement with [113]. Then, use the semiclassical LB method, and set the fugacity  $z$  in small number  $z = 0.00001$  which makes it in classical limit, the results are shown in Fig. 5.20(b), and it can recover the classical cases Fig. 5.20(a).

Up to now, we have shown that present semiclassical LB method in classical limit could recover the results of conventional LB method, moreover, the present semiclassical LB method can be used to calculate lid driven cavity filled with dilute quantum gas. The kinematic viscosity  $\nu$  of the fluid could be obtained from the given Reynolds number and the relaxation time  $\tau$  is calculated according to (2.20), rather than the classical one  $\tau_c = \frac{\nu}{T} + \frac{\delta t}{2}$ . The velocity vectors of dilute quantum gas of  $Re_\infty = 100$  are shown in Fig. 5.21 for BE statistics and Fig. 5.21 for FD statistics. Also the pressure contours and streamlines are provided in different quantum statistics, Fig. 5.25, Fig. 5.22, Fig. 5.26 and Fig. 5.23. In Fig. 5.31, the velocity profiles of two different statistics (BE and FD) with two different initialization fugacity  $z = 0.1$  and  $z = 0.2$  are shown. The solid lines represent the results of BE statistics and dashed lines represent the results of FD statistics. The differences between these two different fugacities is tiny and hard to be delineated.

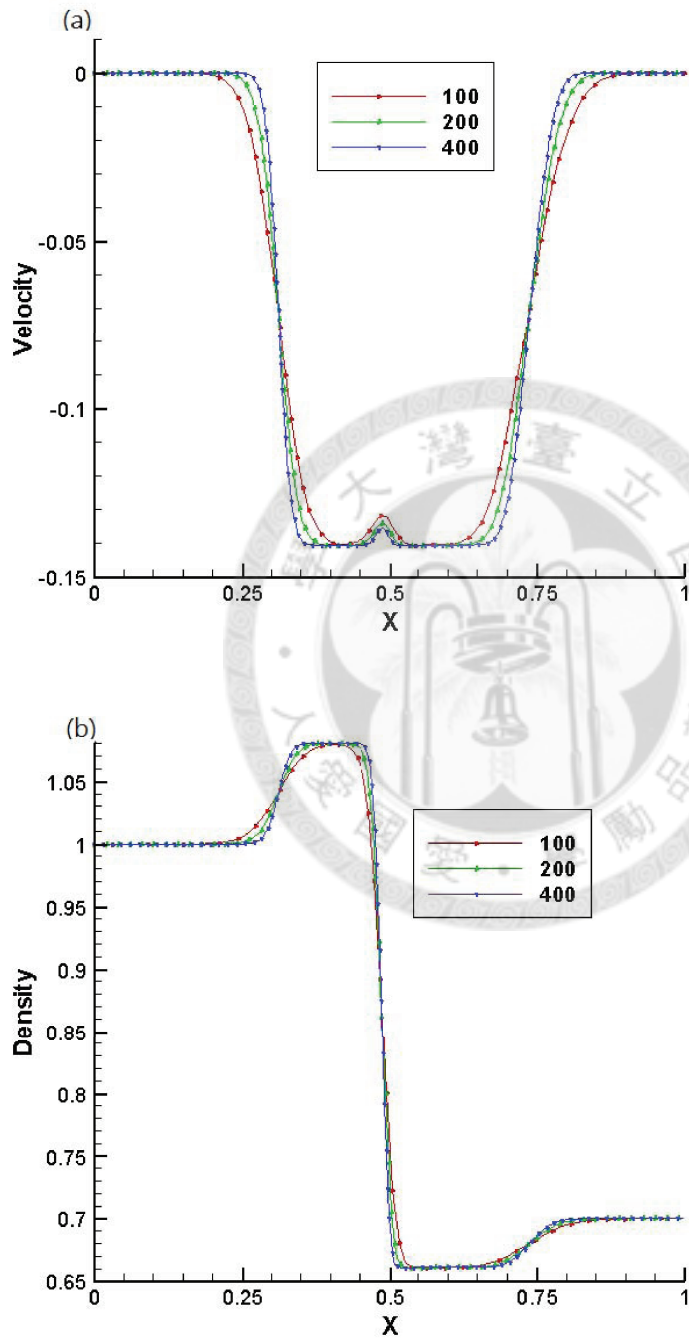
Table 5.1: Comparisons of drag coefficient of different boundary conditions in LB method

Re	IB method	BB method
20	2.383	3.626
40	1.819	1.433
100	1.428	2.621
200	1.339	3.108

Table 5.2: Comparisons of the average Nusselt number and the maximum velocity components across the cavity center. The data in parentheses are the locations of the maxima.

Ra		$Nu_{ave}$	$u_{max}(y)$	$v_{max}(x)$
$10^3$	Present	1.1194	3.5519(0.8203)	3.6091(0.1875)
$129 \times 129$	Ref [79]	1.1168	3.6554(0.8125)	3.6985(0.1797)
$10^4$	Present	2.2015	15.7489(0.8203)	19.4241(0.1328)
$129 \times 129$	Ref [114]	2.2442	16.1802(0.8265)	19.6295(0.1193)
$10^5$	Present	4.5327	34.4184(0.8477)	72.4886(0.0742)
$257 \times 257$	Ref [114]	4.5216	34.7399(0.8558)	68.6396(0.0657)





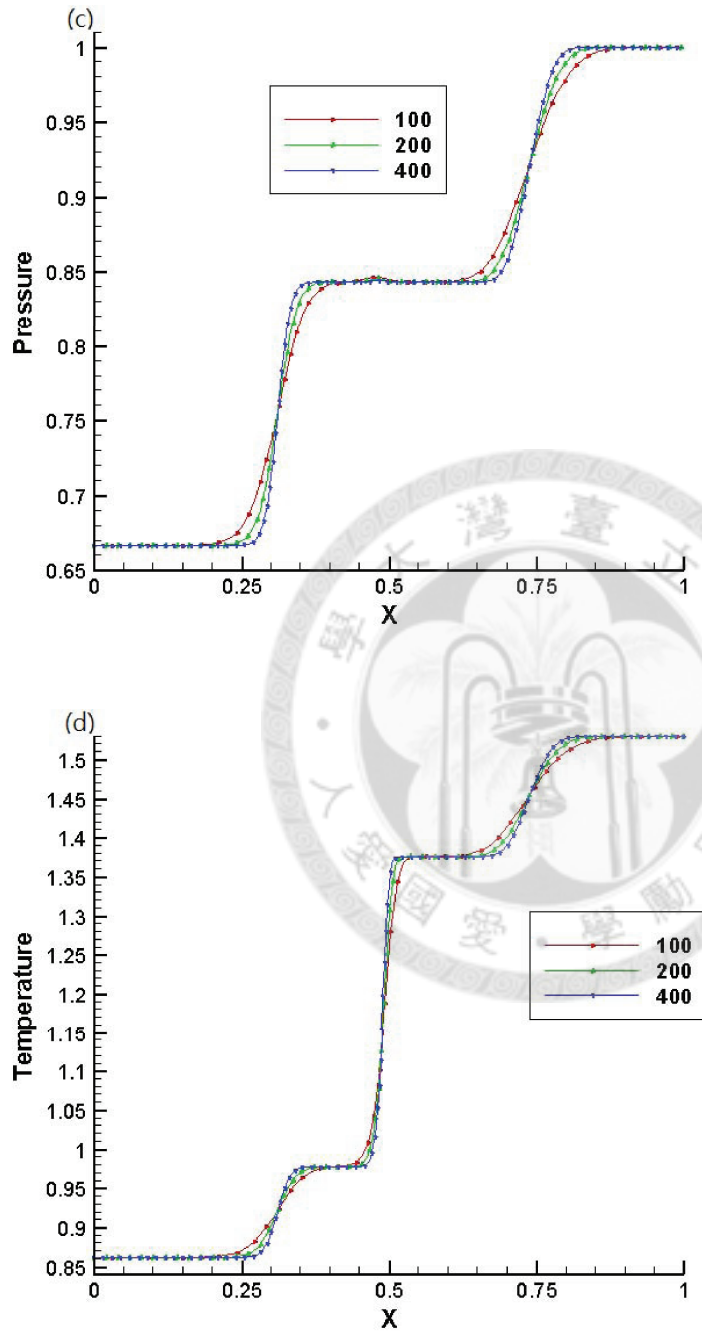
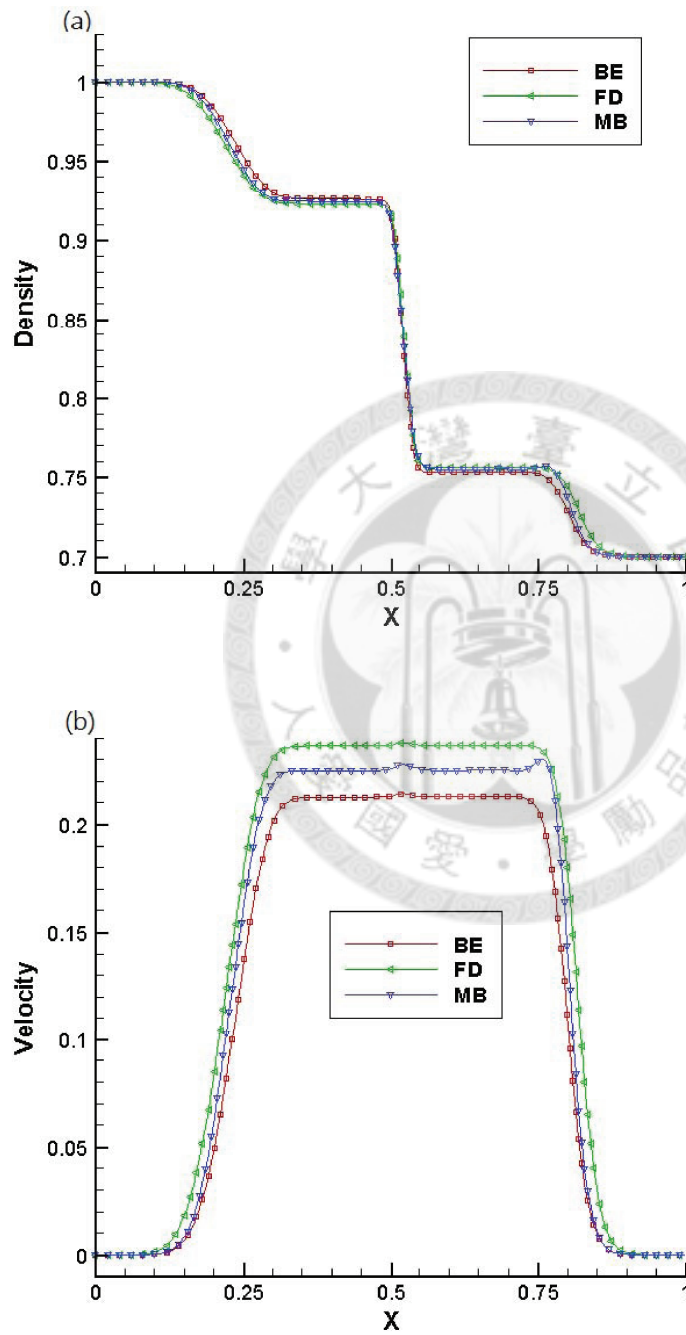


Figure 5.1: Convergence of solution with refined grids, the cells number is 100, 200, and 400. (a) Velocity, (b) Density, (a) Pressure, (d) Temperature.



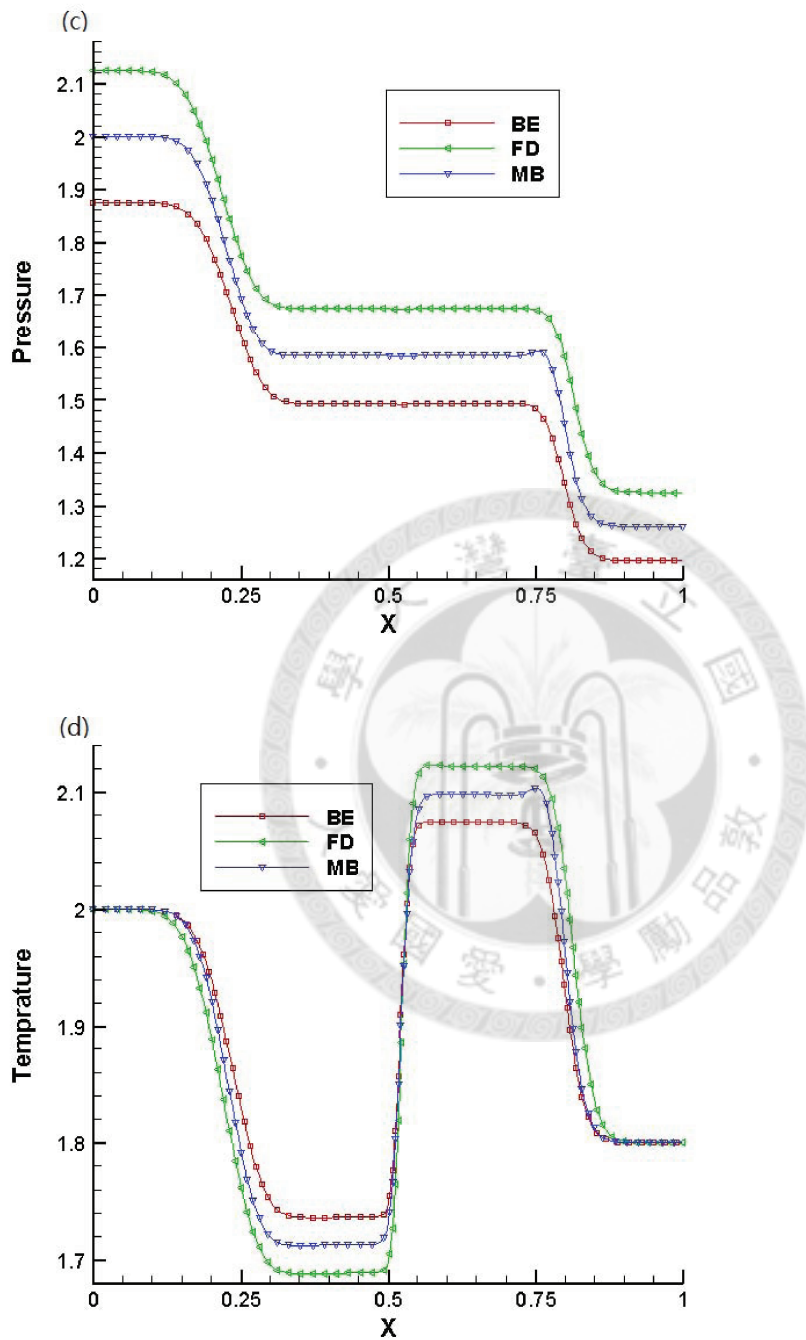
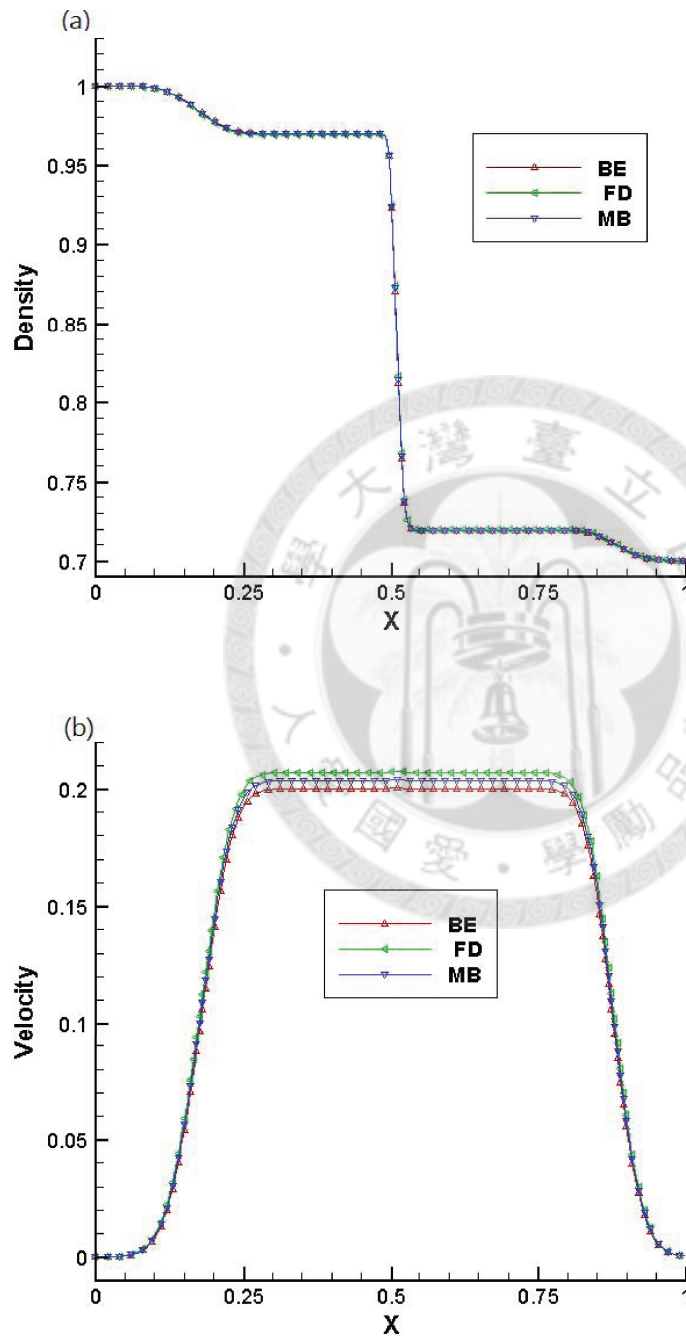


Figure 5.2: Shock tube flow in a quantum gas. The effect due to different particle statistics; Bose-Einstein: BE, Fermi-Dirac: FD, Maxwell-Boltzmann: MB. (a) Density, (b) Velocity, (c) Pressure, (d) Temperature.



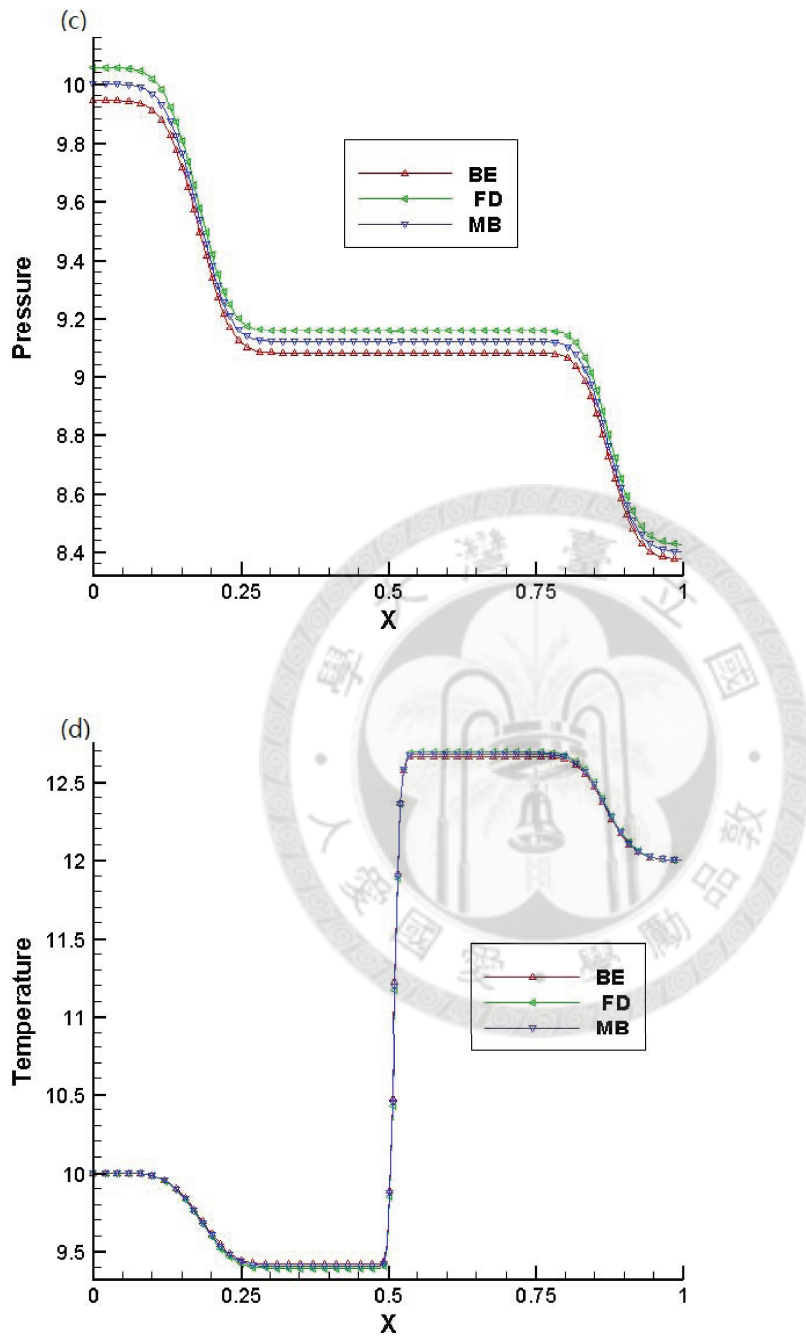


Figure 5.3: Shock tube flow in a quantum gas. The effect in high temperature limit; Bose-Einstein: BE, Fermi-Dirac: FD, Maxwell-Boltzmann: MB. (a) Density, (b) Velocity, (c) Pressure, (d) Temperature.

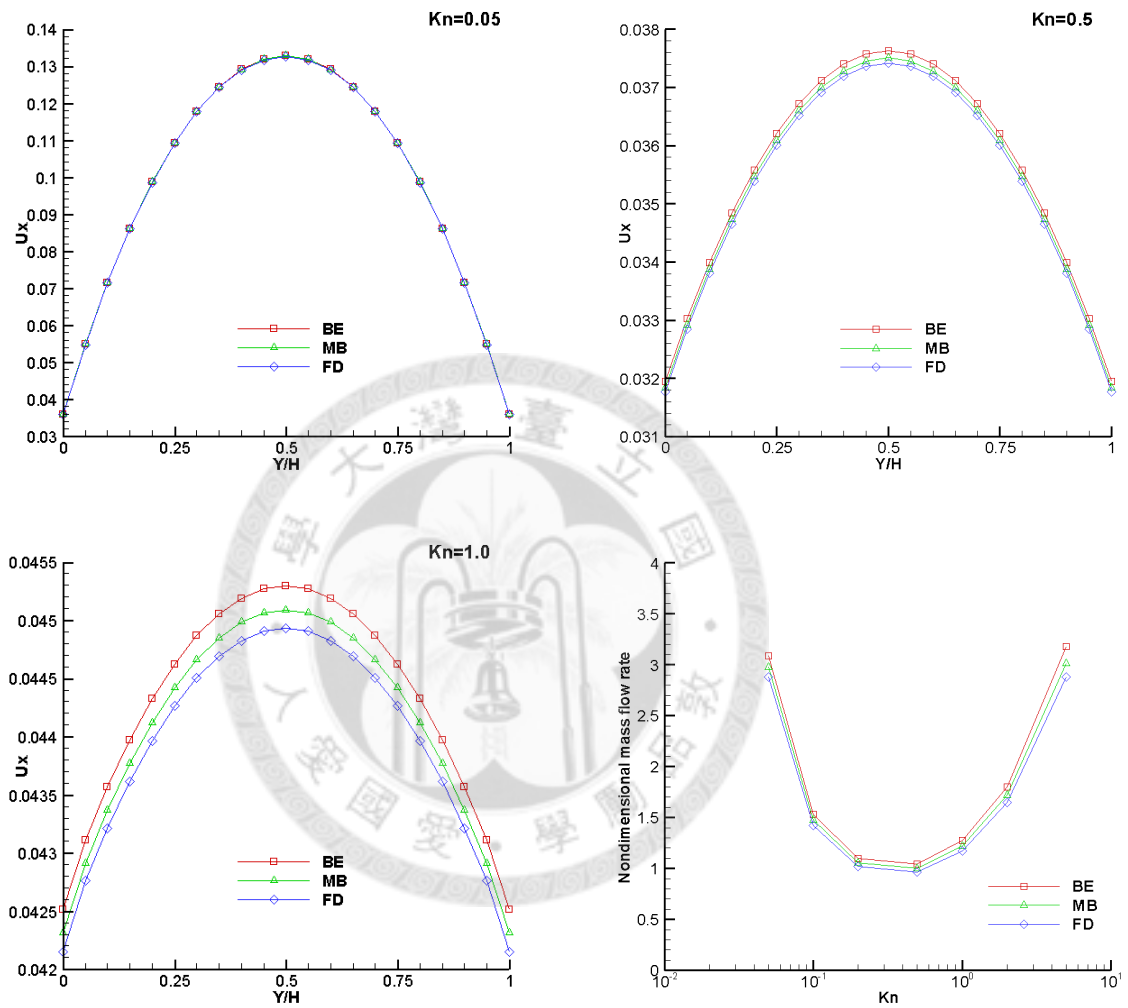


Figure 5.4: Velocity profiles in a channel flow of gases of arbitrary statistics (gas with  $z = 0.2$ ). (a)  $Kn=0.05$ , (b)  $Kn=0.5$ , (c)  $Kn=1$ . (d) Normalized mass flux in a channel flow as a function of  $Kn$  number.

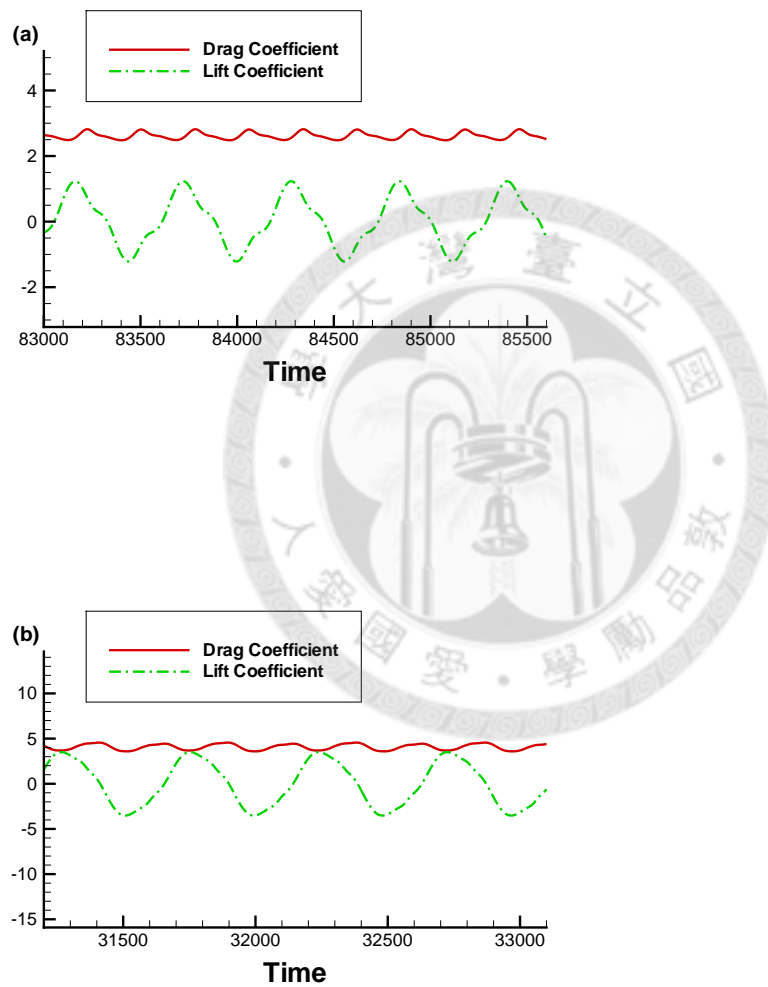


Figure 5.5: Drag and lift coefficients in classical limit. (a)  $Re = 100$ , (b)  $Re = 500$ .



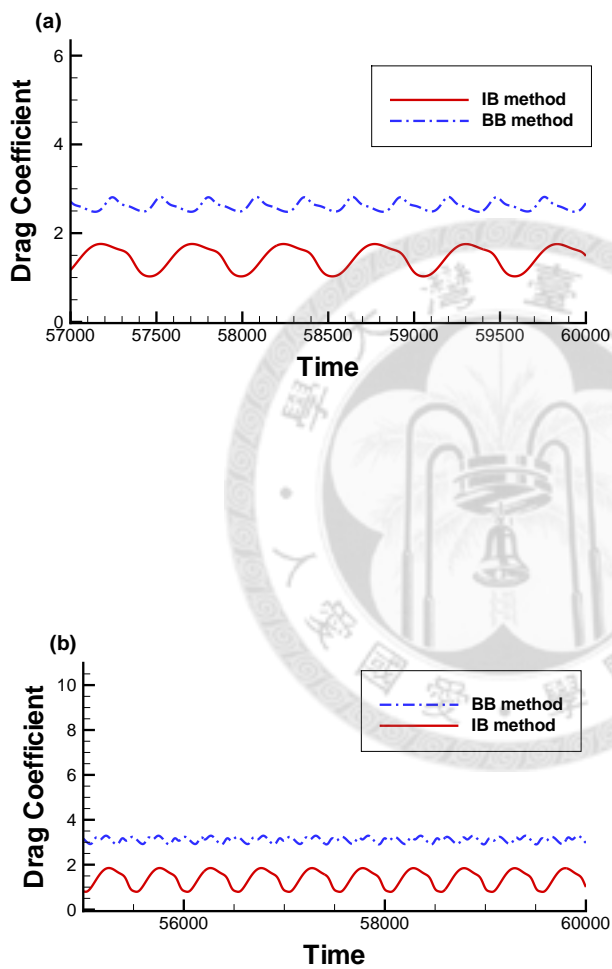


Figure 5.6: Drag and lift coefficients in different boundary conditions (immersed boundary condition and bounce back boundary condition). (a)  $Re = 100$ , (b)  $Re = 200$ .

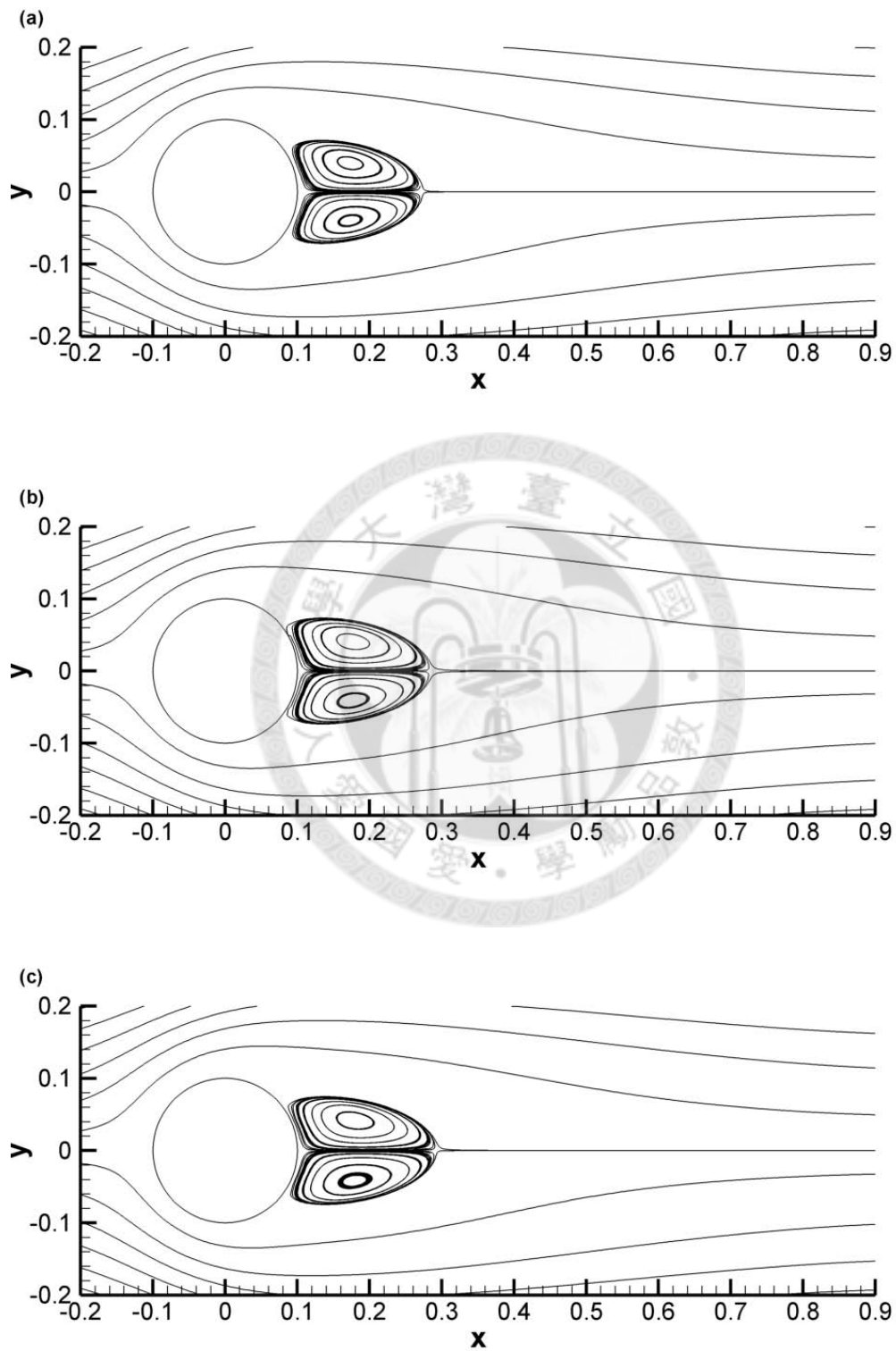


Figure 5.7: Streamlines of uniform flow over a circular cylinder in a quantum gas with  $z = 0.2$  and  $Re_\infty = 20$ . (a) BE gas, (b) MB gas, (c) FD gas.

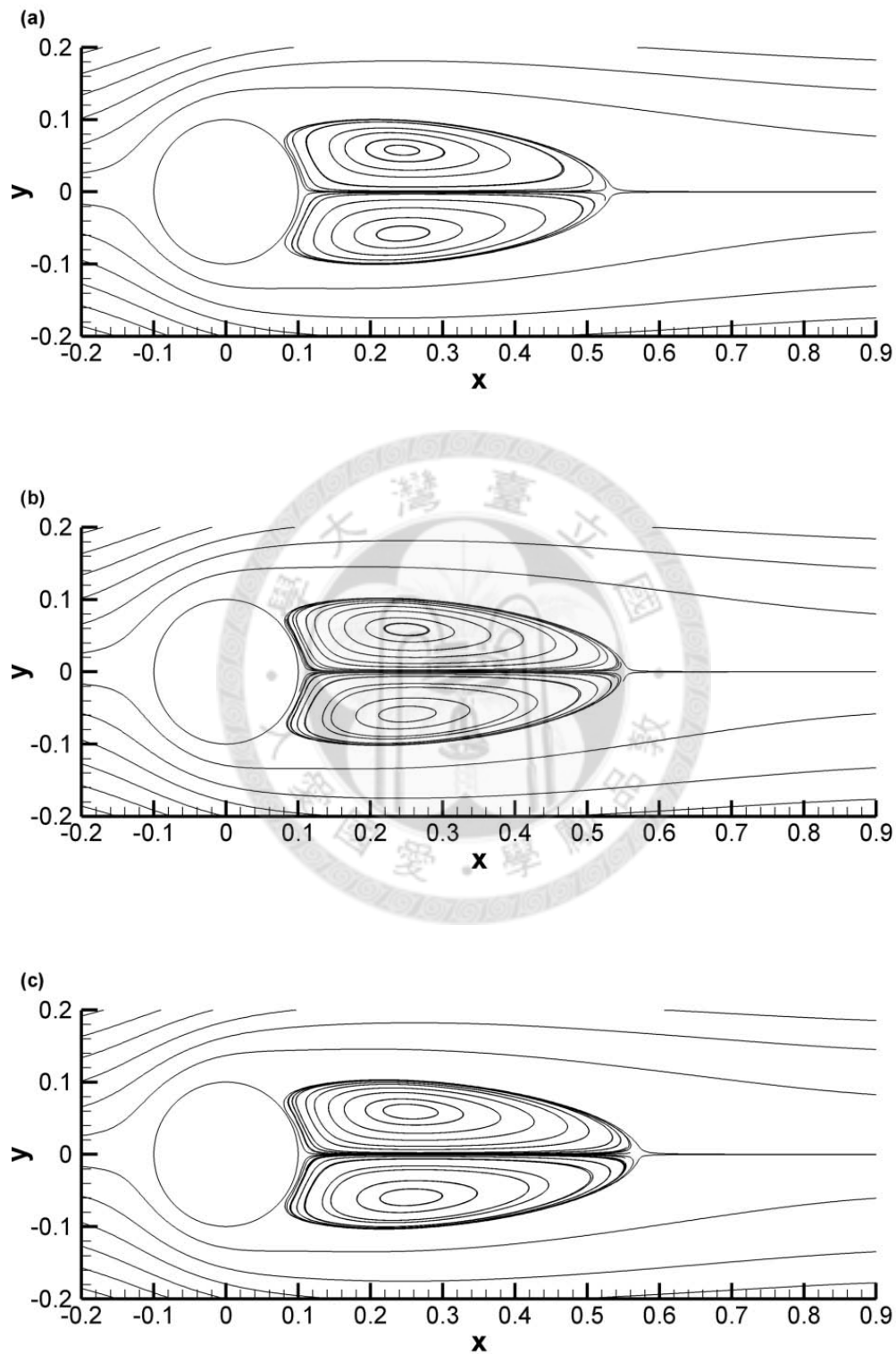


Figure 5.8: Streamlines of uniform flow over a circular cylinder in a quantum gas with  $z = 0.2$  and  $Re_\infty = 40$ . (a) BE gas, (b) MB gas, (c) FD gas.

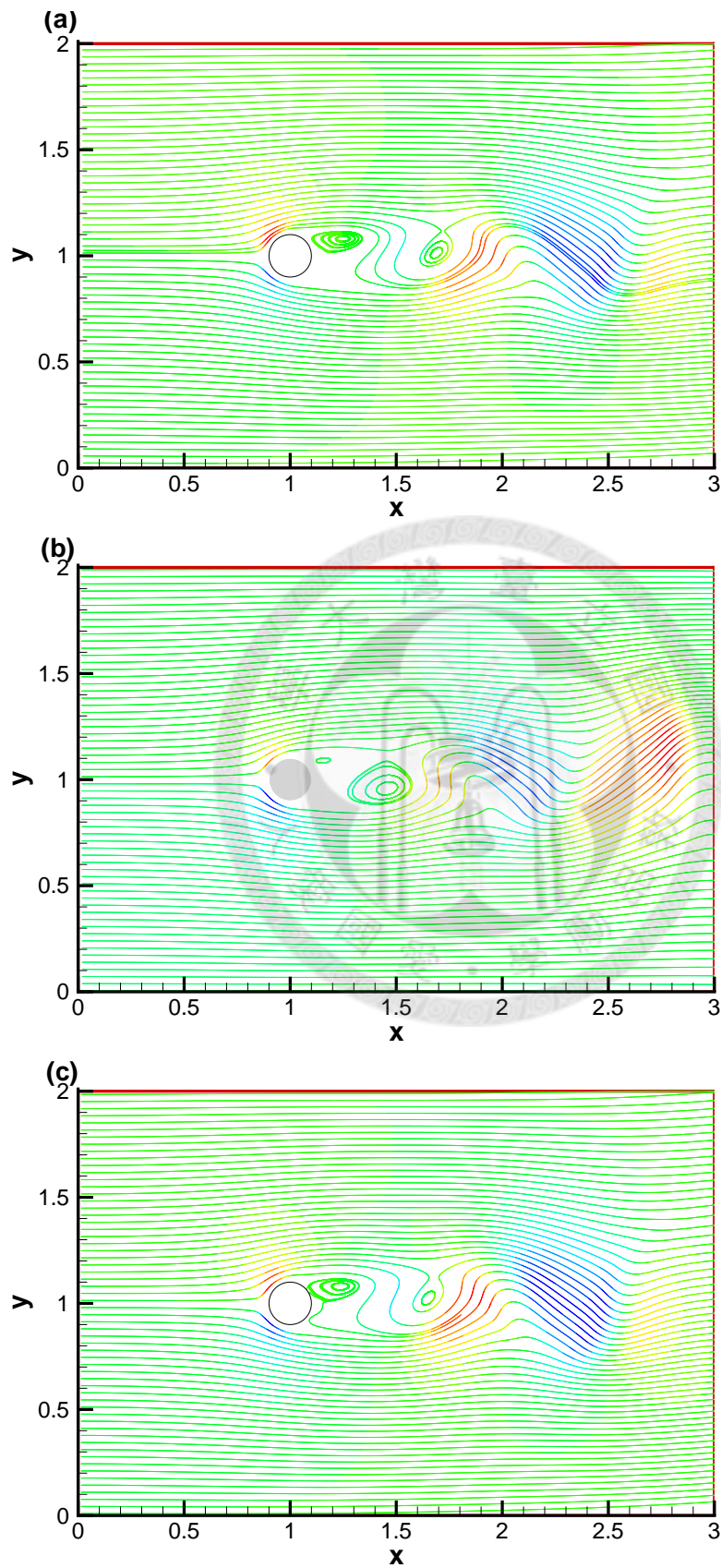


Figure 5.9: Streamlines of uniform flow over a circular cylinder in a quantum gas with  $z = 0.2$  and  $Re_\infty = 200$ . (a) BE gas, (b) MB gas, (c) FD gas.

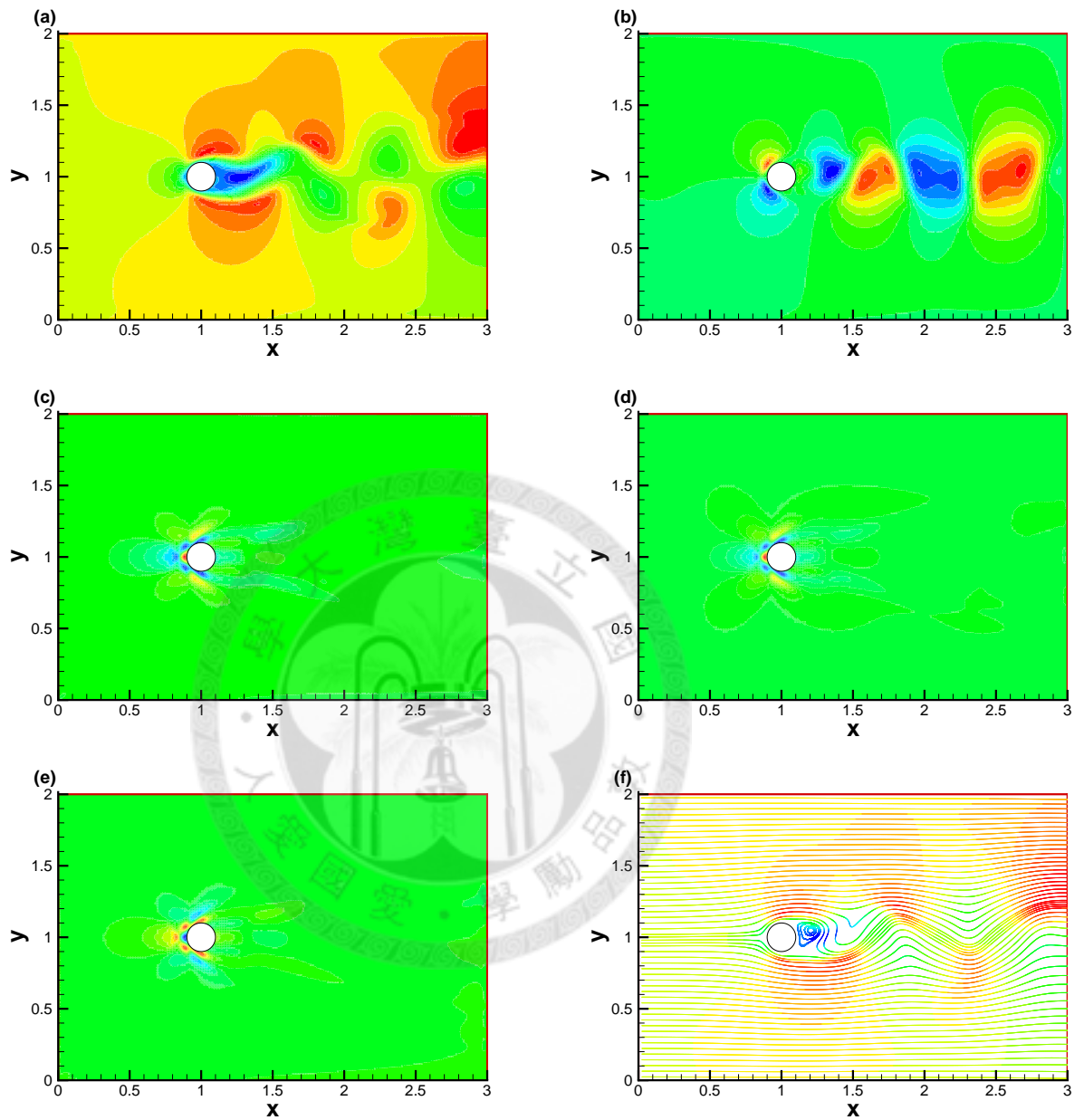


Figure 5.10: Different contours and streamlines of uniform flow over a circular cylinder in a quantum gas in a classical limit with  $Re_\infty = 200$ , steps=94200. (a) X-direction velocity( $u_x$ ), (b) y-direction velocity( $u_y$ ), (c) fugacity( $z$ ), (d) density( $\rho$ ), (e) temperature( $\theta$ ), (f) streamlines.

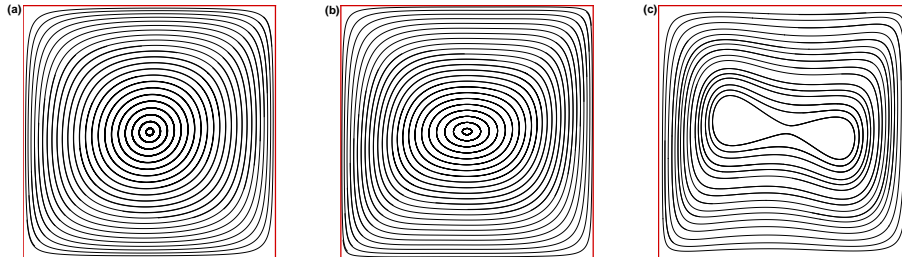


Figure 5.11: Streamlines for different Rayleigh numbers of natural convection.

(a)  $Ra = 10^3$ , (b)  $Ra = 10^4$ , (c)  $Ra = 10^5$ .

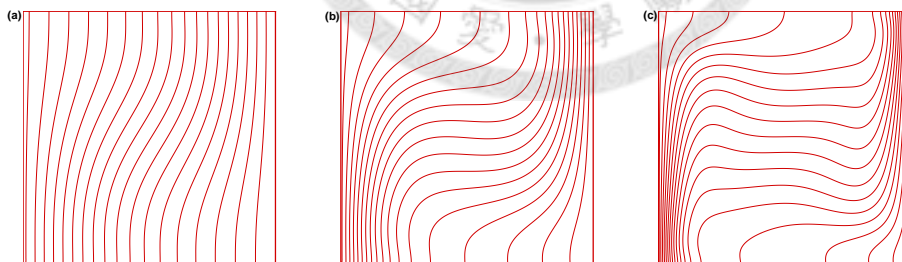


Figure 5.12: Isotherm lines for different Rayleigh numbers of natural convection.

(a)  $Ra = 10^3$ , (b)  $Ra = 10^4$ , (c)  $Ra = 10^5$ .

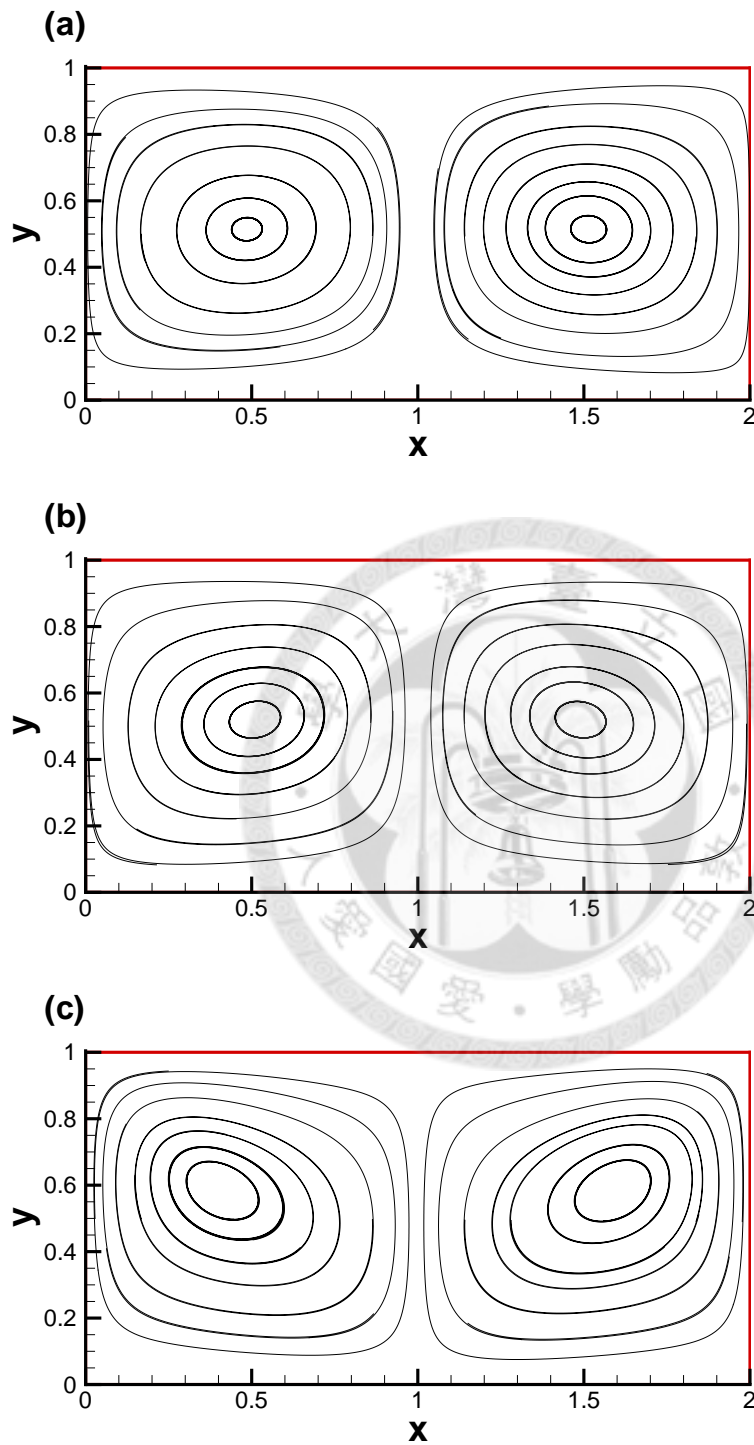


Figure 5.13: Streamlines of Rayleigh-Bénard convection for different Rayleigh numbers. (a)  $Ra = 4000$ , (b)  $Ra = 10000$ , (c)  $Ra = 50000$ .

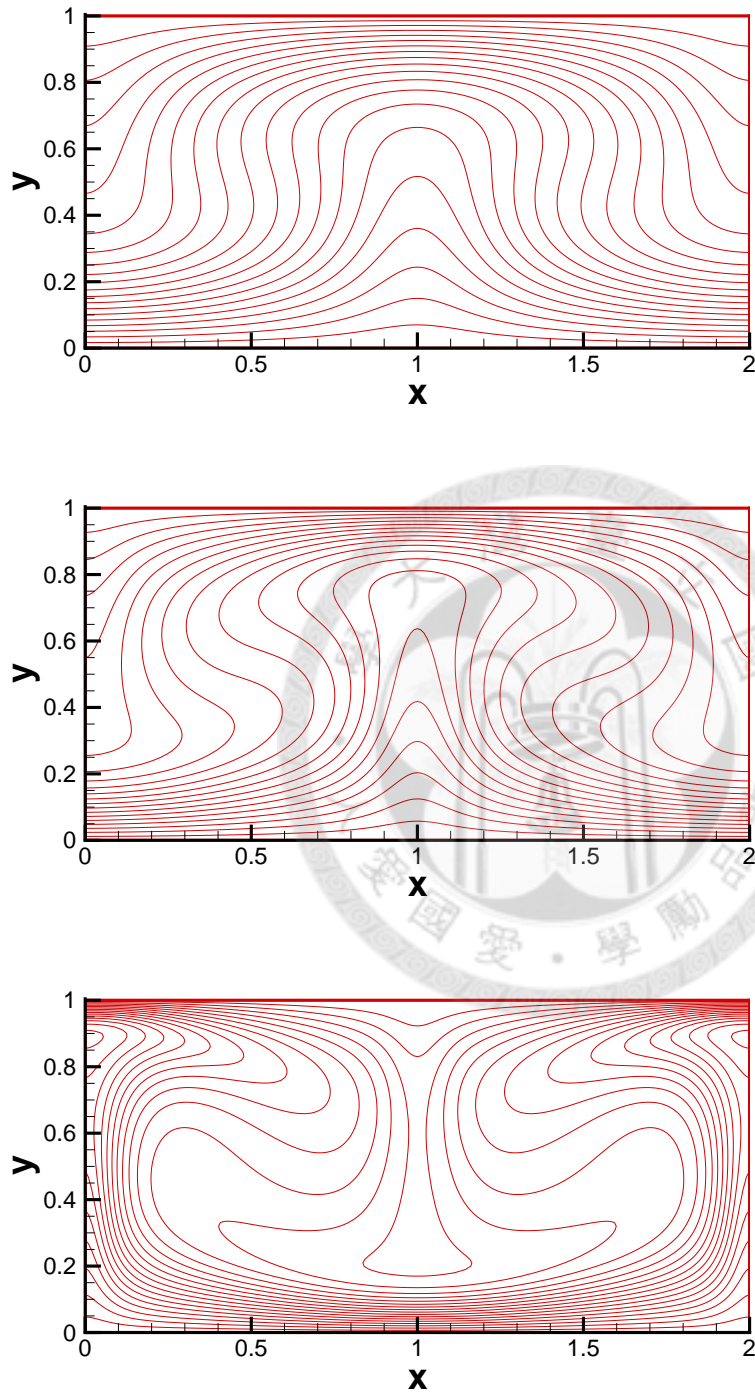


Figure 5.14: Isotherms of Rayleigh-Bénard convection for different Rayleigh numbers. (a)  $Ra = 4000$ , (b)  $Ra = 10000$ , (c)  $Ra = 50000$ .



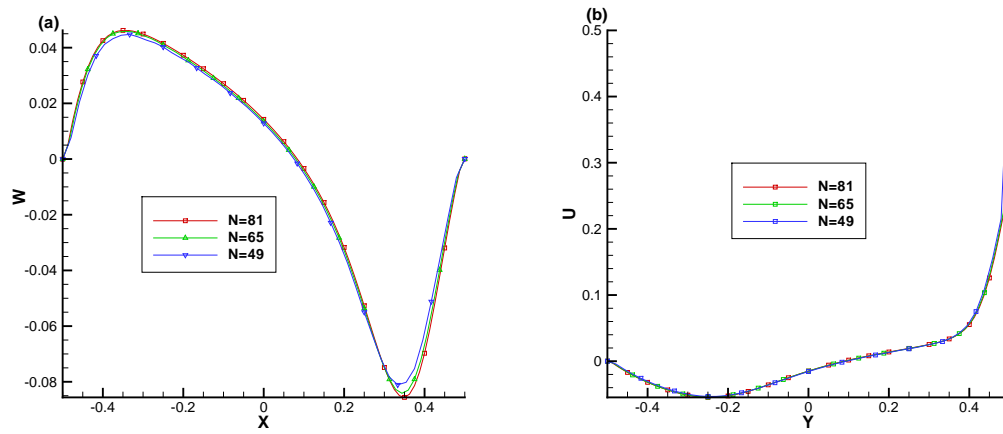


Figure 5.15: Grid refinement of three dimensional lid driven simulation,  $Re = 400$  for two different centerlines. (a)  $(x, 0, 0)$ , (b)  $(0, 0, z)$ .

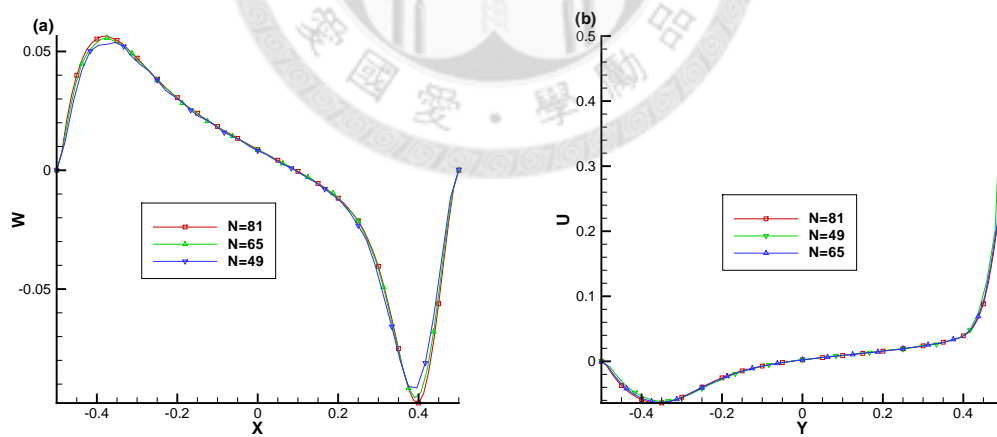


Figure 5.16: Grid refinement of three dimensional lid driven simulation,  $Re = 1000$  for two different centerlines. (a)  $(x, 0, 0)$ , (b)  $(0, 0, z)$ .

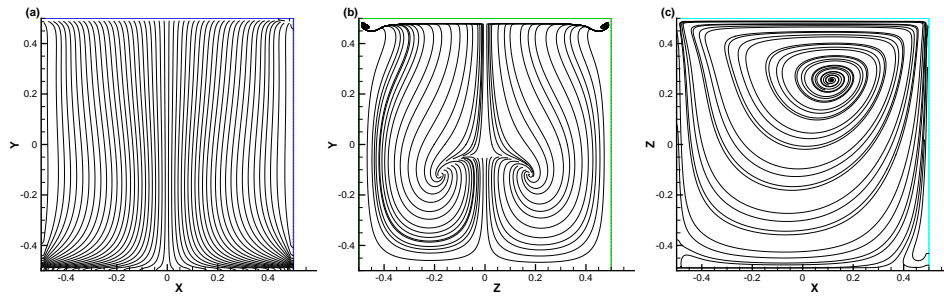


Figure 5.17: Streamlines of MB statistics in three mid-planes,  $Re = 100$ . (a) xy planes, (b) zy planes, (c) xz planes.

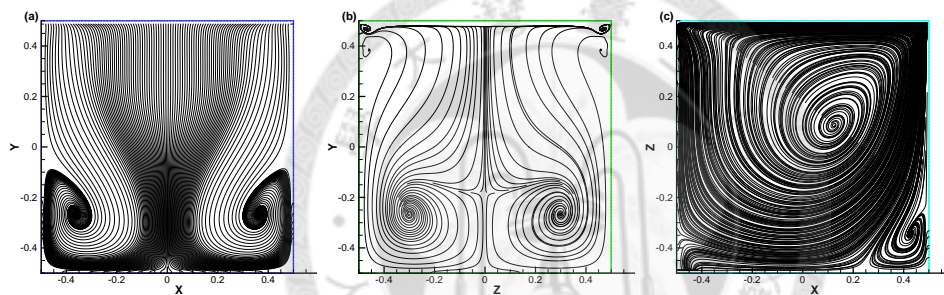


Figure 5.18: Streamlines of MB statistics in three mid-planes,  $Re = 400$ . (a) xy planes, (b) yz planes, (c) xz planes.

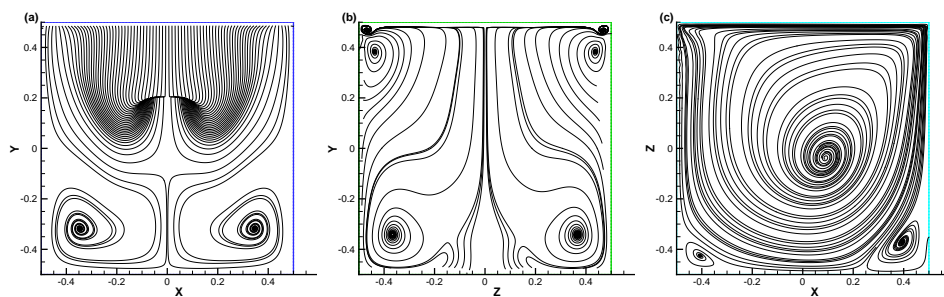


Figure 5.19: Streamlines of MB statistics in three mid-planes,  $Re = 1000$ . (a) xy planes, (b) yz planes, (c) xz planes.

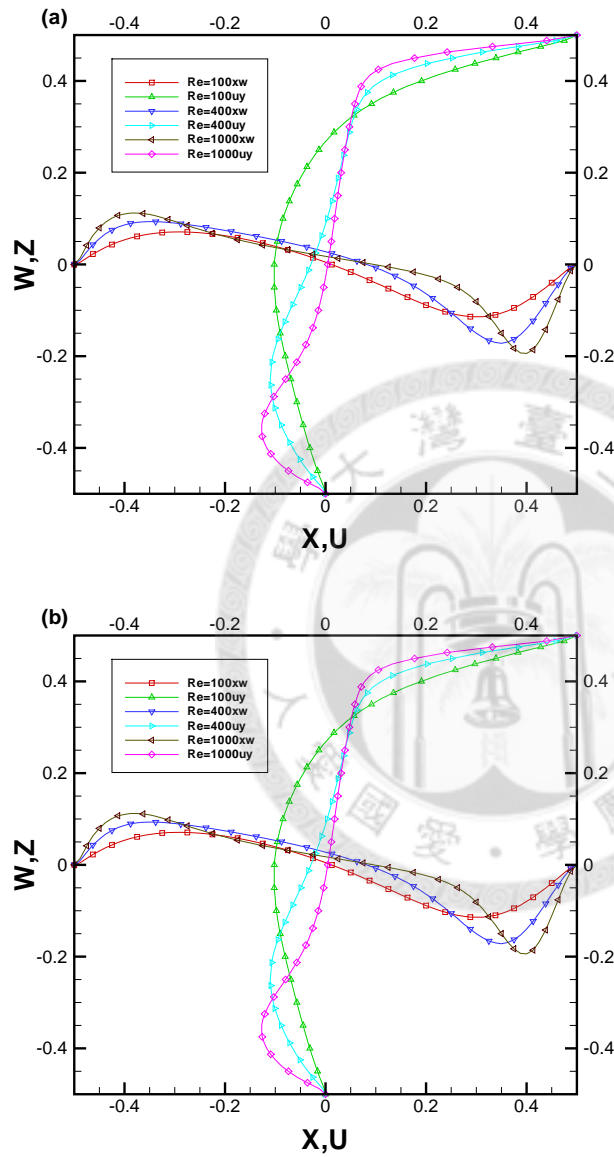


Figure 5.20: Centerlines velocity of classical and semiclassical model. (a) Classical, (b) semiclassical

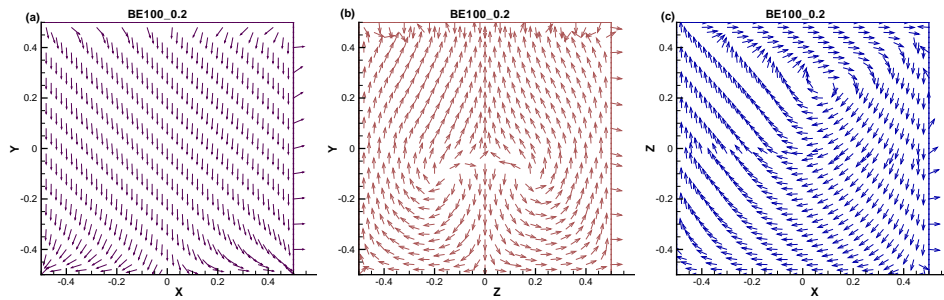


Figure 5.21: Velocity vectors of BE statistics in three mid-planes,  $Re = 100$ ,  $z = 0.2$ . (a) xy planes, (b) yz planes, (c) xz planes.

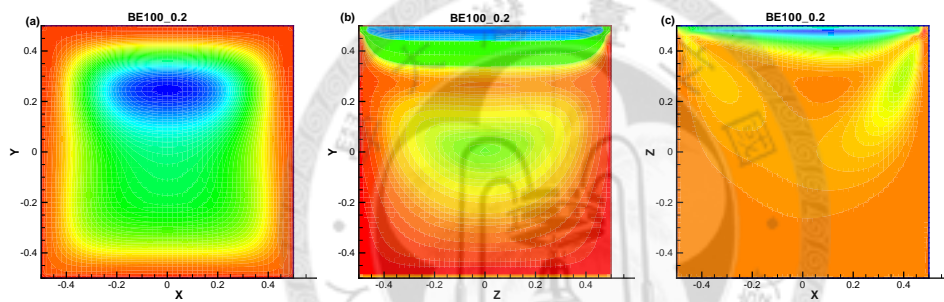


Figure 5.22: Pressure contours of BE statistics in three mid-planes,  $Re = 100$ ,  $z = 0.2$ . (a) xy planes, (b) yz planes, (c) xz planes.

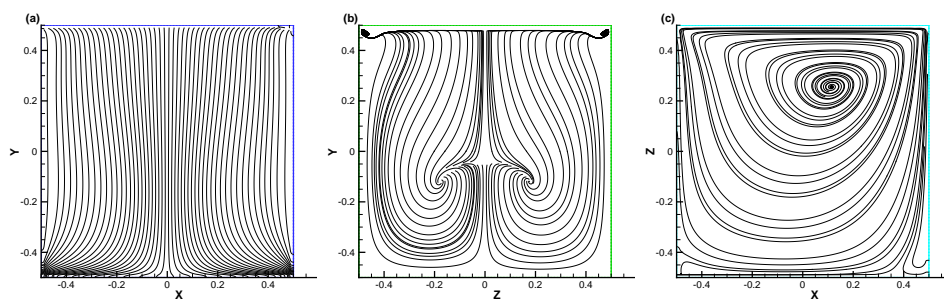


Figure 5.23: Streamlines patterns of BE statistics in three mid-planes,  $Re = 100$ ,  $z = 0.2$ . (a) xy planes, (b) yz planes, (c) xz planes.

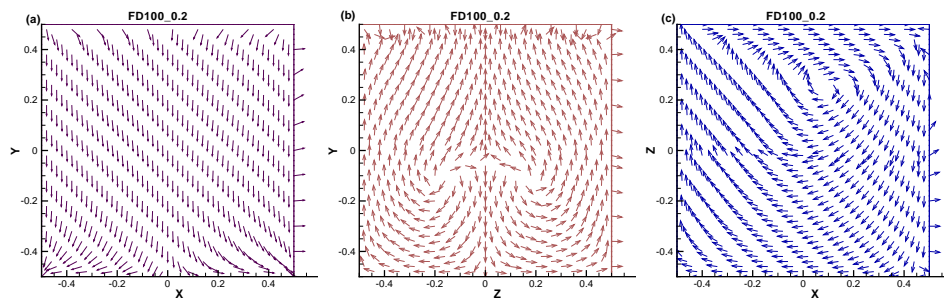


Figure 5.24: Velocity vectors of FD statistics in three mid-planes,  $Re = 100$ ,  $z = 0.2$ . (a) xy planes, (b) yz planes, (c) xz planes.

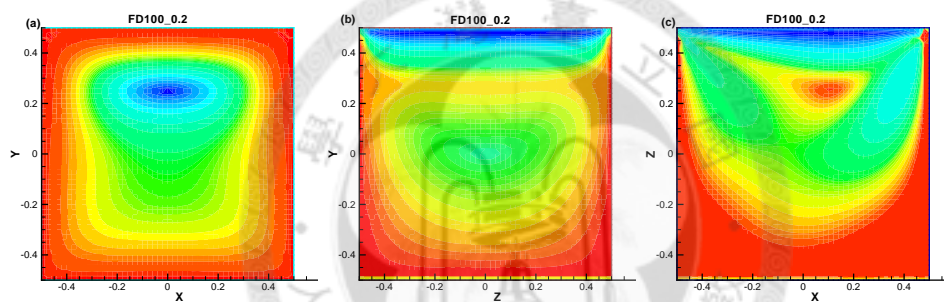


Figure 5.25: Pressure contours of FD statistics in three mid-planes,  $Re = 100$ ,  $z = 0.2$ . (a) xy planes, (b) yz planes, (c) xz planes.

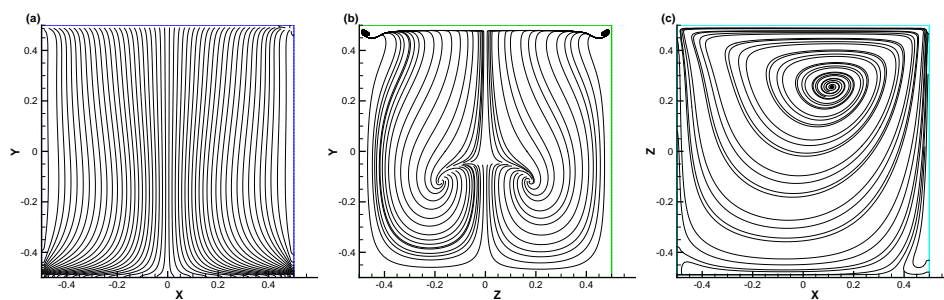


Figure 5.26: Streamlines patterns of FD statistics in three mid-planes,  $Re = 100$ ,  $z = 0.2$ . (a) xy planes, (b) yz planes, (c) xz planes.



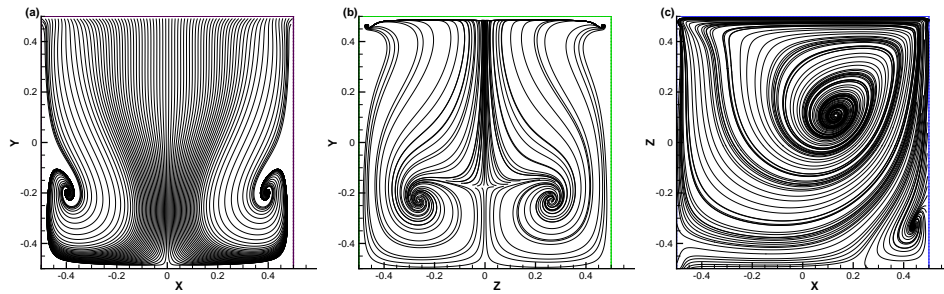


Figure 5.27: Streamlines patters of FD statistics in three mid-planes,  $Re = 400$ ,  $z = 0.2$ . (a) xy planes, (b) yz planes, (c) xz planes.

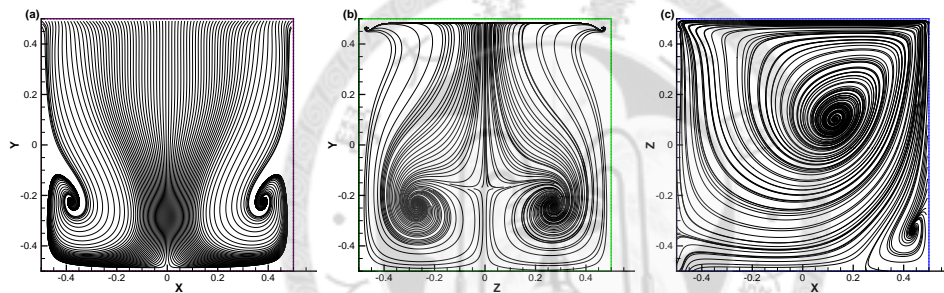


Figure 5.28: Streamlines patters of BE statistics in three mid-planes,  $Re = 400$ ,  $z = 0.2$ . (a) xy planes, (b) yz planes, (c) xz planes.

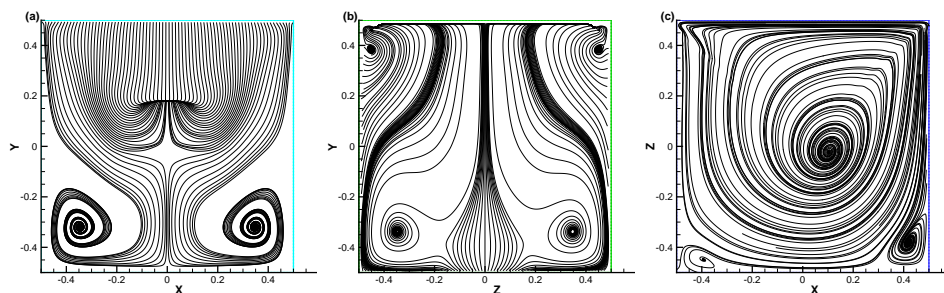


Figure 5.29: Streamlines patters of FD statistics in three mid-planes,  $Re = 1000$ ,  $z = 0.2$ . (a) xy planes, (b) yz planes, (c) xz planes.

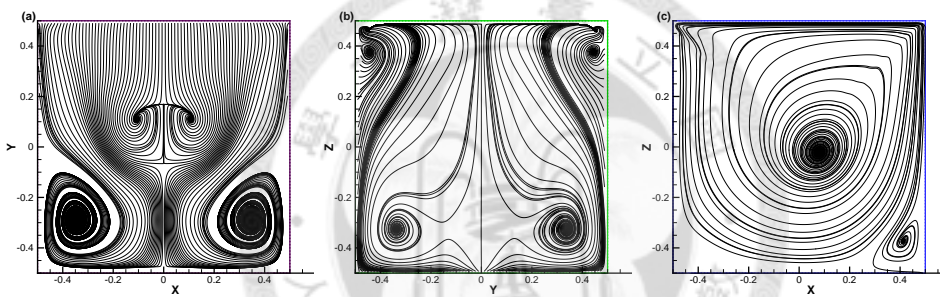


Figure 5.30: Streamlines patterns of BE statistics in three mid-planes,  $Re = 1000$ ,  $z = 0.2$ . (a) xy planes, (b) yz planes, (c) xz planes.

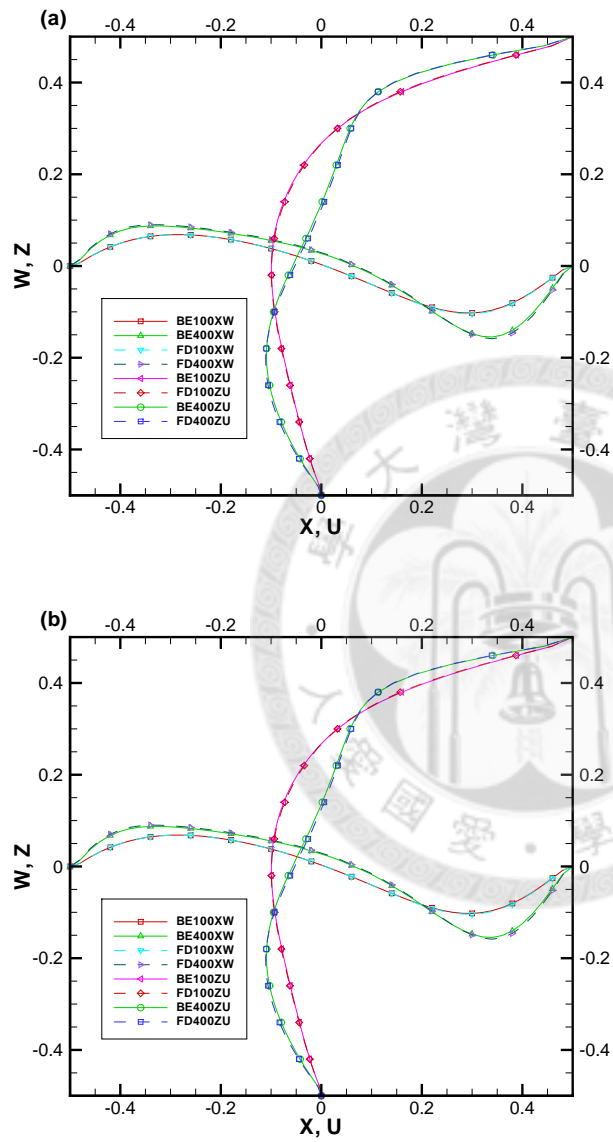


Figure 5.31: Centerlines velocity of different quantum statistics,  $z = 0.1$  and  $z = 0.2$



# Conclusions and Future Work

---

## Contents

---

<b>6.1 Accomplishments</b> . . . . .	<b>101</b>
<b>6.2 Future Work</b> . . . . .	<b>103</b>

---

## 6.1 Accomplishments

In this dissertation, I have derived a general LB method which is called semiclassical LB method, and also made several contributions to the analysis of this method. This method is suitable for analyzing dilute quantum gas hydrodynamics and beyond. The present work is different from Boltzmann equation with quantum collision (Wigner distribution, density matrix), or quantum LB method. It solves the Boltzmann equation with BGK approximation together with BE distribution function and FD distribution function on phase space. The following is a summary of my major accomplishments.

1. We proposed a new semiclassical LB method which is obtained by first projecting the UUB-BGK equations onto the Hermite polynomial basis as pioneered by Grad [5][18]. The equilibrium distribution of LB equations for simulating hydrodynamical flows is derived through expanding BE (or FD) distribution function onto Hermite polynomial basis which is

done in a *a priori* manner and is free of usual *ad hoc* parameter-matching. Finite order expansions up to third order are considered and compared with traditional classical LB-BGK methods. The present work can be considered as an extension and generalization of the work of Shan and He [17] for quantum gas and share equally many desirable properties claimed by them, such as free of drawbacks in conventional higher-order hydrodynamic formulations. The present work recovers the classical results in [17] when the classical limit is taken. The hydrodynamics beyond the semiclassical Navier-Stokes equations can also be explored if higher than third order expansion is taken. Lastly, the present development of semiclassical LB method provides a unified framework for a parallel treatment of gas systems of particles of arbitrary statistics.

2. The present construction provides quantum Navier-Stokes order solution and beyond. Several computational examples of both BE and FD gases in one dimensional shock tube flow have been simulated and the results exhibit similar flow characteristics of their corresponding classical cases. The effect of quantum statistics on the hydrodynamics is clearly delineated.
3. Several computational examples of both BE and FD gases in two-dimensional microchannel flows have been simulated over Knudsen numbers representing the Knudsen, slip and Poiseuille regions. The Knudsen minimum phenomena is captured for all the gas statistics. Moreover, this semiclassical LB method recovers the classical results when the classical limit is taken.
4. In two dimensional flows over circular cylinder, the length of vortex after the circular cylinder are different from different quantum statistics. The

drag coefficient and lift coefficient are also provided, It is always shown that the one in classical limit is within the other quantum statistics.

5. In three dimensional lid driven cavity flow, the velocity vectors and the velocity of the centerlines of three slices are shown. The one in classical limit matches with previous works, it validates the semiclassical LB method in classical limit.

## 6.2 Future Work

Since the semiclassical LB methods have been derived, however, there exist some works to do in the future.

1. The experimental results for quantum hydrodynamics are rare and we only validate our results with the corresponding classical counterpart in classical limit. There are some experiments dealing with quantum fluids in microchannel flow. For example, in [106], first observation of the Knudsen minimum in normal liquid  $^3\text{He}$  was reported. Also, Knudsen minima has been found for phonons at different Knudsen numbers have been reported, see [107][108]. The present work should be compared with quantum fluid experiments and also validated according to more experiments.
2. A new coupled thermal LB method based on double distribution functions with two relaxation times is derived for thermohydrodynamic Navier-Stokes equations in Appendix 2. The method is obtained by first projecting the governing two relaxation kinetic model equations onto the Hermite polynomial basis as pioneered by [79] and [16]. And the coupled thermal LB method should be possibly used for developing double

distribution function semiclassical LB method.

3. The present work is developed based on expanding the distribution function (including equilibrium distribution function  $f^{eq}$ ) onto Hermite polynomials. Although this strategy for building LB method attracts lots of attentions in recent years, there are still some criticisms concerning entropy and Galilean invariance on these procedures [115][116]. One of the disadvantages of expanding the equilibrium distribution function onto Hermite polynomials is that the roots of Hermite polynomials are irrational, the corresponding discrete velocities can not be fitted into a regular space filling lattice. Such that, the resulting off-lattice models make the exact space discretization of the advection step which is the major advantage of the LB methods broken. Another drawback is that the solution of projecting the equilibrium distribution function in a finite dimensional Hermite basis will lose the positivity of the distribution function in the truncation of Hermite polynomial expansions. One of the methods for solving these problems mentioned above is through the entropic formulation [117][118] which evaluates the Boltzmann H function at the nodes of the given quadrature instead of equilibrium distribution function. And in recent years, this idea is extended to derive a generalized Maxwell distribution function for LB method [119], in that work, all the previously introduced equilibria for LB are found as special cases of the generalized Maxwellian. Moreover, in [120] taking advantage of the closed-form generalized Maxwell distribution function and splitting the relaxation to the equilibrium in two steps, they proposed an entropic quasiequilibrium kinetic model for the simulation of low Mach number flows. The future development of semiclassical LB method may follow

the new trend of LB method.





# Nomenclature

---

$n$	number density
$\rho$	density, $Kg/m^3$
$\mu$	viscosity, or chemical potential
$\mathbf{c}$	lattice velocity
$c_s$	speed of sound
$D$	dimension of system
$\xi_i$	lattice streaming vector in $i$ direction
$e$	kinetic energy
$F$	external force
$f$	distribution function
$g$	acceleration due to gravity
$H$	height, m
$p$	pressure
$Pr$	Prandtl number
$q$	heat flux vector
$\mathbf{x}$	position vector
$Ra$	Rayleigh number
$U$	maximum velocity at the inlet
$U_0$	top lid velocity
$\mathbf{u}$	fluid velocity, $ms^{-1}$
$u, v, w$	x, y and z components of flow velocity

$V$	discrete velocity space
$\Pi_{ij}$	momentum stress tensor
$m$	mass, kg
$t$	time, s
$T$	temperature, K
$\delta_x$	lattice spacing, m
$\delta_t$	time step, s

### *Subscripts*

$i, j, k$	Cartesian coordinate system Greek symbols
$x, y, z$	Cartesian coordinate system Greek symbols
$a$	velocity component

### *Superscripts*

$eq$	equilibrium distribution function
$(0)$	equilibrium distribution function after discretizing velocity space
$N$	order of the discretized equilibrium distribution function
$Q$	semiclassical distribution function
$C$	classical distribution function

### *Abbreviations*

LB	Lattice Boltzmann
WKB	Wentzel-Kramers-Brillouin
UUB	Uehling-Uhlenbeck-Boltzmann
BGK	Bhatnagar-Gross-Krook
FD	Fermi-Dirac
BE	Bose-Einstein



---

MB	Maxwell-Boltzmann
DdQq	d Dimension, q velocity





# Chapman-Enskog Analysis of semiclassical LB method

---

## B.1 Chapman-Enskog Analysis of Single Relaxation Time semiclassical LB method

In this section, the generic evolution equation of single relaxation time semiclassical LB method is inspected by means of a Chapman-Enskog analysis. In LB method, the choice of lattice types is very important and it affects the accuracy and stability of LB simulation. The lattice must verify some symmetry conditions to yield the desired asymptotic PDE. It requires appropriate lattice velocities  $\mathbf{c}_a$  and weights  $w_a$  in developing LB method such that the following relations are verified:

$$\begin{aligned}
 (a) \quad & \sum_a w_a = 1 \\
 (b) \quad & \sum_a w_a c_{ai} = 0 \\
 (c) \quad & \sum_a w_a c_{ai} c_{aj} = c_s^2 \delta_{ij} \\
 (d) \quad & \sum_a w_a c_{ai} c_{aj} c_{ak} = 0 \\
 (e) \quad & \sum_a w_a c_{ai} c_{aj} c_{ak} c_{al} = c_s^4 (\delta_{ij} \delta_{kl} + \delta_{ik} \delta_{lj} + \delta_{il} \delta_{kj})
 \end{aligned} \tag{B.1}$$

Now, the LB-BGK equation (3.4) and semiclassical equilibria (3.38) up to third order are used and listed below.

$$f_a(\mathbf{x} + \boldsymbol{\zeta}_a \delta_t, t + \delta_t) - f_a(\mathbf{x}, t) = -\frac{(f_a - f_a^{(0)})}{\tau} \quad (\text{B.2})$$

$$f_a^{(0)} = w_a n \left\{ 1 + \boldsymbol{\zeta}_a \cdot \mathbf{u} + \frac{1}{2} [(\mathbf{u} \cdot \boldsymbol{\zeta}_a)^2 - u^2 + (T \frac{g_{5/2}(z)}{g_{3/2}(z)} - 1)(\boldsymbol{\zeta}_a^2 - D)] \right\} \\ + \frac{\boldsymbol{\zeta}_a \cdot \mathbf{u}}{6} [(\mathbf{u} \cdot \boldsymbol{\zeta}_a)^2 - 3u^2 + 3(T \frac{g_{5/2}(z)}{g_{3/2}(z)} - 1)(\boldsymbol{\zeta}_a^2 - D - 2)] \quad (\text{B.3})$$

First, computing all the following summations by the semiclassical equilibria with the aids of (B.1) as:

$$\sum_a f_a^{(0)} = n \quad (\text{B.4})$$

$$\sum_a \zeta_{ai} f_a^{(0)} = n u_i \quad (\text{B.5})$$

$$\sum_a \zeta_{ai} \zeta_{aj} f_a^{(0)} = n [T \frac{g_{5/2}}{g_{3/2}} \delta_{ij} + u_i u_j] \quad (\text{B.6})$$

$$\sum_a \zeta_{ai} \zeta_{aj} \zeta_{ak} f_a^{(0)} = n T \frac{g_{5/2}}{g_{3/2}} [\delta_{ij} u_k + \delta_{kj} u_i + \delta_{ki} u_j] \quad (\text{B.7})$$

Introducing the following expansions

$$f_a(\mathbf{x} + \boldsymbol{\zeta}_a \delta_t, t + \delta_t) = \sum_{n=0}^{\infty} \frac{\varepsilon^n}{n!} (\partial_t + \boldsymbol{\zeta}_a \cdot \nabla) f_a \simeq f_a^0 + \varepsilon f_a^1 + \varepsilon^2 f_a^2 + \dots \quad (\text{B.8})$$

$$t_1 = t \varepsilon \quad (\text{B.9})$$

$$t_2 = t \varepsilon^2 \quad (\text{B.10})$$

$$(i, j, k)_1 = (i, j, k) \varepsilon \quad (\text{B.11})$$

$$\partial_t = \varepsilon \partial_{t_1} + \varepsilon^2 \partial_{t_2} \quad (\text{B.12})$$

The above expressions of the derivatives are substituted into (B.2), and

terms involving different orders of  $\varepsilon$  are separated as:

$$0 = \frac{-1}{\tau}[f_a^0 - f_a^{(0)}] \quad (\text{B.13})$$

$$\partial_{t_1} f_a^0 + \zeta_{aj} \partial_{j_1} f_a^0 = -\frac{1}{\tau} f_a^1 \quad (\text{B.14})$$

$$\partial_{t_2} f_a^0 + \left(\frac{2\tau - 1}{2\tau}\right)(\partial_{t_1} f_a^1 + \zeta_{aj} \partial_{j_1} f_a^1) = -\frac{1}{\tau} f_a^2 \quad (\text{B.15})$$

After summation with respect to  $a$ , the three different order mass conservation equations are recovered below:

$$-\frac{1}{\tau} \sum_a [f_a^0 - f_a^{(0)}] = 0 \quad (\text{B.16})$$

$$\partial_{t_1} \sum_a f_a^0 + \partial_{j_1} \sum_a f_a^0 \zeta_{aj} = -\frac{1}{\tau} \sum_a f_a^1 \quad (\text{B.17})$$

$$\partial_{t_2} \sum_a f_a^0 + \left(\frac{2\tau - 1}{2\tau}\right)(\partial_{t_1} \sum_a f_a^1 + \partial_{j_1} \sum_a f_a^1 \zeta_{aj}) = -\frac{1}{\tau} \sum_a f_a^2 \quad (\text{B.18})$$

After multiplying with  $m\zeta_{ai}$  and summing with respect to  $a$ , the three different order momentum conservation equations are recovered below:

$$-\frac{1}{\tau} \sum_a m[f_a^0 - f_a^{(0)}] = 0 \quad (\text{B.19})$$

$$\partial_{t_1} \sum_a m f_a^0 \zeta_{ai} + \partial_{j_1} \sum_a m f_a^0 \zeta_{ai} \zeta_{aj} = -\frac{1}{\tau} \sum_a m f_a^1 \zeta_{ai} \quad (\text{B.20})$$

$$\begin{aligned} \partial_{t_2} \sum_a m f_a^0 \zeta_{ai} + \left(\frac{2\tau - 1}{2\tau}\right)(\partial_{t_1} \sum_a m f_a^1 \zeta_{ai} + \partial_{j_1} \sum_a m f_a^1 \zeta_{ai} \zeta_{aj}) \\ = -\frac{1}{\tau} \sum_a m f_a^2 \zeta_{ai} \end{aligned} \quad (\text{B.21})$$

The local number density  $n$  and the local velocity  $\mathbf{u}$  are

$$\begin{aligned} n &= \sum_a f_a = \sum_a f_a^{(0)} \\ \mathbf{u} &= \frac{1}{n} \sum_a f_a \zeta_a = \frac{1}{n} \sum_a f_a^{(0)} \zeta_a \end{aligned}$$

From zeroth-order mass and momentum equations (B.16) and (B.19), we get

$$\sum_a f_a^l = 0 \quad (\text{B.22})$$

$$\sum_a f_a^l \zeta_a = 0, (l \geq 1) \quad (\text{B.23})$$

For deriving the Navier-Stokes equation, we add the first and second order momentum equations (B.20) and (B.21).

$$\partial_t(\rho u_i) + \partial_j P_{ij} = 0 \quad (\text{B.24})$$

where the momentum flux density tensor  $P_{ij}^{(1)}$  is given by

$$P_{ij} = P_{ij}^0 + \varepsilon \left( \frac{2\tau - 1}{2\tau} \right) P_{ij}^1 \quad (\text{B.25})$$

$$P_{ij}^0 = m \sum_a \zeta_{ai} \zeta_{aj} f_a^0 = p \delta_{ij} + \rho u_i u_j \quad (\text{B.26})$$

$$P_{ij}^1 = m \sum_a \zeta_{ai} \zeta_{aj} f_a^1 = -\tau \rho T \frac{g_{\frac{5}{2}}}{g_{\frac{3}{2}}} [\partial_{i_1} u_j + \partial_{j_1} u_i] \quad (\text{B.27})$$

The  $P_{ij}^{(1)}$  is calculated as:

$$\begin{aligned} P_{ij}^1 &= m \sum_a \zeta_{ai} \zeta_{aj} (-\tau \partial_{t_1} f_a^{(0)} - \tau \zeta_{ak} \partial_{k_1} f_a^0) = -\tau m \partial_{t_1} \\ & [T \frac{g_{\frac{5}{2}}}{g_{\frac{3}{2}}} n \delta_{ij} + \rho u_i u_j] - \tau m T \frac{g_{\frac{5}{2}}}{g_{\frac{3}{2}}} [\delta_{ij} \partial_{k_1} (n u_k) + \partial_{i_1} (n u_j) + \partial_{j_1} (n u_i)] = -\tau m \partial_{t_1} \\ & [T \frac{g_{\frac{5}{2}}}{g_{\frac{3}{2}}} n \delta_{ij} + \rho u_i u_j] - \tau m T \frac{g_{\frac{5}{2}}}{g_{\frac{3}{2}}} [\delta_{ij} (u_k \partial_{k_1} n + n \partial_{k_1} u_k) + (u_j \partial_{i_1} n + n \partial_{i_1} u_j) + (u_i \partial_{j_1} n + n \partial_{j_1} u_i)] \end{aligned} \quad (\text{B.28})$$

Then, we use (B.17) and (B.20) to get

$$\partial_{t_1} (n T \frac{g_{\frac{5}{2}}}{g_{\frac{3}{2}}}) = -T \frac{g_{\frac{5}{2}}}{g_{\frac{3}{2}}} \partial_{k_1} (n u_k) \quad (\text{B.29})$$

$$\begin{aligned} \partial_{t_1} (\rho u_i u_j) &= -T \frac{g_{\frac{5}{2}}}{g_{\frac{3}{2}}} [u_i \partial_{j_1} n + u_j \partial_{i_1} n] - \partial_{k_1} (u_i u_j u_k) \\ &\simeq -T \frac{g_{\frac{5}{2}}}{g_{\frac{3}{2}}} [u_i \partial_{j_1} n + u_j \partial_{i_1} n] \end{aligned} \quad (\text{B.30})$$

After putting (B.29) and (B.30) into (B.28), we can get (B.27). Finally, put (B.25),(B.26) and (B.27) into (B.24), we can get the final form of the momentum equation as

$$\partial_t(\rho u_i) + \partial_j(\rho u_i u_j) = -\partial_i p + \nu \partial_j[\rho \partial_i u_j + \rho \partial_j u_i] \quad (\text{B.31})$$

In symbolic notation the equation is

$$\partial_t(\rho \mathbf{u}) + \nabla \cdot (\rho \mathbf{u} \mathbf{u}) = -\nabla p + \nu \nabla \cdot [\rho \nabla \mathbf{u} + \rho (\nabla \mathbf{u})^T] \quad (\text{B.32})$$

The Navier-Stokes equation is recovered from this equation in the incompressible limit( $\partial_j u_j = 0$ ) or ( $\nabla \cdot \mathbf{u} = 0$ )

$$\partial_t u_i + u_j \partial_j u_i = -\frac{1}{\rho} \partial_i p + \nu \nabla^2 u_i \quad (\text{B.33})$$

$$\nu = \left(\tau - \frac{1}{2}\right) T \frac{g_{\frac{3}{2}}}{g_{\frac{3}{2}}} \quad (\text{B.34})$$

In symbolic notation the equation is

$$\partial_t \mathbf{u} + \mathbf{u} \cdot \nabla \mathbf{u} = -\frac{1}{\rho} \nabla p + \nu \nabla^2 \mathbf{u} \quad (\text{B.35})$$

Notice that  $\nabla \cdot (\nabla)^T = \nabla(\nabla \cdot \mathbf{u})$





# Derivations of Double Distribution Function LB method

---

In this chapter, we provide another possible way to solve the defects of single relaxation time semiclassical LB method from the ideas of developing thermal LB methods. Historically, the existing thermal LB methods can be classified into three categories. The first category is the passive-scalar approach [121] and the basic approach of this method is assuming that the viscous heat dissipation and the compression work done by the pressure can be neglected. As a consequence, the temperature can be simulated by a scalar density distribution function. The other two categories include the multi-speed distribution function approach [122][123][124] and the double distribution functions (DDF) approach [125][126][127][79]. The multi-speed approach is achieved by increasing the numbers of discrete velocities, then, the compressible Navier-Stokes equations could be recovered by those increasing degrees of freedom. Although the multi-speed approach can reach a thermal LB method, but it suffers from severe numerical instability and a narrow range of temperature variation. Moreover, the Prandtl number is usually fixed at constant. On the other hand, the DDF approach utilizes two distribution functions, one is for describing the velocity field, the other is for describing the internal energy or total energy. The DDF approach can achieve a better numerical stability than the multi-speed approach. We derive a thermal LB method which is

based on DDF method and should be suitable for developing DDF semiclassical LB method, in which both the Maxwell equilibrium velocity distribution function and a total energy equilibrium distribution function are expanded on tensor Hermite polynomials according to [79][16]. By choosing a proper reference velocity, the coupling of lattice velocities and the local temperature is avoided and the uncoupling process between velocity field and temperature field as done in [79] is not necessary, thus, some of limitations mentioned such as valid only to small temperature variation and transport coefficients are independent of temperature can be overcome. We also apply the Chapman-Enskog method to the present coupled thermal LB-BGK equations to obtain the relations between the relaxation time and viscosity and thermal conductivity. Hydrodynamics based on moments up to third order expansions are presented. Computational examples to illustrate the methods are given, and the results are carefully studied with the published result [114]. This new scheme provides a possible way for extending the current semiclassical LB method to double distribution functions semiclassical LB method.

## C.1 Two Relaxation Times Kinetic Model

In this section we briefly describe the coupled kinetic model equations based on double distribution functions for the later development of thermal LB method. We adopt the two relaxation times kinetic model equations proposed by Guo et al [79]. The double distribution functions in terms of two relaxation times

can be expressed as follow:

$$\partial_t f + \boldsymbol{\xi} \cdot \nabla_{\mathbf{x}} f + \mathbf{a} \cdot \nabla_{\boldsymbol{\xi}} f = -\frac{1}{\tau_f} [f - f^{eq}], \quad (\text{C.1})$$

$$\begin{aligned} \partial_t h + \boldsymbol{\xi} \cdot \nabla_{\mathbf{x}} h + \mathbf{a} \cdot \nabla_{\boldsymbol{\xi}} h &= -\frac{1}{\tau_h} [h - h^{eq}] \\ &+ \frac{Z}{\tau_{hf}} [f - f^{eq}] + f \boldsymbol{\xi} \cdot \mathbf{a}, \end{aligned} \quad (\text{C.2})$$

where  $f^{(0)}$  and  $h^{(0)}$  are given by

$$f^{eq} = \frac{\rho}{(2\pi RT)^{D/2}} \exp\left[-\frac{(\boldsymbol{\xi} - \mathbf{u})^2}{2RT}\right], \quad (\text{C.3})$$

$$h^{eq} = \frac{\rho \boldsymbol{\xi}^2}{2(2\pi RT)^{D/2}} \exp\left[-\frac{(\boldsymbol{\xi} - \mathbf{u})^2}{2RT}\right]. \quad (\text{C.4})$$

Here,  $f(\boldsymbol{\xi}, \mathbf{x}, t)$  and  $h(\boldsymbol{\xi}, \mathbf{x}, t) = \boldsymbol{\xi}^2 f/2$  are respectively the velocity distribution function and total energy distribution function,  $\boldsymbol{\xi}$  is the particle velocity,  $\mathbf{x}$  the physical space position,  $\mathbf{a}$  the acceleration due to external force and  $t$  is time. In (C.1) and (C.2),  $\tau_f$  and  $\tau_h$  are the relaxation times characterizing, respectively, the momentum change and internal energy change during particle collisions and  $\tau_{hf}^{-1} = \tau_h^{-1} + \tau_f^{-1}$ ,  $Z = \boldsymbol{\xi} \cdot \mathbf{u} - u^2/2$  where  $\mathbf{u}(\mathbf{x}, t)$  is the mean velocity. In (C.3) and (C.4),  $\rho(\mathbf{x}, t)$  is the density,  $T$  the local temperature,  $R$  is the gas constant and  $D$  is the space dimension.

Once the distribution functions  $f$  and  $h$  are known, the macroscopic quantities, e.g., the density  $\rho$ , mean velocity  $\mathbf{u}$ , and energy density  $E$  are defined, respectively, by

$$\rho(\mathbf{x}, t) = \int f d\boldsymbol{\xi}, \quad (\text{C.5})$$

$$\rho \mathbf{u}(\mathbf{x}, t) = \int \boldsymbol{\xi} f d\boldsymbol{\xi}, \quad (\text{C.6})$$

$$\rho E(\mathbf{x}, t) = \rho \left( \varepsilon + \frac{u^2}{2} \right) = \int h d\boldsymbol{\xi} \quad (\text{C.7})$$

Through the Chapman-Enskog expansion of the two relaxation time kinetic model equations, the thermal-hydrodynamic equations at the compressible

Navier-Stokes level can be obtained:

$$\partial_t \rho + \nabla \cdot (\rho \mathbf{u}) = 0, \quad (\text{C.8})$$

$$\partial_t (\rho \mathbf{u}) + \nabla \cdot (\rho \mathbf{u} \mathbf{u}) = -\nabla p + \nabla \cdot \boldsymbol{\tau} + \rho \mathbf{a}, \quad (\text{C.9})$$

$$\begin{aligned} \partial_t (\rho E) + \nabla \cdot [(p + \rho E) \mathbf{u}] &= \nabla \cdot (\kappa \nabla T) + \nabla \cdot (\boldsymbol{\tau} \cdot \mathbf{u}) \\ &+ \rho \mathbf{u} \cdot \mathbf{a}, \end{aligned} \quad (\text{C.10})$$

where  $p = \rho RT$  is the pressure and  $\boldsymbol{\tau} = \mu[[\nabla \mathbf{u} + (\nabla \mathbf{u})^T] - (2/D)(\nabla \cdot \mathbf{u})\mathbf{I}]$  is the viscous stress tensor. The transport coefficients viscosity  $\mu$  and thermal conductivity  $\kappa$  are given, respectively, by

$$\mu = \tau_f p, \quad \kappa = \frac{(D+2)R}{2} \tau_h p = c_p \tau_h p \quad (\text{C.11})$$

where  $c_p = (D+2)R/2$  is the specific heat ratio at constant pressure. Using the momentum equation, we can also deduce the temperature equation from the the total energy equation as

$$c_v [\partial_t (\rho T) + \nabla \cdot (\rho \mathbf{u} T)] = \nabla \cdot (\kappa \nabla T) - p \nabla \cdot \mathbf{u} + \boldsymbol{\tau} \cdot \nabla \mathbf{u}, \quad (\text{C.12})$$

where  $c_v = DR/2$  is the specific heat at constant volume. The Prandtl number of the kinetic system is  $Pr = \mu c_p / \kappa = \tau_f / \tau_h$  and can be made arbitrary by tuning the two relaxation times.

Introduce the characteristic (or reference) length  $L$ , time  $t_0$  and velocity  $c_0 = \sqrt{RT_0}$  scales, where  $T_0$  is a reference temperature and with  $t_0 = L/c_0$ , we have the dimensionless quantities as follows:

$$\begin{aligned} \hat{\mathbf{x}} = \frac{\mathbf{x}}{L}, (\hat{\boldsymbol{\xi}}, \hat{\mathbf{u}}, \hat{\mathbf{c}}) &= \frac{(\boldsymbol{\xi}, \mathbf{u}, \mathbf{c})}{c_0}, \hat{t} = \frac{t}{(L/c_0)}, (\hat{\tau}_f, \hat{\tau}_h) = \frac{(\tau_f, \tau_h)}{L/c_0}, \\ (\hat{f}, \hat{f}^{(0)}) &= \frac{(f, f^{(0)})}{\rho_0/c_0^D}, (\hat{h}, \hat{h}^{(0)}) = \frac{(h, h^{(0)})}{\rho_0/c_0^{D-2}}. \end{aligned} \quad (\text{C.13})$$

Substituting the above dimensionless variables into the (C.1) and (C.2), it is straightforward to find that the resulting governing kinetic equations become

dimensionless and remain unchanged in form and the equilibrium distribution functions,  $\hat{f}^{(0)}$  and  $\hat{h}^{(0)}$  are given by

$$\hat{f}^{eq} = \frac{\hat{\rho}}{(2\pi\hat{\theta})^{D/2}} \exp\left[-\frac{\hat{c}^2}{2\hat{\theta}}\right], \quad (\text{C.14})$$

$$\hat{h}^{eq} = \frac{\hat{\rho}\hat{\xi}^2}{2(2\pi\hat{\theta})^{D/2}} \exp\left[-\frac{\hat{c}^2}{2\hat{\theta}}\right], \quad (\text{C.15})$$

where  $\theta \equiv RT$  and  $\hat{\theta} \equiv RT/c_0^2$ .

## C.2 Expansion of the Equilibrium Distribution Functions

In this section, following the approach in [16], we adopt the Grad's moment expansion approach and seek solutions to (C.1) and (C.2) by expanding  $f(\mathbf{x}, \boldsymbol{\xi}, t)$  and  $h(\mathbf{x}, \boldsymbol{\xi}, t)$  in terms of Hermite polynomials,

$$f(\mathbf{x}, \boldsymbol{\xi}, t) = \omega(\boldsymbol{\xi}) \sum_{n=0}^{\infty} \frac{1}{n!} \mathbf{a}^{(n)}(x, t) \mathcal{H}^{(n)}(\boldsymbol{\xi}) \quad (\text{C.16})$$

$$h(\mathbf{x}, \boldsymbol{\xi}, t) = \omega(\boldsymbol{\xi}) \sum_{n=0}^{\infty} \frac{1}{n!} \mathbf{b}^{(n)}(x, t) \mathcal{H}^{(n)}(\boldsymbol{\xi}) \quad (\text{C.17})$$

where  $\omega(\boldsymbol{\xi}) = \frac{1}{(2\pi)^{D/2}} e^{-\boldsymbol{\xi}^2/2}$  is the weighting function,  $\mathbf{a}^{(n)}$ ,  $\mathbf{b}^{(n)}$  and  $\mathcal{H}^{(n)}(\boldsymbol{\xi})$  are rank- $n$  tensors and the product on the right-hand side denotes full contraction. Here and throughout the manuscript, the shorthand notations of [18] for fully symmetric tensors have been adopted. The equilibrium distribution functions  $f^{(0)}$  and  $h^{(0)}$  are also similarly expanded. Here the expansion to finite  $N$ -th order can be expressed as follow:

$$f^{(0),N}(\mathbf{x}, \boldsymbol{\xi}, t) = \omega(\boldsymbol{\xi}) \sum_{n=0}^N \frac{1}{n!} \mathbf{a}_0^{(n)}(x, t) \mathcal{H}^{(n)}(\boldsymbol{\xi}) \quad (\text{C.18})$$

$$h^{(0),N}(\mathbf{x}, \boldsymbol{\xi}, t) = \omega(\boldsymbol{\xi}) \sum_{n=0}^N \frac{1}{n!} \mathbf{b}_0^{(n)}(x, t) \mathcal{H}^{(n)}(\boldsymbol{\xi}) \quad (\text{C.19})$$

and,

$$\mathbf{a}_0^{(n)}(\mathbf{x}, t) = \int f^{(0)}(\mathbf{x}, \boldsymbol{\xi}, t) \mathcal{H}^{(n)}(\boldsymbol{\xi}) d\boldsymbol{\xi} \quad (\text{C.20})$$

$$\mathbf{b}_0^{(n)}(\mathbf{x}, t) = \int h^{(0)}(\mathbf{x}, \boldsymbol{\xi}, t) \mathcal{H}^{(n)}(\boldsymbol{\xi}) d\boldsymbol{\xi} \quad (\text{C.21})$$

### C.3 Discretization of Velocity Space

It is essential to realize that as a partial sum of Hermite series with finite terms, the truncated distribution functions can be completely and uniquely determined by its values at a set of discrete abscissae. This is true because with  $f$  (or  $h$ ) truncated to order  $N$ , the integrand on the right-hand side of (C.20) can be written as:

$$f^N(\mathbf{x}, \boldsymbol{\xi}, t) = \omega(\boldsymbol{\xi}) p(\mathbf{x}, \boldsymbol{\xi}, t), h^N(\mathbf{x}, \boldsymbol{\xi}, t) = \omega(\boldsymbol{\xi}) q(\mathbf{x}, \boldsymbol{\xi}, t), \quad (\text{C.22})$$

where  $p(\mathbf{x}, \boldsymbol{\xi}, t)$  (or  $q(\mathbf{x}, \boldsymbol{\xi}, t)$ ) is a polynomial in  $\boldsymbol{\xi}$  of a degree not greater than  $2N$ . Using the Gauss-Hermite quadrature,  $\mathbf{a}^{(n)}$  (or  $\mathbf{b}^{(n)}$ ) can be precisely expressed as a weighted sum of the functional values of  $p(\mathbf{x}, \boldsymbol{\xi}, t)$  (or  $q(\mathbf{x}, \boldsymbol{\xi}, t)$ ):

$$\begin{aligned} \mathbf{a}^{(n)} &= \int \omega(\boldsymbol{\xi}) p(\mathbf{x}, \boldsymbol{\xi}, t) = \sum_{a=1}^d w_a p(\mathbf{x}, \boldsymbol{\xi}_a, t) \\ &= \sum_{a=1}^d \frac{w_a}{\omega(\boldsymbol{\xi}_a)} f^N(\mathbf{x}, \boldsymbol{\xi}_a, t) \mathcal{H}^{(n)}(\boldsymbol{\xi}_a), \end{aligned} \quad (\text{C.23})$$

where  $w_a$  and  $\boldsymbol{\xi}_a$ ,  $a = 1, 2, \dots, d$ , are, respectively, the weights and abscissae of a Gauss-Hermite quadrature of a degree  $\geq 2N$ . Similar expressions can be given for  $\mathbf{b}^{(n)}$  and  $h^N(\mathbf{x}, \boldsymbol{\xi}_a, t)$ . Hence, the set of discrete distribution function values  $f^N(\boldsymbol{\xi}_a)$  and  $h^N(\boldsymbol{\xi}_a)$  now serve as a new set of fundamental variables for

defining the fluid system in place of the conventional thermohydrodynamic variables. For further details, see Shan et al. [16].

Notice that with the weighting function, we have:

$$f^{(0)} = \frac{\rho}{(\hat{\theta})^{D/2}} \omega\left(\frac{\hat{c}}{\sqrt{\hat{\theta}}}\right), \quad (\text{C.24})$$

the  $\hat{\cdot}$  will be taken off hereinafter, and all the velocities should be considered as nondimensional variables. After a change of variable  $\boldsymbol{\eta} \equiv \mathbf{c}/\sqrt{\theta}$ , we have

$$\mathbf{a}_0^{(n)} = \rho \int \omega(\boldsymbol{\eta}) \mathcal{H}^{(n)}(\sqrt{\theta}\boldsymbol{\eta} + \mathbf{u}) d\boldsymbol{\eta} \quad (\text{C.25})$$

and some of the first few tensor Hermite polynomials are given here,  $\mathcal{H}^{(0)}(\mathbf{x}) = 1$ ,  $\mathcal{H}_i^{(1)}(\mathbf{x}) = x_i$ ,  $\mathcal{H}_{ij}^{(2)}(\mathbf{x}) = x_i x_j - \delta_{ij}$ , and  $\mathcal{H}_{ijk}^{(3)}(\mathbf{x}) = x_i x_j x_k - x_i \delta_{jk} - x_j \delta_{ik} - x_k \delta_{ij}$ , etc.

The Hermite expansion coefficients  $\mathbf{a}_0^{(n)}$  can be calculated as

$$\begin{aligned} \mathbf{a}_0^{(0)} &= \rho, \\ \mathbf{a}_0^{(1)} &= \rho \mathbf{u}, \\ \mathbf{a}_0^{(2)} &= \rho[\mathbf{u}\mathbf{u} + (\theta - 1)\delta], \\ \mathbf{a}_0^{(3)} &= \rho[\mathbf{u}\mathbf{u}\mathbf{u} + (\theta - 1)\delta\mathbf{u}]. \end{aligned} \quad (\text{C.26})$$

Similarly, the expansion coefficients  $\mathbf{b}_0^{(n)}$  can be obtained as:

$$\begin{aligned} \mathbf{b}_0^{(0)} &= \rho E, \\ \mathbf{b}_0^{(1)} &= (p + \rho E)\mathbf{u}, \\ \mathbf{b}_0^{(2)} &= (2p + \rho E)\mathbf{u}\mathbf{u} + (p + \rho E(\theta - 1))\delta. \end{aligned}$$

After obtaining  $\mathbf{a}_0^{(n)}$  and  $\mathbf{b}_0^{(n)}$ , we can calculate  $f_a^{(0),N}$  and  $h_a^{(0),N}$  from E(C.16) and (C.17). For  $N = 3$  in velocity distribution function and  $N = 2$  in total energy distribution function, we get the explicit Hermite expansion of

these two distribution functions at the discrete velocities  $\boldsymbol{\xi}_a$  as:

$$f_a^{(0),3} = \omega_a \rho \left\{ 1 + \boldsymbol{\xi}_a \cdot \mathbf{u} + \frac{(\boldsymbol{\xi}_a \cdot \mathbf{u})^2}{2} - \frac{u^2}{2} + (\theta - 1) \frac{(\boldsymbol{\xi}_a^2 - D)}{2} \right. \\ \left. + \frac{\boldsymbol{\xi}_a \cdot \mathbf{u}}{6} [(\boldsymbol{\xi}_a \cdot \mathbf{u})^2 - 3u^2 + 3(\boldsymbol{\xi}_a - 1)(\boldsymbol{\xi}_a^2 - D - 2)] \right\} \quad (\text{C.27})$$

$$h_a^{(0),2} = \omega_a \rho \left\{ E + \left( \frac{p}{\rho} + E \right) \boldsymbol{\xi}_a \cdot \mathbf{u} + \left( \frac{p}{\rho} + \frac{E}{2} \right) [(\boldsymbol{\xi}_a \cdot \mathbf{u})^2 - u^2] \right. \\ \left. + \frac{p}{2\rho} (\boldsymbol{\xi}_a^2 - D) + E(\theta - 1)(\boldsymbol{\xi}_a^2 - D) \right\} \\ = \omega_a p [\boldsymbol{\xi}_a \cdot \mathbf{u} + (\boldsymbol{\xi}_a \cdot \mathbf{u})^2 - u^2 + \frac{1}{2}(\boldsymbol{\xi}_a^2 - D)] + E f_a^{(0),2} \quad (\text{C.28})$$

where  $D = \delta_{ii}$  and  $f_a^{(0),2}$  is the expansion of  $f_a^{(0)}$  to  $N = 2$  order.

The governing equations for the coupled LB-BGK method are

$$\partial_t f_a + \boldsymbol{\xi}_a \cdot \nabla_{\mathbf{x}} f_a = -\frac{1}{\tau_f} [f_a - f_a^{(0),3}] + F_a, \quad (\text{C.29})$$

$$\partial_t h_a + \boldsymbol{\xi}_a \cdot \nabla_{\mathbf{x}} h_a = -\frac{1}{\tau_h} [h_a - h_a^{(0),2}] \\ + \frac{Z_a}{\tau_{hf}} [f_a - f_a^{(0),3}] + q_a, \quad (\text{C.30})$$

where  $F_a$  and  $q_a$  are given respectively, by

$$F_a = \omega_a \rho (\boldsymbol{\xi} \cdot \mathbf{a} + (\boldsymbol{\xi}_a \cdot \mathbf{a})(\boldsymbol{\xi}_a \cdot \mathbf{u}) - \mathbf{a} \cdot \mathbf{u}), \quad (\text{C.31})$$

$$q_a = \omega_a \rho E \boldsymbol{\xi}_a \cdot \mathbf{a} + f_a \boldsymbol{\xi}_a \cdot \mathbf{a}. \quad (\text{C.32})$$

come from the similar procedures expanding the forcing terms onto Hermite polynomials.

At this stage, some notes are in order. First, we note that the above development follows closely the works presented in [16]. The model presented here is a coupled LB model, that is, the local temperature  $\theta = RT$  appears in both equilibrium velocity distribution function  $f_a^{(0)}$  and equilibrium total energy distribution function  $h_a^{(0)}$ , as also mentioned in [16] and [47], by choosing a proper reference velocity  $c_0 = \sqrt{\theta_0}$ , the particle velocity  $\boldsymbol{\xi}$  depends on



a constant  $c_0$ , but not local temperature  $\theta$  and the resultant discrete velocity model is consistent with the original kinetic model where the particle velocity,  $\xi$ ,  $\mathbf{x}$  and  $t$  are independent variables. Second, in contrast to [79], where all the local temperatures appearing in their truncated equilibrium distribution functions are replaced by a constant reference temperature  $T_0$ . Although the zeroth- and first-order moments of their  $f^{(0),2}$  and the zeroth order moment of  $h^{(0),2}$  are the same as those of the EDFs with local temperature, however, the higher-order moments required in the derivation of the Navier-Stokes equations are different when one replaces the local temperature  $T$  by  $T_0$ . Third, with our formulation, the conventional LB scheme still can be used, and we do not need to uncouple (C.27) and (C.28) as described in [79].

## C.4 Time Discretization

The detailed descriptions of the time discretization of thermal LB method based DDF can be found in [79]. First, by integrating the (C.29) along the characteristic line can leads to

$$\begin{aligned} & f_a(x + c_a \delta_t, t + \delta_t) - f_a(x, t) \\ &= \int_0^{\delta_t} [\Omega_f(x + c_a t', t + t') + F_a(x + c_a t', t + t')] dt' \end{aligned} \quad (\text{C.33})$$

where  $\delta_t$  is the time step and  $\Omega_f = (f_a^{(0),3} - f_a)/\tau_f$ . Then, by applying trapezoidal rule leads to the following equation.

$$\begin{aligned} & f_a(x + c_a \delta_t, t + \delta_t) - f_a(x, t) \\ &= \frac{\delta_t}{2} [\Omega_f(x + c_a \delta_t, t + \delta_t) + F_a(x + c_a \delta_t, t + \delta_t)] \\ &+ \frac{\delta_t}{2} [\Omega_f(x, t) + F_a(x, t)] \end{aligned} \quad (\text{C.34})$$

Introducing the following distribution function:

$$\bar{f}_a = f_a - \frac{\delta_t}{2}(\Omega_f + F_a) \quad (\text{C.35})$$

Then, one can get

$$f_a - f_a^{(0),3} = \frac{\bar{f}_a - f_a^{(0),3} + \frac{\delta_t}{2}F_a}{1 + \frac{\delta_t}{2\tau_f}} \quad (\text{C.36})$$

$$\bar{f}_a - f_a = -\frac{\delta_t}{2}(\Omega_f + F_a). \quad (\text{C.37})$$

From above equations, one can get the governing equation of distribution function with time discretization,

$$\begin{aligned} \bar{f}_a(x + c_a\delta_t, t + \delta_t) - \bar{f}_a(x, t) = & -\omega_f[\bar{f}_a(x, t) - f^{(0),3}(x, t)] \\ & + \delta_t(1 - \frac{\omega_f}{2})F_a, \end{aligned} \quad (\text{C.38})$$

where  $\omega_f = \frac{1}{\tau_f}$ . The macroscopic density  $\rho$  and velocity  $\mathbf{u}$  are determined by

$$\rho = \sum_a \bar{f}_a, \quad (\text{C.39})$$

$$\rho\mathbf{u} = \sum_a c_a\bar{f}_a + \frac{\delta_t}{2}\rho\mathbf{a}. \quad (\text{C.40})$$

By the similar procedures, the governing equation of total energy distribution function with time discretization is shown as following, together with the determination of the total energy.

$$\begin{aligned} \bar{h}_a(x + c_a\delta_t, t + \delta_t) - \bar{h}_a(x, t) \\ = -\omega_h[\bar{h}_a(x, t) - h^{(0),2}(x, t)] + \delta_t(1 - \frac{\omega_h}{2})q_a \\ + (\omega_h - \omega_f)Z_a(\bar{f}_a(x, t) - f^{(0),2}(x, t) + \frac{\delta_t}{2}F_a) \end{aligned} \quad (\text{C.41})$$

where  $\omega_h = \frac{1}{\tau_h}$  can be calculated from Prandtl number as  $Pr = \gamma \frac{\tau_f - 0.5}{\tau_h - 0.5}$  once  $\tau_f$  has been determined as described in Appendix. And also notice that

$$\bar{h}_a = h_a - \frac{\delta_t}{2}(\Omega_h + F_a) \quad (\text{C.42})$$

The determination of energy  $E$  can be found by

$$\rho E = \sum_a \bar{h}_a + \frac{\delta_t}{2} \rho \mathbf{u} \cdot \mathbf{a}. \quad (\text{C.43})$$

## C.5 Chapman-Enskog Analysis of Double Distribution Functions LB method

In this section, detail derivations of the Chapman-Enskog analysis of double distribution functions LB method are given. Following summations are computed by the MB equilibrium distribution function (C.27) and total energy distribution function (C.28).

$$\sum_a f_a^{(0),3} = \rho, \quad (\text{C.44})$$

$$\sum_a \xi_a f_a^{(0),3} = \rho \mathbf{u}, \quad (\text{C.45})$$

$$\sum_a \xi_a \xi_a f_a^{(0),3} = p \delta + \rho \mathbf{u} \mathbf{u}, \quad (\text{C.46})$$

$$\sum_a \xi_a \xi_a \xi_a f_a^{(0),3} = p [\delta \mathbf{u}]_s + \rho \mathbf{u} \mathbf{u} \mathbf{u} \quad (\text{C.47})$$

$$\sum_a \xi_a h_a^{(0),2} = (p + \rho E) \mathbf{u}, \quad (\text{C.48})$$

$$\sum_a \xi_a \xi_a h_a^{(0),2} = p(1 + E) \delta + (2p + \rho E) \mathbf{u} \mathbf{u}, \quad (\text{C.49})$$

where  $\delta$  is the Kronecker delta with two indices. Herein after,  $f^{(0)}$  is used to represent  $f^{(0),3}$  and  $h^{(0)}$  is used to represent  $h^{(0),2}$ . Introduce the following

expansions:

$$\begin{aligned}
 f_a &\simeq f_a^0 + \varepsilon f_a^1 + \varepsilon^2 f_a^2 + \dots \\
 h_a &\simeq h_a^0 + \varepsilon h_a^1 + \varepsilon^2 h_a^2 + \dots \\
 F_a &= \varepsilon F_a^1, \quad q_a = \varepsilon q_a^1 + \varepsilon^2 q_a^2 + \dots \\
 t_1 &= t\varepsilon, \quad t_2 = t\varepsilon^2, \quad r_1 = r\varepsilon
 \end{aligned}$$

such that the time and space derivative are expressed as

$$\begin{aligned}
 \partial_t &= \varepsilon \partial_{t_1} + \varepsilon^2 \partial_{t_2} \\
 \nabla &= \varepsilon \nabla_1
 \end{aligned}$$

The above expressions of the derivatives are substituted into (C.29) and (C.30), and terms involving different orders of  $\varepsilon$  are separated as:

$$\varepsilon^0 : f_a^0 = f_a^{(eq)} \tag{C.50}$$

$$\varepsilon^1 : \partial_{t_1} f_a^0 + \xi_a \nabla_1 f_a^{(0)} = -\frac{1}{\tau_f} f_a^{(1)} + F_a^{(1)} \tag{C.51}$$

$$\varepsilon^2 : \partial_{t_2} f_a^{(0)} + \partial_{t_1} f_a^{(1)} + \xi_a \nabla_1 f_a^{(1)} = -\frac{1}{\tau_f} f_a^{(2)} \tag{C.52}$$

and

$$\varepsilon^0 : h_a^0 = h_a^{(eq)} \tag{C.53}$$

$$\varepsilon^1 : \partial_{t_1} h_a^0 + \xi_a \nabla_1 h_a^{(0)} = -\frac{1}{\tau_h} h_a^{(1)} + \frac{Z_a}{\tau_{hf}} f_a^{(1)} + q_a^1 \tag{C.54}$$

$$\varepsilon^2 : \partial_{t_2} h_a^{(0)} + \partial_{t_1} h_a^{(1)} + \xi_a \nabla_1 h_a^{(1)} = -\frac{1}{\tau_h} h_a^{(2)} + \frac{Z_a}{\tau_{hf}} f_a^{(2)} + q_a^2 \tag{C.55}$$

From the above equations, we have

$$\begin{aligned}
 f_a^0 &= f_a^{(eq)}, \quad h_a^0 = h_a^{(eq)} \\
 \sum_a F_a &= 0, \quad \sum_a \boldsymbol{\xi}_a F_a = \rho \mathbf{a}, \quad \sum_a \boldsymbol{\xi}_a \boldsymbol{\xi}_a F_a = \rho [\mathbf{a} \mathbf{u}]_s \\
 \sum_a q_a &= \rho \mathbf{u} \cdot \mathbf{a}, \quad \sum_a \boldsymbol{\xi}_a q_a = (\rho E \mathbf{I} + \mathbf{P}) \cdot \mathbf{a}, \\
 \sum_a f_a^{(l)} &= 0, \quad \sum_a f_a^{(l)} \boldsymbol{\xi}_a = 0, \quad (l \geq 1), \\
 \sum_a h_a^{(l)} &= 0, \quad \sum_a h_a^{(l)} \boldsymbol{\xi}_a = 0, \quad (l \geq 1)
 \end{aligned}$$

where  $\mathbf{P} = \sum_a \boldsymbol{\xi}_a \boldsymbol{\xi}_a f_a$ .

From (C.51) and (C.54), we obtain the following first order thermal hydrodynamic equations:

$$\partial_{t_1} \rho + \nabla_1 \cdot (\rho \mathbf{u}) = 0 \quad (\text{C.56})$$

$$\partial_{t_1} (\rho \mathbf{u}) + \nabla_1 \cdot (\rho \mathbf{u} \mathbf{u} + p \mathbf{I}) = \rho \mathbf{a}_1 \quad (\text{C.57})$$

$$\partial_{t_1} (\rho E) + \nabla_1 \cdot ((p + \rho E) \mathbf{u}) = \rho \mathbf{u} \cdot \mathbf{a}_1 \quad (\text{C.58})$$

From (C.52) and (C.55), we get the following second order thermal hydrodynamic equations:

$$\partial_{t_2} \rho = 0 \quad (\text{C.59})$$

$$\partial_{t_2} (\rho \mathbf{u}) + \nabla_1 \cdot \mathbf{P}^{(1)} = 0 \quad (\text{C.60})$$

$$\partial_{t_2} (\rho E) + \nabla_1 \cdot \mathbf{q}^{(1)} = 0 \quad (\text{C.61})$$

wherein,  $\mathbf{P}^{(1)} \equiv \sum_a \boldsymbol{\xi}_a \boldsymbol{\xi}_a f_a^{(1)}$ , and  $\mathbf{q}^{(1)} \equiv \sum_a \boldsymbol{\xi}_a h_a^{(1)}$ . For calculating  $\mathbf{P}^{(1)}$ , and  $\mathbf{q}^{(1)}$  we use (C.51) to get

$$\frac{-1}{\tau_f} \mathbf{P}^{(1)} = \partial_{t_1} \mathbf{P}^{(0)} + \nabla_1 \cdot \sum_a \boldsymbol{\xi}_a \boldsymbol{\xi}_a \boldsymbol{\xi}_a f_a^{(0)} - \sum_a \boldsymbol{\xi}_a \boldsymbol{\xi}_a F_a^{(1)} \quad (\text{C.62})$$

With the aids of (C.44) and notice that from (C.56), (C.57) and (C.58) we have

$$\partial_{t_1}(\rho\mathbf{u}\mathbf{u}) = -\nabla_1(p\mathbf{u}) - \nabla_1(\rho\mathbf{u}\mathbf{u}\mathbf{u}) + \rho\mathbf{a}\mathbf{u} \quad (\text{C.63})$$

$$\partial_{t_1}p = -\nabla_1(p\mathbf{u}) - \frac{2}{D}p\nabla_1 \cdot \mathbf{u} \quad (\text{C.64})$$

such that,

$$\mathbf{P}^{(1)} = p(\mathbf{S}_1 - \frac{2}{D}(\nabla_1 \cdot \mathbf{u})\mathbf{I}) \quad (\text{C.65})$$

And, use (C.54), we can get

$$\begin{aligned} -\frac{1}{\tau_h}\mathbf{q}^{(1)} &= -\frac{1}{\tau_{hf}}P^{(1)} \cdot \mathbf{u} + \partial_{t_1}\mathbf{q}^{(0)} \quad (\text{C.66}) \\ &+ \nabla_1 \cdot \sum_a \boldsymbol{\xi}_a \boldsymbol{\xi}_a h_a^{(0)} + \nabla_a \cdot \sum_a \boldsymbol{\xi}_a q_a^1 \\ &= \partial_{t_1}[(p + \rho E)\mathbf{u}] + \nabla_1[p(1 + E)\delta + (2p + \rho E)\mathbf{u}\mathbf{u}] \\ &- \frac{1}{\tau_{hf}}P^{(1)}\mathbf{u} - [(p + \rho E)\mathbf{a} + \rho(\mathbf{u}\mathbf{a}_1)\mathbf{u}] = [\partial_{t_1}(p\mathbf{u}) \\ &+ \nabla_1(p\delta + p\mathbf{u}\mathbf{u})] + \{\partial_{t_1}(\rho E\mathbf{u}) + \nabla_1[pE\delta + (p + \rho E)\mathbf{u}\mathbf{u}]\} \\ &+ \frac{\tau_f}{\tau_{hf}}p\mathbf{S}^{(1)}\mathbf{u} - [(p + \rho E)\mathbf{a} + \rho(\mathbf{u} \cdot \mathbf{a}_1)\mathbf{u}] \\ &= pa_1 + \rho(\mathbf{u} \cdot \mathbf{a}_1)\mathbf{u} + E\rho\mathbf{a} + p\mathbf{u}\nabla_1\mathbf{u} + p\nabla_1E + E\nabla_1p \\ &+ \frac{\tau_f}{\tau_{hf}}p\mathbf{S}^{(1)}\mathbf{u} - [(p + \rho E)\mathbf{a} + \rho(\mathbf{u} \cdot \mathbf{a}_1)\mathbf{u}] \\ &= p(\mathbf{u}\nabla\mathbf{u} + \nabla E) + \frac{\tau_f}{\tau_{hf}}p\mathbf{S}^{(1)}\mathbf{u} = pc_\nu\nabla\theta + p\mathbf{S}^{(1)} \\ &+ \frac{\tau_f}{\tau_{hf}}p\mathbf{S}^{(1)}\mathbf{u} = pc_\nu\nabla\theta + \frac{\tau_f}{\tau_h}p\mathbf{S}^{(1)}\mathbf{u} \end{aligned}$$

Then, we can get  $\mathbf{q}^{(1)}$ . In deriving above equation we need the following equations derived from (C.56), (C.57) and (C.58)

$$\begin{aligned} \partial_{t_1}(\rho E\mathbf{u}) &= -\nabla_1[(p + \rho E)\mathbf{u}\mathbf{u}] + \rho\mathbf{u}(\mathbf{u} \cdot \mathbf{a}_1) \\ &+ \rho E\mathbf{a}_1 - E\nabla p + p\mathbf{u} \cdot \nabla\mathbf{u} \quad (\text{C.67}) \end{aligned}$$

$$\partial_{t_1}(p\mathbf{u}) = -\nabla_1(p\mathbf{u}\mathbf{u}) - \theta\nabla_1p + p\mathbf{a}_1 - \frac{2}{D}(\nabla_1 \cdot \mathbf{u})p\mathbf{u} \quad (\text{C.68})$$

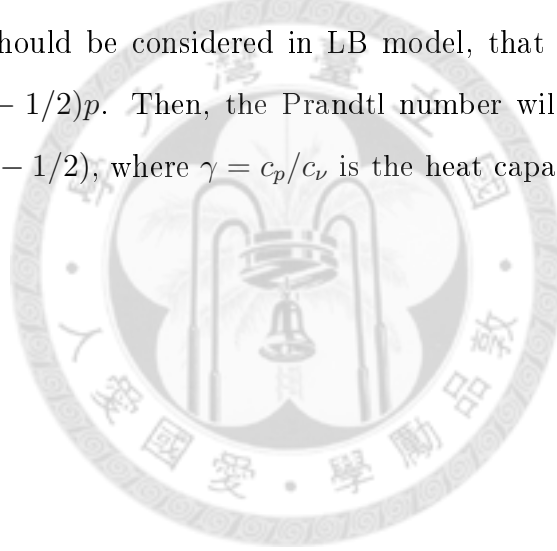
Finally, based on equations from (C.56) to (C.61), together with (C.65) and (C.66), we obtain the following thermal-hydrodynamic equations at the Navier-Stokes level:

$$\partial_t \rho + \nabla \cdot (\rho \mathbf{u}) = 0, \quad (\text{C.69})$$

$$\partial_t (\rho \mathbf{u}) + \nabla \cdot (\rho \mathbf{u} \mathbf{u}) = -\nabla p + \nabla \cdot \boldsymbol{\tau} + \rho \mathbf{a}, \quad (\text{C.70})$$

$$\partial_t (\rho E) + \nabla \cdot [(p + \rho E) \mathbf{u}] = \nabla \cdot (\kappa \nabla \theta) + \nabla \cdot (\boldsymbol{\tau} \cdot \mathbf{u}) + \rho \mathbf{u} \cdot \mathbf{a}, \quad (\text{C.71})$$

where  $\boldsymbol{\tau} = \mu[[\nabla \mathbf{u} + (\nabla \mathbf{u})^T] - (2/D)(\nabla \cdot \mathbf{u})\mathbf{I}]$  and thermal conductivity  $\kappa = \frac{D}{2} \tau_h p = c_\nu \tau_h p$ . Here, the viscosity is given by  $\mu = \tau_f p$ . Notice that the discrete effect should be considered in LB model, that is,  $\mu = (\tau_f - 1/2)p$  and  $\kappa = c_\nu(\tau_h - 1/2)p$ . Then, the Prandtl number will be  $Pr = c_p \mu / \kappa = \gamma(\tau_f - 1/2) / (\tau_h - 1/2)$ , where  $\gamma = c_p / c_\nu$  is the heat capacity ratio.







# Bibliography

- [1] F. J. Higuera and J. Jimenez. Boltzmann approach to lattice gas simulations. *Europhys. Lett.*, 9:663, 1989. 1
- [2] G. R. McNamara and G. Zanetti. Use of the boltzmann equation to simulate lattice-gas automata. *Phys. Rev. Lett.*, 61:2332, 1988. 1, 4
- [3] U. Frisch, B. Hasslacher, and Y. Pomeau. Lattice-gas automata for the navier-stokes equation. *Phys. Rev. Lett.*, 56(14):1505–1508, Apr 1986. 1, 4
- [4] S. Chapman and T. G. Cowling. *The mathematical theory of non-uniform gases*. Cambridge University Press, 1970. 1, 2, 3
- [5] H. Grad. Note on n-dimensional hermite polynomials. *Commun. Pure Appl. Maths*, 2(4):325 – 330, 1949. 1097-0312. 1, 2, 25, 101
- [6] S. Chen and G. D. Doolen. Lattice boltzmann method for fluid flows. *Annual Review of Fluid Mechanics*, 30(1):329–364, 1998. 1, 4
- [7] D. Yu, R. Mei, L. S. Luo, and W. Shyy. Viscous flow computations with the method of lattice boltzmann equation. *Progress in Aerospace Sciences*, 39(5):329 – 367, 2003. 1, 4
- [8] C. K. Aidun and J. R. Clausen. Lattice-boltzmann method for complex flows. *Annual Review of Fluid Mechanics*, 42(1):439–472, 2010. 1, 4
- [9] Y. H. Qian, D. d’Humières, and P. Lallemand. Lattice bgk models for navier-stokes equation. *Europhys. Lett.*, 17:479, 1992. 1

- [10] H. Chen, S. Chen, and W. H. Matthaeus. Recovery of the navier-stokes equations using a lattice-gas boltzmann method. *Phys. Rev. A*, 45:R5339, 1992. 1
- [11] Y. H. Qian and S. A. Orszag. Lattice bgk models for the navier-stokes equation: nonlinear deviation in compressible regimes. *Europhys. Lett.*, 21:255, 1993. 1
- [12] P. L. Bhatnagar, E. P. Gross, and M. Krook. A model for collision processes in gases. i: small amplitude processes in charged and neutral one-component system. *Phys. Rev.*, 94:511, 1954. 1, 13
- [13] D. H. Rothman and S. Zaleski. Lattice-gas models of phase separation: interfaces, phase transitions and multiphase flow. *Rev. Mod. Phys.*, 66:1417, 1994. 2
- [14] X. He and L. S. Luo. Theory of the lattice boltzmann method: From the boltzmann equation to the lattice boltzmann equation. *Phys. Rev. E*, 56(6):6811–6817, Dec 1997. 2, 54
- [15] L. S. Luo. Comment on "discrete boltzmann equation for microfluidics.". *Phys. Rev. Lett.*, 92:139401, 2004. 2
- [16] X. Shan, X. F. Yuan, and H. Chen. Kinetic theory representation of hydrodynamics : a way beyond the navier-stokes equation. *J. Fluid Mech.*, 550(-1):413–441, 2006. 2, 25, 29, 33, 34, 35, 103, 118, 121, 123, 124
- [17] X. Shan and X. He. Discretization of the velocity space in the solution of the boltzmann equation. *Phys. Rev. Lett.*, 80(1):65–68, Jan 1998. 2, 25, 54, 102

- [18] H. Grad. On the kinetic theory of rarefied gases. *Commun. Pure Appl. Maths*, 2(4):331 – 407, 1949. 2, 25, 101, 121
- [19] B. C. Eu and K. Mao. Quantum kinetic theory of irreversible thermodynamics: Low-density gases. *Phys. Rev. E*, 50(6):4380–4398, Dec 1994. 2
- [20] J. F. Lutsko. Approximate solution of the enskog equation far from equilibrium. *Phys. Rev. Lett.*, 78(2):243–246, Jan 1997. 2
- [21] E. A. Uehling and G. E. Uhlenbeck. Transport phenomena in einstein-bose and fermi-dirac gases. i. *Phys. Rev.*, 43(7):552–561, Apr 1933. 2, 6, 8, 13
- [22] E. A. Uehling. Transport phenomena in einstein-bose and fermi-dirac gases. ii. *Phys. Rev.*, 46(10):917–929, Nov 1934. 2, 6, 8
- [23] T. Nikuni and A. Griffin. Hydrodynamic damping in trapped bose gases. *Journal of Low Temperature Physics*, 111(5):793–814, Jun 1998. 2, 13, 17
- [24] M. Lundstrom. *Fundamentals of carrier transport*. Cambridge University Press, 2000. 3
- [25] J. Y. Yang and Y. H. Shi. A kinetic beam scheme for the ideal quantum gas dynamics. *Proc. Roy. Soc. Lond. A*, 462:1553, 2006. 3, 7
- [26] J. Y. Yang, T.Y. Hsieh, and Y. H. Shi. Kinetic flux vector splitting schemes for ideal quantum gas dynamics. *SIAM J. Sci. Comput.*, 29(1):221–244, 2007. 3, 7

- [27] Y. H. Shi and J. Y. Yang. A gas-kinetic bgk scheme for semiclassical boltzmann hydrodynamic transport. *J. Comput. Phys.*, 227(22):9389 – 9407, 2008. 3, 7
- [28] J. Y. Yang and L. H. Hung. Lattice uehling-uhlenbeck boltzmann-bhatnagar-gross-krook hydrodynamics of quantum gases. *Phys. Rev. E*, 79(5):056708, May 2009. 3, 6
- [29] F. J. Higuera and J. Jiménez. Boltzmann approach to lattice gas simulations. *Europhys. Lett.*, 9:663, 1989. 4
- [30] F. J. Higuera, S. Succi, and R. Benzi. Lattice gas dynamics with enhanced collisions. *Europhys. Lett.*, 9:345, 1989. 4
- [31] R. Benzi, S. Succi, and M. Vergassola. The lattice boltzmann equation: theory and applications. *Phys. Rep.*, 222:145, 1992. 4
- [32] C. E. Frouzakis I. V. Karlin, S. Ansumali. Elements of the lattice boltzmann method i:linear advection equation. *Comm. in Comput. Phys.*, 1(1):1, Aug 2006. 4
- [33] C. E. Frouzakis I. V. Karlin, S. Ansumali. Elements of the lattice boltzmannmethod ii:kinetics and hydrodynamics in one dimension. *Comm. in Comput. Phys.*, 2(2):196–238, Apr 2007. 4
- [34] B. C. Eu. *Nonequilibrium Statistical Mechanics*. Kluwer Academic Publishers, 1998. 5
- [35] J. Y. Yang, L. H. Hung, and S. H. Hu. semiclassical lattice hydrodynamics of rarefied channel flows. *Applied Mathematics and Computation*, In Press, Corrected Proof:–, 2010. 6

- [36] J. Y. Yang, L. H. Hung, and Y. T. Kuo. semiclassical axisymmetric lattice boltzmann method. *Adv. Appl. Math. Mech.*, 2(5):626–639, Oct 2010. 6
- [37] S. Succi and R. Benzi. Lattice boltzmann equation for quantum mechanics. *Physica D: Nonlinear Phenomena*, 69(3-4):327 – 332, 1993. 6, 7
- [38] S. Succi. Numerical solution of the schrödinger equation using discrete kinetic theory. *Phys. Rev. E*, 53(2):1969–1975, Feb 1996. 6, 7
- [39] B. C. Shi and Z. L. Guo. Lattice boltzmann model for the one-dimensional nonlinear dirac equation. *Phys. Rev. E*, 79(6):066704, Jun 2009. 7
- [40] B. C. Shi and Z. L. Guo. Lattice boltzmann model for nonlinear convection-diffusion equations. *Phys. Rev. E*, 79(1):016701, Jan 2009. 7
- [41] J. Zhang and G. Yan. Lattice boltzmann model for the complex ginzburg-landau equation. *Phys. Rev. E*, 81(6):066705, Jun 2010. 7
- [42] B. B. Iwo. Weyl, dirac, and maxwell equations on a lattice as unitary cellular automata. *Phys. Rev. D*, 49(12):6920–6927, Jun 1994. 7
- [43] B. M. Boghosian and W. Taylor. Quantum lattice-gas model for the many-particle schrödinger equation in  $d$  dimensions. *Phys. Rev. E*, 57(1):54–66, Jan 1998. 7
- [44] J. Yopez. Quantum lattice-gas model for computational fluid dynamics. *Phys. Rev. E*, 63(4):046702, Mar 2001. 7

- [45] S. Palpacelli, S. Succi, and R. Spigler. Ground-state computation of bose-einstein condensates by an imaginary-time quantum lattice boltzmann scheme. *Phys. Rev. E*, 76(3):036712, Sep 2007. 7
- [46] G. A. Bird. *Molecular gas dynamics and the direct simulation of gas flows*. Oxford University Press, Oxford, 1994. 13
- [47] P. C. Philippi, Jr. L. A. Hegele, L. O. E. dos Santos, and R. Surmas. From the continuous to the lattice boltzmann equation: The discretization problem and thermal models. *Phys. Rev. E*, 73(5):056702, 2006. 25, 124
- [48] H. Grad. The profile of a steady plane shock wave. *Commun. Pure Appl. Maths*, 5(3):257–300, 1952. 25
- [49] L. Giraud, D. D’Humières, and P. Lallemand. A lattice boltzmann model for jeffreys viscoelastic fluid. *Europhys. Lett.*, 42:625, 1998. 35
- [50] P. Lallemand and L. S. Luo. Theory of the lattice boltzmann method: Dispersion, dissipation, isotropy, galilean invariance, and stability. *Phys. Rev. E*, 61(6):6546–6562, Jun 2000. 35
- [51] R. Zhang, X. Shan, and H. Chen. Efficient kinetic method for fluid simulation beyond the navier-stokes equation. *Phys. Rev. E*, 74(4):046703, Oct 2006. 35, 65, 67
- [52] X. Shan and H. Chen. A general multiple-relaxation-time boltzmann collision model. *Int. J. Mod. Phys. C*, 18:635, 2007. 35
- [53] P. A. Skordos. Initial and boundary conditions for the lattice boltzmann method. *Phys. Rev. E*, 48(6):4823–4842, Dec 1993. 44, 45

- [54] Joris C. G. Verschaeve. Analysis of the lattice boltzmann bhatnagar-gross-krook no-slip boundary condition: Ways to improve accuracy and stability. *Phys. Rev. E*, 80(3):036703, Sep 2009. 44
- [55] A. Caiazzo. Analysis of lattice boltzmann initialization routines. *J. Stat. Phys.*, 121(.):37 48, . 2005. 45
- [56] L. S. Luo R. Mei, P. Lallemand, and D. d’Humières. Consistent initial conditions for lattice boltzmann simulations. *J. Comp. Phys.*, 35(.):855 862, . 2006. 45
- [57] H. Yu, S. S. Girimaji, and L. S. Luo. Lattice boltzmann simulations of decaying homogeneous isotropic turbulence. *Phys. Rev. E*, 71(1):016708, Jan 2005. 45
- [58] J. Zhang, B. Li, and D. Y. Kwok. Mean-field free-energy approach to the lattice boltzmann method for liquid-vapor and solid-fluid interfaces. *Phys. Rev. E*, 69:032602, 2004. 46
- [59] R. Cornubert, D. d’Humeières, and D. Levermore. A knudsen layer theory for lattice gases. *Phys. D*, 47:241, 1991. 47, 50
- [60] I. Ginzbourg and P. Adler. Boundary flow condition analysis for the three-dimensional lattice boltzmann model. *J. Phys. II*, 4:191, 1994. 47
- [61] D. Kandhai, A. Koponen, A. Hoekstra, M. Kataja, J. Timonen, and PMA. Slood. Implementation aspects of 3d lattice-bgk: boundaries, accuracy, and a new fast relaxation method. *J. Comput. Phys.*, 150:482, 1999. 47

- [62] A. J. C. Ladd. Numerical simulations of particulate suspensions via a discretized boltzmann equation. part 1. theoretical foundation. *J. Fluid Mech.*, 271:285, 1994. 47
- [63] D. P. Ziegler. Boundary conditions for lattice boltzmann simulations. *J. Stat. Phys.*, 71:1171, 1993. 47, 50
- [64] D. R. Noble and J. R. Torczynski. A lattice-boltzmann method for partially saturated computational cells. *Int. J. Mod. Phys. C*, 9:1189, 1998. 48
- [65] D. Holdych, D. Rovas, J. Georgiadis, and R. Buckius. An improved hydrodynamics formulation for multiphase flow lattice-boltzmann models. *Int. J. Mod. Phys. C*, 9:1393, 1998. 48
- [66] O. E. Strack and B. K. Cook. Three-dimensional immersed boundary conditions for moving, solids in the lattice-boltzmann method. *Int. J. Numer. Methods Fluids*, 55:103, 2007. 48
- [67] J. Wu and C. K. Aidun. Simulating 3d deformable particle suspensions using lattice boltzmann method with discrete external boundary force. *Int. J. Numer. Methods Fluids*, 2009. 48
- [68] O. Filippova and D. Hänel. Grid refinement for lattice-bgk models. *J. Comput. Phys.*, 147(1):219 – 228, 1998. 48
- [69] R. Mei, L.-S. Luo, and W. Shyy. An accurate curved boundary treatment in the lattice boltzmann method. *J. Comput. Phys.*, 155(2):307 – 330, 1999. 48



- [70] M. Bouzidi, M. Firdaouss, and P. Lallemand. Momentum transfer of a boltzmann-lattice fluid with boundaries. *Phys. Fluids*, 13:3452, 2001. 48
- [71] P. Lallemand and L. S. Luo. Theory of the lattice boltzmann method: Acoustic and thermal properties in two and three dimensions. *Phys. Rev. E*, 68(3):036706, Sep 2003. 48
- [72] R. Verberg and AKC Ladd. Accuracy and stability of a lattice-boltzmann model with subgrid scale boundary conditions. *Phys. Rev. E*, 65:016701, 2001. 49
- [73] D. R. Noble, S. Chen, J. G. Georgiadis, and R. O. Buckius. A consistent hydrodynamic boundary condition for the lattice boltzmann method. *Phys. Fluids*, 7:203, 1995. 49, 50
- [74] Q. Zou and X. He. On pressure and velocity boundary conditions for the lattice boltzmann bgk model. *Phys. Fluids.*, 9:1591, 1997. 50
- [75] S. Chen, D. Martinez, and R. Mei. On boundary conditions in lattice boltzmann methods. *Phys. Fluids*, 8:2527, 1996. 50
- [76] Z. L. Guo, C. G. Zheng, and B. C. Shi. An extrapolation method for boundary conditions in lattice boltzmann method. *Physics of Fluids*, 14(6), 2002. 50
- [77] L. Zheng, B. C. Shi, and Z. L. Guo. Multiple-relaxation-time model for the correct thermohydrodynamic equations. *Phys. Rev. E*, 78(2):026705, Aug 2008. 50

- [78] S. Chen, J. Tölke, S. Geller, and M. Krafczyk. Lattice boltzmann model for incompressible axisymmetric flows. *Phys. Rev. E*, 78(4):046703, Oct 2008. 50
- [79] Z. L. Guo, C. G. Zheng, B. C. Shi, and T. S. Zhao. Thermal lattice boltzmann equation for low mach number flows: Decoupling model. *Phys. Rev. E*, 75(3):036704, 2007. 50, 71, 72, 76, 103, 117, 118, 125
- [80] Z. L. Guo, H. Han, B. C. Shi, and C. G. Zheng. Theory of the lattice boltzmann equation: Lattice boltzmann model for axisymmetric flows. *Phys. Rev. E*, 79(4):046708, Apr 2009. 50
- [81] C. S. Peskin. *Flow patterns around heart valves: a digital computer method for solving the equations of motion*. PhD thesis, Univ. Microfilms., 1972. 52
- [82] D. Goldstein, R. Handler, and L. Sirovich. Modeling a no-slip flow boundary with an external force field. *J. Comput. Phys.*, 105(2):354 – 366, 1993. 52
- [83] M. C. Lai and C. S. Peskin. An immersed boundary method with formal second-order accuracy and reduced numerical viscosity. *J. Comput. Phys.*, 160(2):705 – 719, 2000. 52
- [84] M. N. Linnick and H. F. Fasel. A high-order immersed interface method for simulating unsteady incompressible flows on irregular domains. *J. Comput. Phys.*, 204(1):157 – 192, 2005. 52
- [85] A. L. F. Lima E Silva, A. Silveira-Neto, and J. J. R. Damasceno. Numerical simulation of two-dimensional flows over a circular cylinder using

- the immersed boundary method. *J. Comput. Phys.*, 189(2):351 – 370, 2003. 52
- [86] Z. G. Feng and E. E. Michaelides. The immersed boundary-lattice boltzmann method for solving fluid-particles interaction problems. *J. Comput. Phys.*, 195(2):602 – 628, 2004. 52, 53, 70
- [87] Z. G. Feng and E. E. Michaelides. Proteus: a direct forcing method in the simulations of particulate flows. *J. Comput. Phys.*, 202(1):20 – 51, 2005. 52, 53
- [88] E. A. Fadlun, R. Verzicco, P. Orlandi, and J. Mohd-Yusof. Combined immersed-boundary finite-difference methods for three-dimensional complex flow simulations. *J. Comput. Phys.*, 161(1):35 – 60, 2000. 53
- [89] M. Uhlmann. An immersed boundary method with direct forcing for the simulation of particulate flows. *J. Comput. Phys.*, 209(2):448 – 476, 2005. 53
- [90] C. Shu, N. Liu, and Y. T. Chew. A novel immersed boundary velocity correction-lattice boltzmann method and its application to simulate flow past a circular cylinder. *J. Comput. Phys.*, 226(2):1607 – 1622, 2007. 53
- [91] P. Lallemand, L. S. Luo, and Y. Peng. A lattice boltzmann front-tracking method for interface dynamics with surface tension in two dimensions. *J. Comput. Phys.*, 226:1367, 2007. 53, 70
- [92] M. Knudsen. Die gesetze der molecular stromung und dieinneren reibungstromung der gase durch rohren. *J. Comput. Phys.*, 28:75–130, 1909. 53, 65

- [93] S. Ansumali and I. V. Karlin. Kinetic boundary conditions in the lattice boltzmann method. *Phys. Rev. E*, 66:026311, 2002. 54, 56
- [94] W. Q. Tao G. H. Tang and Y. L. He. Lattice boltzmann method for gaseous microflows using kinetic theory boundary conditions. *Phys. Fluids*, 17:058101, 2005. 54
- [95] S. Succi. Mesoscopic modeling of slip motion at fluid-solid interfaces with heterogeneous catalysis. *Phys. Rev. Lett.*, 89:064502, 2002. 55
- [96] F. Toschi and S. Succi. Lattice boltzmann method at finite knudsen numbers. *Europhys. Lett.*, 69:549, 2005. 56
- [97] R. W. Whitworth. Experiments on the flow of heat in liquid helium below 0.7 degrees k. *Proc. R. Soc. A*, 246:390, 1958. 65
- [98] D. Benin and H. Maris. Phonon heat transport and knudsen's minimum in liquid helium at low temperatures. *Phys. Rev. B*, 18:3112, 1978. 65
- [99] H. H. Jensen, H. Smith, P. Wölfle, K. Nagai, and T. M. Bisgaard. Boundary effects in fluid flow. application to quantum liquids. *J. Low Temp. Phys.*, 41:473, 1980. 65
- [100] D. Sawkey and J. P. Harrison. Volume flow in liquid  $^3\text{he}$  in the knudsen and poiseuille regions. *Physica B*, 112:329, 2003. 65
- [101] T. Kanki and S. Iuchi. Poiseuille flow and thermal creep of a rarefied gas between parallel plates. *Phys. Fluids*, 16:594, 1973. 65
- [102] M. Gad el Hak. The fluid mechanics of microdevices. *J. Fluids Eng.*, 121:5, 1999. 66

- [103] G. E. Karniadakis, A. Beskok, and N. Aluru. *Micro flows: Fundamentals and Simulation*. Springer-Verlag, 2001. 66
- [104] C. M. Ho and Y. C. Tai. Micro-electro-mechanical-systems (mems) and fluid flows. *Ann. Rev. Fluid Mech.*, 30:579, 1998. 66
- [105] Y. Zhang, R. Qin, and D. R. Emerson. Lattice boltzmann simulation of rarefied gas flows in microchannels. *Phys. Rev. E*, 71(4):047702, Apr 2005. 67
- [106] M. J. Rice. Size-dependent transport-coefficient effects in fermi liquids. *Phys. Rev.*, 165(1):288–292, Jan 1968. 68, 103
- [107] B. C. Eu. Generalized hydrodynamics approach to the knudsen problem. *Phys. Rev. A*, 40(11):6395–6402, Dec 1989. 68, 69, 103
- [108] J. M. Parpia and T. L. Rhodes. First observation of the knudsen minimum in normal liquid  $^3\text{he}$ . *Phys. Rev. Lett.*, 51(9):805–808, Aug 1983. 68, 69, 103
- [109] M. Kardar. *Statistical physics of particles*. Cambridge University Press, 2007. 69, 71
- [110] B. Hasslacher P. Lallemand U. Frisch, D. d’Humières and J.P. Rivet. Lattice gas hydrodynamics in two and three dimensions. *Complex Syst.*, 1:649, 1987. 70, 74
- [111] S. Hou, Q. Zou, S. Chen, G. D. Doolen, and A. C. Cogley. Simulation of cavity flow by the lattice boltzmann method. *J. Comput. Phys.*, 118(2):329 – 347, 1995. 74

- [112] J. Y. Yang, S. C. Yang, Y. N. Chen, and C. A. Hsu. Implicit weighted eno schemes for the three-dimensional incompressible navier-stokes equations. *J. Comput. Phys.*, 146(1):464 – 487, 1998. 74
- [113] S. Albensoeder and H. C. Kuhlmann. Accurate three-dimensional lid-driven cavity flow. *J. Comput. Phys.*, 206(2):536 – 558, 2005. 74
- [114] M. Hortmann, M. Pericacute, and G. Scheuerer. Finite volume multigrid prediction of laminar natural convection: Bench-mark solutions. *Int. J. Numer. Methods Fluids*, 11(2):189–207, 1990. 1097-0363. 76, 118
- [115] S. S. Chikatamarla, S. Ansumali, and I. V. Karlin. Grad’s approximation for missing data in lattice boltzmann simulations. *EPL (Europhysics Letters)*, 74(2):215, 2006. 104
- [116] S. S. Chikatamarla and I. V. Karlin. Lattices for the lattice boltzmann method. *Phys. Rev. E*, 79(4):046701, Apr 2009. 104
- [117] I. V. Karlin, A. Ferrante, and H. C. Öttinger. Perfect entropy functions of the lattice boltzmann method. *Europhys. Lett.*, 47:182, 1999. 104
- [118] S. Ansumali and I. V. Karlin. Stabilization of the lattice boltzmann method by the h theorem: a numerical test. *Phys. Rev. E*, 62:7999, 2000. 104
- [119] P. Asinari and I. V. Karlin. Generalized maxwell state and  $h$  theorem for computing fluid flows using the lattice boltzmann method. *Phys. Rev. E*, 79(3):036703, Mar 2009. 104
- [120] P. Asinari and I. V. Karlin. Quasiequilibrium lattice boltzmann models with tunable bulk viscosity for enhancing stability. *Phys. Rev. E*, 81(1):016702, Jan 2010. 104

- [121] X. Shan. Simulation of rayleigh-benard convection using a lattice boltzmann method. *Phys. Rev. E*, 55(3):2780–2788, Mar 1997. 117
- [122] F. J. Alexander, S. Chen, and J. D. Sterling. Lattice boltzmann thermohydrodynamics. *Phys. Rev. E*, 47(4):R2249–R2252, Apr 1993. 117
- [123] K. Takeshi and T. Michihisa. Lattice boltzmann model for the compressible navier-stokes equations with flexible specific-heat ratio. *Phys. Rev. E*, 69(3):035701, Mar 2004. 117
- [124] Y. Chen, H. Ohashi, and M. Akiyama. Thermal lattice bhatnagar-gross-krook model without nonlinear deviations in macrodynamic equations. *Phys. Rev. E*, 50(4):2776–2783, Oct 1994. 117
- [125] X. He, S. Chen, and G. D. Doolen. A novel thermal model for the lattice boltzmann method in incompressible limit. *J. Comput. Phys.*, 146(1):282 – 300, 1998. 117
- [126] Y. Peng, C. Shu, and Y. T. Chew. Simplified thermal lattice boltzmann model for incompressible thermal flows. *Phys. Rev. E*, 68(2):026701, Aug 2003. 117
- [127] Y. Shi, T. S. Zhao, and Z. L. Guo. Thermal lattice bhatnagar-gross-krook model for flows with viscous heat dissipation in the incompressible limit. *Phys. Rev. E*, 70(6):066310, Dec 2004. 117